

LieAugmenter: Equivariant Learning by Discovering Symmetries with Learnable Augmentations

Eduardo Santos-Escriche^{1,2}, Ya-Wei Eileen Lin^{1,2}, and Stefanie Jegelka^{1,2,3,4}

¹Technical University of Munich (School of CIT)

²Munich Center for Machine Learning

³Munich Data Science Institute

⁴MIT (Department of EECS and CSAIL)

Abstract

Data augmentation is a powerful mechanism in equivariant machine learning, encouraging symmetry by training networks to produce consistent outputs under transformed inputs. Yet, effective augmentation typically requires the underlying symmetry to be specified *a priori*, which can limit generalization when symmetries are unknown or only approximately valid. To address this, we introduce *LieAugmenter*, an end-to-end framework that discovers task-relevant continuous symmetries through *learnable augmentations*. Specifically, the augmentation generator is parameterized using the theory of Lie groups and trained jointly with the prediction network using the augmented views. The learned augmentations are task-adaptive, enabling effective and interpretable symmetry discovery. We provide a theoretical analysis of identifiability and show that our method yields symmetry-respecting models for the identified groups. Empirically, LieAugmenter outperforms baselines on image classification, as well as on the prediction of N -body dynamics and molecular properties. In addition, it can also provide an interpretable signature for detecting the absence of symmetries.

1. Introduction

Equivariant machine learning [Bronstein et al., 2017, Villar et al., 2021, Van der Pol et al., 2020] has emerged as a principled approach for incorporating known symmetries into learning systems, leading to improved sample efficiency [Wang et al., 2022a, Tahmasebi and Jegelka, 2024], generalization [Elesedy and Zaidi, 2021, Sokolic et al., 2017], and interpretability [Crabbé and van der Schaar, 2023, Wang and Wang, 2021] across a wide range of domains [Bronstein et al., 2021, Kondor and Trivedi, 2018]. When the target function respects a symmetry, e.g., translation equivariance in vision [LeCun et al., 1989, Worrall et al., 2017], rotational equivariance in molecular modeling [Batzner et al., 2022, Schütt et al., 2021], or Euclidean symmetry in physical systems [Smidt et al., 2021], explicitly encoding the symmetry can substantially reduce the effective hypothesis space [Cohen and Welling, 2016]. Among the various paradigms for incorporating symmetry, *data augmentation* [Shorten and Khoshgoftaar, 2019, Mumuni and Mumuni, 2022] is arguably the most widely used in practice: it is architecture-agnostic, straightforward to integrate into existing pipelines, and naturally accommodates *approximate* symmetries [van der Ouderaa et al., 2022, Petrache and Trivedi, 2023, Tahmasebi and Weber, 2025]. Yet, similar to equivariant architectures which impose hard equivariance by design [Maron et al., 2019a,b, Weiler et al., 2018, Liao and Smidt, 2023], augmentation-based approaches typically require the symmetry to be specified *a priori* to be effective. In practice, the relevant symmetry is often unknown, partially present, or holds only approximately [Gross, 1996, Cubuk et al., 2019, Davies et al., 2016, Mitra et al., 2006, 2013, Liu and Tegmark, 2022].

These challenges motivate *symmetry discovery*: learning transformations from data rather than specifying them by hand [Zhou et al., 2021, Benton et al., 2020, Yang et al., 2024, Dehmamy et al., 2021, Ko et al., 2024]. A growing line of work explores unsupervised or weakly supervised discovery of continuous symmetries by learning latent group actions, e.g., via Lie algebra-based architectures, adversarial distribution matching in data space, latent-space formulations for nonlinear actions, or post-hoc extraction from trained predictors [Yang et al., 2023, Moskalev et al., 2022, Hu et al., 2025b, Shaw et al., 2024, Krippendorf and Syvaeri, 2020, van der Ouderaa et al., 2023]. Yet, two limitations commonly arise. First, many discovery objectives target distributional symmetry, encouraging transformed samples to match the observed input distribution [Yang et al., 2023, Desai et al., 2022, Hu et al., 2025b]. Prior methods find symmetries by assuming that the data distribution is invariant under a transformation (i.e., uniform over group orbits). However, this criterion can

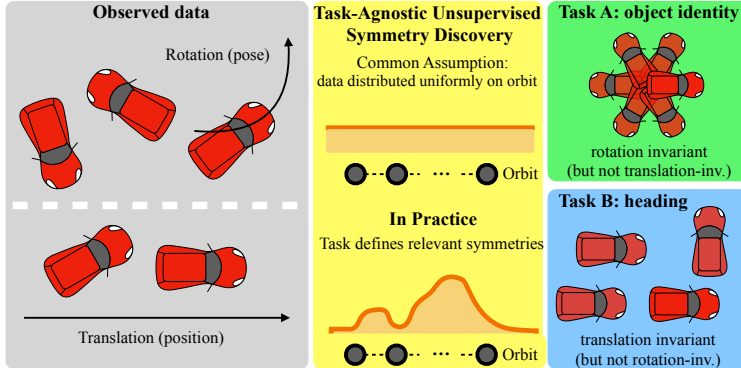


Figure 1: Data exhibits latent transformations, e.g., rotation and translation, but which of these transformations should be treated as symmetries is often unknown. Symmetry discovery infers this. Existing unsupervised symmetry discovery methods can have two drawbacks: (i) they often assume the data is uniformly distributed across an orbit; this is not always true in practice [Lawrence et al., 2025]; (ii) symmetries can differ across target tasks.

fail to capture symmetries that are relevant for the downstream task, as symmetries can be task-dependent (see Figure 1), and imposing the wrong symmetry can degrade performance [Benton et al., 2020, Rommel et al., 2022, Miao et al., 2023]. Second, many symmetry discovery methods are used post hoc or as a separate preprocessing step: a symmetry (or Lie algebra) is estimated from unlabeled data or a trained model, and then a second model is trained or redesigned to exploit it [Moskalev et al., 2022, Yang et al., 2023, Hu et al., 2025b]. Such separation can complicate model selection and prevents task supervision from refining the symmetry estimate end-to-end. Hence, this paper seeks to address the following question:

Can we train an end-to-end unconstrained architecture to jointly achieve both interpretable symmetry discovery and approximately equivariant predictions?

Our Approach: Task-Adaptive Symmetry Discovery via Learnable Lie Augmentations. We propose *LieAugmenter*, an end-to-end framework that formulates symmetry discovery as learning task-dependent data augmentations over a continuous transformation family. *LieAugmenter* parameterizes candidate symmetries using a set of learnable Lie algebra generators. During training, we sample group elements and apply the corresponding transformations to inputs. We jointly optimize (i) the parameters of the augmentation generator and (ii) a symmetry-agnostic prediction network that receives the augmented data to learn equivariant predictions. The multi-task loss includes a supervised prediction loss and an equivariance loss that encourages equivariance under sampled transformations. Figure 2 illustrates our model. It is worth noting that rather than imposing equivariance architecturally, *LieAugmenter* promotes approximate equivariance through the end-to-end loss, allowing the learned transformations to adapt to the task while yielding an interpretable Lie algebra basis for the discovered symmetry.

We theoretically characterize the symmetry discovery mechanism by establishing an identifiability result for learned transformations. We also show that the approximate learned equivariance improves robustness under transformation-shifted test distributions. Empirically, we demonstrate the effectiveness of our approach on image classification, N -body dynamics prediction, and molecular property prediction. *LieAugmenter* learns interpretable symmetries *end-to-end* and achieves strong predictive performance compared to oracle augmentation and two-stage symmetry discovery baselines. Moreover, our method can detect the absence of symmetry for datasets with no nontrivial continuous symmetry and provides an interpretable *no-symmetry* signature.

2. Related Work

We briefly review the most relevant Lie-based symmetry discovery methods related to our approach. For a more comprehensive and detailed discussion of related literature, see Appendix B. Augerino [Benton et al., 2020] and LieGAN [Yang et al., 2023] are the most related symmetry discovery methods to ours since they also parameterize learnable continuous symmetries with Lie algebra bases. Different from *LieAugmenter*, Augerino is a supervised method solely based on the task loss, and the discovered symmetry is restricted to a subgroup of a pre-specified group. To avoid having to pre-specify this group, the Augerino+ variant

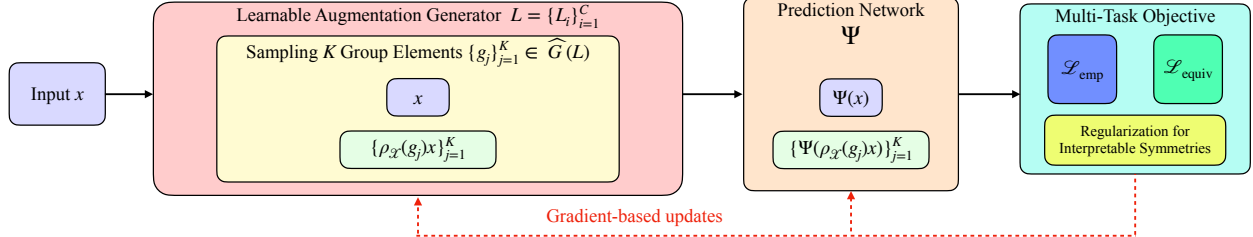


Figure 2: Illustration of LieAugmenter for task-dependent soft-equivariant models. LieAugmenter performs end-to-end task-dependent symmetry discovery by learning augmentation generators $L = \{L_i\}$ used to sample transformations $g_j \in \widehat{G}(L)$. Sampling K group elements $\{g_j\}_{j=1}^K$ induces K learned augmentations $\{\rho_{\mathcal{X}}(g_j)x\}_{j=1}^K$, which are passed to the prediction network Ψ . During training, Ψ and L are optimized jointly using the supervised task loss and the equivariance loss computed on the learned augmentations.

[Yang et al., 2023] fixes the search space to the general linear group. LieGAN learns fully unknown groups via generative adversarial training on the input distribution. However, it is an unsupervised symmetry discovery approach that is task-agnostic. It discovers symmetries as transformations that preserve the data distribution, making its performance sensitive to symmetry acting uniformly on the data [Hu et al., 2025b], and hindering its adaptability to different tasks. In addition, to use the learned symmetry in a task, an additional downstream model is needed. Our method, in contrast to these approaches, is end-to-end and it incorporates an equivariance loss in the objective to promote task-adaptive approximate symmetries.

3. Preliminaries

We briefly review relevant background. For additional details and used notation, we refer to Appendix A.

Matrix Lie Group and Lie Algebras. A matrix Lie group G is a subgroup of the general linear group $\text{GL}(d, \mathbb{R})$ that is also a smooth manifold s.t. multiplication and inversion are smooth maps [Baker, 2003, Erdmann and Wildon, 2006]. In this paper, we primarily consider connected matrix Lie groups. The associated Lie algebra $\mathfrak{g} = T_{\text{Id}}G$ is the tangent space of G at the identity element. Each element $A \in \mathfrak{g}$ is an infinitesimal generator of one-parameter subgroups $t \mapsto \exp(tA)$ for $t \in \mathbb{R}$. Let $\{L_i\}_{i=1}^{\dim \mathfrak{g}}$ be a basis of \mathfrak{g} . For matrix Lie groups, the exponential map $\exp : \mathfrak{g} \rightarrow G$ is given by the matrix exponential, which is a local diffeomorphism in a neighborhood of the identity. If G is connected and compact, \exp is surjective [Kirillov, 2008, Hall, 2013], hence every $g \in G$ can be written as $g = \exp(\sum_i w_i L_i)$ with $w_i \in \mathbb{R}$.

Group Actions and Equivariance. We consider inputs $x \in \mathcal{X} \subseteq \mathbb{R}^n$ and outputs $y \in \mathcal{Y} \subseteq \mathbb{R}^m$. A linear action of G on \mathcal{X} is specified by a representation $\rho_{\mathcal{X}} : G \rightarrow \text{GL}(n)$, and similarly on \mathcal{Y} by $\rho_{\mathcal{Y}} : G \rightarrow \text{GL}(m)$. A function $f : \mathcal{X} \rightarrow \mathcal{Y}$ is G -equivariant if $f(\rho_{\mathcal{X}}(g)x) = \rho_{\mathcal{Y}}(g)f(x)$ for all $g \in G$ and $x \in \mathcal{X}$. Invariance is a special case of equivariance, where the output action is $\rho_{\mathcal{Y}}(g) = I \forall g \in G$.

4. LieAugmenter

In this section, we introduce *LieAugmenter* for jointly discovering continuous symmetries and training a prediction network using learnable Lie group augmentations under a multi-task objective (see Figure 2 for an illustration).

Problem Setting. We consider a supervised learning setting with a labeled dataset $\mathcal{D} = \{(x_i, y_i)\}_{i=1}^N$, where $x_i \in \mathcal{X} \subseteq \mathbb{R}^n$ and $y_i \in \mathcal{Y} \subseteq \mathbb{R}^m$, and aim to learn a predictor $f : \mathcal{X} \rightarrow \mathcal{Y}$. We assume the data exhibits an unknown *continuous* symmetry modeled by a connected matrix Lie group G with linear representations $\rho_{\mathcal{X}} : G \rightarrow \text{GL}(n)$ and $\rho_{\mathcal{Y}} : G \rightarrow \text{GL}(m)$ (see Appendix A.2 for examples of such groups). Our objective is two-fold: (i) *symmetry discovery*, i.e., to identify an interpretable representation of the latent symmetry via its associated Lie algebra basis, and (ii) *equivariant prediction*, i.e., to learn a function f with strong generalization performance and small equivariance error with respect to the discovered symmetry:

$$f(\rho_{\mathcal{X}}(g)x) \approx \rho_{\mathcal{Y}}(g)f(x) \text{ for all } g \in G \text{ and } x \in \mathcal{X}.$$

4.1. Parameterizing Augmentations using Lie Groups

Central to our model is a learnable data augmentation procedure that learns a Lie algebra basis. For each input $x_i \in \mathcal{X}$ we sample a set of group elements based on the learned symmetry and generate the corresponding transformed inputs, which are then fed to the predictor. To learn symmetry group G from data, we need a differentiable parameterization of group elements that supports gradient-based optimization through the sampling procedure. We thus adopt a reparameterization approach [Price, 2003, Kingma and Welling, 2013] adapted to Lie groups [Falorsi et al., 2019], which samples group elements through the associated Lie algebra.

Let \mathfrak{g} denote the Lie algebra associated with a connected matrix Lie group acting on the representation space of \mathcal{X} . We parameterize a candidate Lie algebra using a learnable set of C generators $L = \{L_i \in \mathbb{R}^{d \times d}\}_{i=1}^C$ ¹ and sample coefficients $w = (w_1, \dots, w_C) \in \mathbb{R}^C$ from a distribution $P(\gamma)$ with parameters γ . Specifically, we consider a uniform distribution $P(\gamma) = \mathcal{U}[-\gamma, \gamma]$. A group element is obtained by mapping the resulting Lie algebra element to the group via the matrix exponential, given by

$$g = \exp \left[\sum_{i=1}^C w_i L_i \right], \quad w_i \sim P(\gamma). \quad (1)$$

By construction, g lies in the matrix Lie subgroup $\widehat{G}(L)$ generated by L (and $\widehat{G}(L)$ coincides with G when the learned generators recover the true Lie algebra). The reparameterized sampling allows gradients to propagate to L .

Given an input x_i , we draw K independent group elements $g_{i,2}, \dots, g_{i,K+1}$ according to Eq. (1) and form the corresponding augmentations using their representations

$$x_{i,j} := \rho_{\mathcal{X}}(g_{i,j}) x_i, \quad j \in [2, \dots, K+1], \quad (2)$$

with the original input $x_{i,1} := x_i$. We then evaluate a symmetry-agnostic network Ψ on $\{x_{i,j}\}_{j=1}^{K+1}$ to produce predictions for the original and transformed inputs, which are used by the training objective in the next subsection.

4.2. Multi-Task Objective for Symmetry Discovery

We now introduce the end-to-end training objective used to learn both the task network and the augmenter. Specifically, we jointly learn (i) a *symmetry-agnostic* prediction network Ψ and (ii) the parameters of the learned augmentation generators. LieAugmenter does not impose the equivariance architecturally; instead, the learned augmentation generators adapt to the task and the prediction model learns symmetry through a training objective that encourages equivariance of the task network Ψ across sampled group transformations.

Our objective consists of two primary terms. The empirical prediction loss measures standard supervised performance on the original inputs, while the equivariance loss promotes symmetry of predictions under transformations sampled from the learned group. In particular, if a sampled transformation does not reflect a valid symmetry of the prediction task, then enforcing equivariance under it leads to discrepancy between predictions and transformed targets, which increases the loss and steers the learned generators away from such transformations. We detail these terms below.

Empirical Prediction Loss. We define the empirical prediction loss on the original, untransformed inputs $x_{i,1} = x_i$. For regression tasks, we use the mean squared error

$$\mathcal{L}_{\text{emp}} = \frac{1}{N} \sum_{i=1}^N \|y_i - \Psi(x_{i,1})\|_2^2, \quad (3)$$

and for classification tasks we use the cross-entropy.

Equivariance Loss. To encourage approximate equivariance w.r.t the sampled transformations, we define an equivariance loss that compares predictions on transformed inputs with transformed targets. Let $g_{i,2}, \dots, g_{i,K+1}$ denote the K group elements sampled for x_i . For regression tasks, we set

$$\mathcal{L}_{\text{equiv}} = \frac{1}{N} \sum_{i=1}^N \frac{1}{K} \sum_{j=2}^{K+1} \|\Psi(\rho_{\mathcal{X}}(g_{i,j})x_i) - \rho_{\mathcal{Y}}(g_{i,j})y_i\|_1, \quad (4)$$

¹For vector-valued data, we take $d = n$ and learn generators in the ambient data representation, i.e., $L_i \in \mathbb{R}^{n \times n}$. For images, we parameterize transformations in coordinate space (e.g., homogeneous $d = 3$), learn $L_i \in \mathbb{R}^{d \times d}$, and realize the induced action $\rho_{\mathcal{X}}(g)$ via differentiable grid warping (see Appendix A.1).

and for classification tasks we use cross-entropy.

The equivariance loss in Eq. (4) links symmetry discovery and prediction: if the learned transformations are incompatible with the data, enforcing consistency across them increases the loss, which in turn discourages incorrect symmetry estimates. In addition, this term can be viewed as a Monte Carlo estimate [Robert et al., 1999] of the expected equivariance violation under the learned sampling distribution over g . It is minimized when $\Psi(\rho_X(g)x) \approx \rho_Y(g)y$ for transformations supported by the data.

Main Objective. We balance predictive accuracy and equivariance with weights $\alpha, \beta \geq 0$:

$$\mathcal{L}_{\text{main}} = \alpha \mathcal{L}_{\text{emp}} + \beta \mathcal{L}_{\text{equiv}}. \quad (5)$$

The coefficient β controls the equivariance constraint, which is important when the underlying symmetry is approximate.

Regularization for Interpretable Symmetries. In addition to $\mathcal{L}_{\text{main}}$, we include regularizers that promote non-trivial and interpretable symmetry representations. First, we discourage near-identity augmentations by penalizing similarity between an input and its transformed variants:

$$\ell_{\text{areg}} = \frac{1}{N} \sum_{i=1}^N \frac{1}{K} \sum_{j=2}^{K+1} |\text{CosSim}(x_i, \rho_X(g_{i,j})x_i)|. \quad (6)$$

Second, we encourage sparse generators:

$$\ell_{\text{bsreg}} = \sum_{i=1}^C \|L_i\|_1. \quad (7)$$

Finally, we promote orthogonality among generators by discouraging highly aligned basis elements:

$$\ell_{\text{bcreg}} = \sum_{i=1}^C \sum_{j=i+1}^C |\text{CosSim}(L_i, L_j)|. \quad (8)$$

Total Training Objective. The final objective is the weighted sum of the main loss and the regularization terms:

$$\mathcal{L}_{\text{total}} = \alpha \mathcal{L}_{\text{emp}} + \beta \mathcal{L}_{\text{equiv}} + \lambda \ell_{\text{areg}} + \nu \ell_{\text{bsreg}} + \eta \ell_{\text{bcreg}}, \quad (9)$$

where $\alpha, \beta, \lambda, \eta, \nu \geq 0$ control the contribution of each term.

We conclude this section with two remarks. First, the multi-task objective in Eq. (9) is designed to prevent degenerate solutions while promoting an interpretable, non-redundant basis (see Appendix C.2). In Appendix E.3, we conduct an ablation study and sensitivity analysis over regularizations and hyperparameters, and find that our method is robust across a broad range of settings. Second, in line with prior Lie group-based symmetry discovery methods [Benton et al., 2020, Yang et al., 2024, 2023, Moskalev et al., 2022], sampling via Eq. (1) is inherently limited to the identity component of the Lie subgroup generated by the learned generators, and may not cover it fully when the exponential map is non-surjective (notably for many non-compact Lie groups) [Kirillov, 2008, Moskowitz and Sacksteder, 2003]. Thus, disconnected symmetries (e.g., reflections) are not reachable without additional discrete structure. See Appendix A.2 for further discussion of recoverable groups. Nevertheless, Lie group actions in our method still capture a broad class of practical continuous symmetries across various application domains [Gross, 1996, Gilmore, 2006, Thomas et al., 2018, Rao and Ruderman, 1998, Finzi et al., 2020, Falorsi et al., 2019, Sola et al., 2018, Kondor and Trivedi, 2018, Sohl-Dickstein et al., 2010, Cohen and Welling, 2014, Dehmamy et al., 2021]. Extending the framework to disconnected symmetries and to more fully address non-compact settings is an important direction for future work.

5. Theoretical Properties of LieAugmenter

In this section, we present the theoretical properties of LieAugmenter. We first state the Monte Carlo nature of the equivariance objective. We then present the identifiability of the discovered symmetry. We further show that LieAugmenter leads to approximately symmetry preserving networks with universal approximation properties and relate approximate equivariance to robustness under transformation shifts. Proofs and additional analysis are in Appendix C.

Let Q_L be the distribution over group elements from Eq. (1) and let the data $(X, Y) \sim P$. We define the population analogues of the losses by $\mathcal{L}_{\text{emp}}^{\text{POP}}(\Psi) = \mathbb{E}[\|Y - \Psi(X)\|_2^2]$, $\mathcal{L}_{\text{equiv}}^{\text{POP}}(\Psi, L) = \mathbb{E}[\mathbb{E}_{g \sim Q_L}[\|\Psi(\rho_X(g)X) - \rho_Y(g)Y\|_1]]$, and set $\mathcal{L}_{\text{main}}^{\text{POP}} = \alpha \mathcal{L}_{\text{emp}}^{\text{POP}} + \beta \mathcal{L}_{\text{equiv}}^{\text{POP}}$.

Lemma 5.1. For fixed (Ψ, L) , the empirical equivariance term in Eq. (4) is a K -sample Monte Carlo estimator of $\mathcal{L}_{\text{equiv}}^{\text{pop}}(\Psi, L)$. Specifically, it is unbiased (up to dataset averaging) and its variance scales as $O(1/K)$.

Lemma 5.1 formalizes that LieAugmenter minimizes an expected equivariance deviation under learned augmentations. Concretely, for fixed augmenter parameters, $\mathcal{L}_{\text{equiv}}$ averages the task loss over K sampled augmentations. This corresponds to a partial augmentation scheme that approximates the group-averaging operator via Monte Carlo sampling. Empirically, we find that using $K = 10$ attains strong performance (see Section 6 and Appendix E).

Theorem 5.2. Let $\alpha, \beta > 0$. Assume $Y = f^*(X)$ almost surely and that f^* is the unique minimizer of $\mathcal{L}_{\text{emp}}^{\text{pop}}(\Psi)$ over the predictor class. In addition, suppose $\mathcal{L}_{\text{equiv}}^{\text{pop}}(f^*, L) = 0$. Let $\widehat{\mathfrak{g}}(L) = \text{span}\{L_1, \dots, L_C\}$ and let $\widehat{G}(L)$ be the connected subgroup generated by $\widehat{\mathfrak{g}}(L)$. Suppose for every g in a neighborhood of the identity in the candidate subgroup $\widehat{G}(L)$, $\rho_{\mathcal{X}}(g)\mathcal{X} \subseteq \mathcal{X}$. Then any global minimizer (Ψ^*, L^*) of $\mathcal{L}_{\text{main}}^{\text{pop}}(\Psi, L)$ satisfies $\Psi^* = f^*$ almost surely and $\widehat{G}(L^*) \subseteq G$. Moreover, if the connected symmetry group of f^* is exactly G and $\dim(\widehat{G}(L^*)) = \dim(G)$, then $\widehat{G}(L^*) = G$ and $\widehat{\mathfrak{g}}(L^*) = \mathfrak{g}$.

Theorem 5.2 explains the symmetry-discovery mechanism, addressing (i) recovering the correct underlying function and (ii) recovering the symmetry. With respect to discovered symmetries, the main objective admits multiple minimizers as any subgroup of G yields zero equivariance loss when $\Psi = f^*$. Therefore, the regularizers in Eq. (9) are designed to break this degeneracy and promote an interpretable basis within the symmetry group. We formalize the role of regularizers as a canonicalization principle in Appendix C.2.

Proposition 5.3. Let $(X, Y) \sim P$ with $Y = f^*(X)$ almost surely for a continuous target function $f^* : \mathcal{X} \rightarrow \mathcal{Y}$ and let f^* be equivariant $\forall g \in \text{supp}(Q_L)$. Assume \mathcal{X} is compact and that $\rho_{\mathcal{X}}(g)\mathcal{X} \subseteq \mathcal{X} \forall g \in \text{supp}(Q_L), x \in \mathcal{X}$. Let the hypothesis class used for Ψ be a universal approximator on \mathcal{X} . Then for any $\varepsilon > 0$, there exists a network Ψ such that

$$\sup_{x \in \mathcal{X}} |\Psi(x) - f^*(x)| < \varepsilon \text{ and } \mathcal{L}_{\text{equiv}}^{\text{pop}}(\Psi, L) < \varepsilon. \quad (10)$$

Proposition 5.3 shows that LieAugmenter can be used with symmetryless networks while retaining universal approximation properties for equivariant targets. Specifically, the universal approximation properties for standard architectures [Leshno et al., 1993, Hornik et al., 1989, Cybenko, 1989] imply the existence of networks Ψ without built-in equivariance that uniformly approximate an equivariant target f^* . In our method, such approximations can be realized while simultaneously optimizing the induced equivariance deviation w.r.t. the learned transformations.

We now connect the approximate equivariance to out-of-distribution (OOD) generalization under transformation shift. We consider the test distribution to be obtained by applying a group element to both inputs and labels.

Proposition 5.4. For $g \in G$, define the transformation-shifted distribution $P^{(g)}$ by $(X', Y') = (\rho_{\mathcal{X}}(g)X, \rho_{\mathcal{Y}}(g)Y)$ with $(X, Y) \sim P$. Let $\ell : \mathcal{Y} \times \mathcal{Y} \rightarrow \mathbb{R}_+$ satisfy: (i) $\ell(\rho_{\mathcal{Y}}(g)a, \rho_{\mathcal{Y}}(g)b) = \ell(a, b) \forall a, b \in \mathcal{Y}, g \in G$, and (ii) there exists $L_\ell > 0$ s.t. $|\ell(u, y) - \ell(v, y)| \leq L_\ell \|u - v\|_1 \forall u, v, y \in \mathcal{Y}$. Then for any network Ψ and any $g \in G$, $\mathcal{R}_{P^{(g)}}(\Psi) \leq \mathcal{R}_P(\Psi) + L_\ell \mathbb{E}[\|\Psi(\rho_{\mathcal{X}}(g)X) - \rho_{\mathcal{Y}}(g)\Psi(X)\|_1]$, where $\mathcal{R}_P(\Psi) := \mathbb{E}[\ell(\Psi(X), Y)]$.

Proposition 5.4 measures how stable the prediction network is under a transformation shift. Specifically, this bound is controlled by the objective optimized in LieAugmenter (see Appendix C.4). We empirically show the advantages of our method under OOD settings in Section 6 and Appendix E.

6. Experiments

We evaluate LieAugmenter on image classification, N -body dynamics prediction, and molecular property prediction. We also examine our method on a dataset without symmetries as a control experiment. Detailed implementation settings, including experimental setup and hyperparameters, are reported in Appendix D. Further empirical results, including runtime analysis, ablations, studies on discovering discrete and partial symmetries, and on data from colorectal cancer detection and Lorentz symmetries in quantum field theory, are provided in Appendix E.

6.1. Image Classification

We first demonstrate the advantage of LieAugmenter for symmetry discovery and equivariant learning in the image domain using a CNN prediction network [LeCun et al., 1989, Krizhevsky et al., 2012]. We use the

RotatedMNIST dataset [Deng, 2012, Larochelle et al., 2007], where each image is randomly rotated in-plane and the digit label is approximately invariant to in-plane rotations, i.e., $\rho_Y(g) \equiv I$ for classification. Here, we consider both in-distribution (ID) and out-of-distribution (OOD) settings. In the ID setting, both training and test images are rotated by angles $\theta \in [0, 360^\circ]$. In the OOD setting, training images are rotated by $\theta \in [-90^\circ, 90^\circ)$ while test images are rotated by angles in the complementary set $\theta \in [90^\circ, 180^\circ) \cup [-180^\circ, -90^\circ)$. Note that from the symmetry discovery perspective, the OOD setting implies that the data has a non-uniform distribution over the orbit, which is a more challenging scenario.

Symmetry Discovery. We compare LieAugmenter with LieGAN and Augerino+ [Yang et al., 2023] for unknown symmetry discovery on RotatedMNIST. Figure 3 shows visualizations of the Lie algebra bases learned by each method. We see that LieAugmenter correctly recovers the Lie algebra basis of the ground-truth SO(2) group in both settings. For a quantitative comparison, Figure 4 reports the absolute cosine similarity and the absolute Frobenius projection between the learned basis and the ground truth. In the ID setting, both LieGAN and LieAugmenter achieve near-perfect directional alignment. In the OOD setting, LieGAN shows degradation and higher variability across runs. In contrast, LieAugmenter remains well aligned and stable, indicating stronger robustness under the shifted distribution.

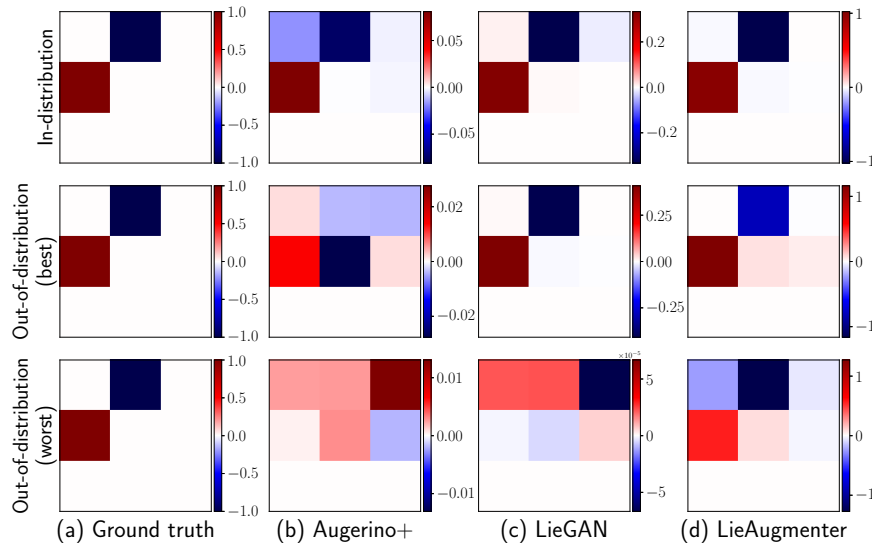


Figure 3: Lie algebra basis for the ground-truth SO(2) group and bases learned by baseline symmetry discovery methods and LieAugmenter on RotatedMNIST. Results are shown for the ID (*top*) and OOD settings. For OOD, we report the best (*middle*) and worst (*bottom*) learned bases across three random seeds.

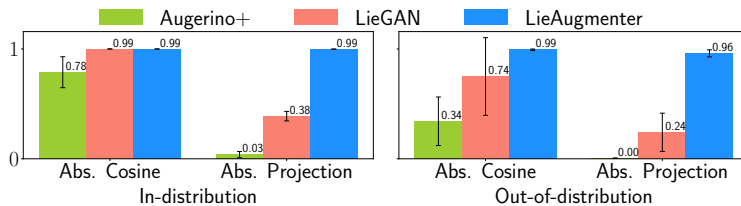


Figure 4: Absolute cosine similarity and absolute Frobenius projection for Lie algebra basis recovery on in-distribution and OOD RotatedMNIST (mean \pm std over three random seeds).

Predictive Performance. We evaluate the prediction performance by comparing LieAugmenter with Augerino+ and the augmentation strategies applied to the base CNN prediction network, including (i) no augmentations, (ii) oracle augmentations using the ground truth SO(2) symmetry, and (iii) augmentations based on the symmetries discovered by LieGAN (denoted by LieGAN Aug). We also include an equivariant architecture baseline, a Group Equivariant Convolutional Network (GCNN) [Cohen and Welling, 2016], which encodes invariance to the discrete $p4$ group through architectural constraints. Table 1 reports test classification accuracy and the equivariance error. We see that in the ID setting LieAugmenter outperforms

the $p4$ equivariant architecture, oracle augmentation, and augmentations from discovered symmetries. In the OOD setting, LieAugmenter matches oracle augmentation. Notably, LieAugmenter attains such strong accuracy and OOD generalization while discovering the symmetry jointly with the prediction network during end-to-end training, rather than relying on prior knowledge of the symmetry (equivariant architectures or oracle augmentation) or a separate symmetry-discovery stage.

Table 1: RotatedMNIST results for in-distribution (ID) and out-of-distribution (OOD) evaluation. We report classification accuracy (higher is better) and equivariance error (lower is better) for an equivariant-architecture baseline (GCNN, $p4$) and for CNN models trained (i) without augmentation (*Trivial*), (ii) with *Oracle* rotation augmentation (ground-truth symmetry), (iii) with symmetry-discovery baselines (Augerino+ and LieGAN Aug.), and (iv) with LieAugmenter (*Ours*). All values are reported as mean \pm std over three random seeds.

	Equivariant architecture	No augmentation	Oracle augmentation	Symmetry discovery		
	GCNN ($p4$)	Trivial	Rotation	Augerino+	LieGAN Aug.	LieAugmenter
ID Acc. (%) (\uparrow)	96.78 \pm 0.36	96.17 \pm 0.34	99.06 \pm 0.00	96.85 \pm 0.30	98.69 \pm 0.16	99.08 \pm 0.06
ID Equiv. Error (\downarrow)	5.31 \pm 1.16	5.52 \pm 0.23	4.01 \pm 0.29	5.09 \pm 0.70	5.04 \pm 0.19	3.10 \pm 0.32
OOD Acc. (%) (\uparrow)	55.60 \pm 1.45	55.24 \pm 1.14	99.09 \pm 0.08	57.68 \pm 1.45	91.59 \pm 1.07	90.82 \pm 6.49
OOD Equiv. Error (\downarrow)	5.78 \pm 1.23	7.19 \pm 0.54	3.87 \pm 0.35	3.97 \pm 0.51	5.82 \pm 0.47	3.26 \pm 0.62

6.2. N -Body Dynamics Prediction

We further examine LieAugmenter on a simulated N -body trajectory dataset from Greydanus et al. [2019]. Following the experimental protocol of Yang et al. [2023], we generate the dynamical data and use an MLP as the prediction network. Specifically, we consider a setting with two bodies of identical mass rotating in nearly circular orbits, where the task is to predict their future coordinates based on past observations. At each timestep, the input and output feature vectors contain $4N$ entries corresponding to the positions and momenta of all bodies $\{q_{i,x}, q_{i,y}, p_{i,x}, p_{i,y}\}_{i=1}^N$. In line with the experimental setting of Yang et al. [2023], we restrict the symmetry search space to transformations that act separately on each body’s position and momentum (see Figure 5 second column). As in Section 6.1, we study both ID and OOD settings, where ID considers the default dataset while in OOD, the training data are constrained so that the first body’s position lies only in the top-left or bottom-right quadrants, and the test set is constructed from the complementary quadrants (top-right or bottom-left). Here, we focus on the one-step prediction (one input timestep to one output timestep), and we provide additional results in Appendix E.5, including a more challenging three-step prediction, where we observe a similarly strong performance.

Symmetry Discovery. In Figure 5, we visualize the learned symmetry structure by showing the resulting 2×2 block-diagonal mask constraint alongside the Lie algebra basis identified by each method. Across both the ID and OOD settings, LieAugmenter correctly recovers the ground-truth Lie algebra basis, demonstrating that it can reliably infer the underlying equivariant transformations even under distribution shift. Additional results under less restrictive symmetry search spaces are provided in Appendix E.5.

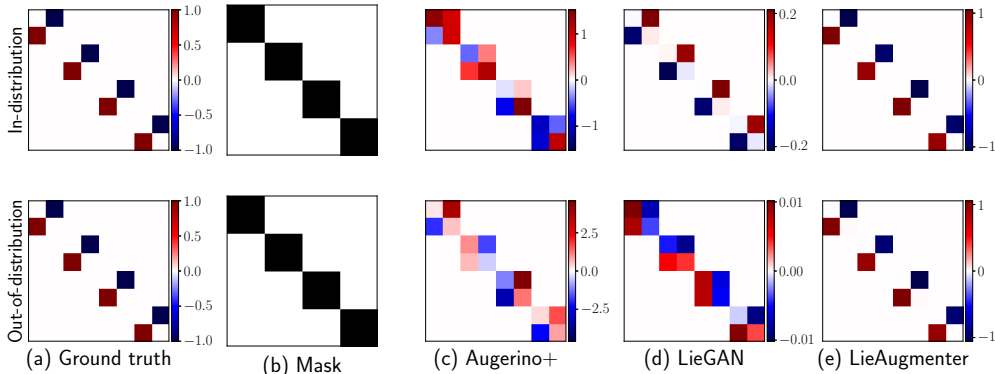


Figure 5: Ground-truth Lie algebra basis, mask of learnable entries, and bases learned by baseline symmetry discovery methods and LieAugmenter for 2-body dynamics prediction. Results are shown for the ID (*top*) and the OOD setting (*bottom*).

Predictive Performance. We compare our method with the analogous augmentation baselines as in Section 6.1. Table 2 reports mean squared error (MSE) and equivariance error. In the ID setting, LieAugmenter achieves the best performance, surpassing oracle augmentation and augmentation based on discovered symmetries. In the OOD setting, the performance of the symmetry-discovery baselines drops markedly, while LieAugmenter still matches oracle performance. Notably, our method attains strong performance without prior knowledge of the symmetry, indicating that it can both recover symmetry and transform it into robust generalization.

Table 2: 2-body dynamics results for ID and OOD evaluations. We report MSE and equivariance error for MLP models trained (i) without augmentation (*Trivial*), (ii) with *Oracle* rotation augmentation (ground-truth symmetry), (iii) with symmetry-discovery baselines (Augerino+ and LieGAN Aug.), and (iv) with LieAugmenter (*Ours*). All values are reported as mean \pm std over three random seeds.

	No augmentation	Oracle augmentation	Symmetry discovery		
	Trivial	Rotation	Augerino+	LieGAN Aug.	LieAugmenter
ID MSE (\downarrow)	5.16e-03 \pm 2.79e-03	2.13e-05 \pm 1.56e-05	9.67e+03 \pm 1.37e+04	1.10e-03 \pm 6.98e-04	1.30e-05 \pm 5.58e-06
ID Equiv. Error (\downarrow)	2.48e-02 \pm 7.37e-03	3.03e-03 \pm 1.03e-03	2.37e-01 \pm 7.53e-02	1.48e-02 \pm 4.80e-03	3.28e-03 \pm 9.36e-04
OOD MSE (\downarrow)	1.86e-02 \pm 3.74e-03	3.03e-05 \pm 8.81e-06	1.48e+05 \pm 2.09e+05	8.94e-03 \pm 9.31e-04	3.73e-05 \pm 2.97e-05
OOD Equiv. Error (\downarrow)	3.33e-02 \pm 2.56e-03	3.70e-03 \pm 1.14e-03	1.95e-01 \pm 9.23e-03	2.73e-02 \pm 1.10e-03	5.96e-03 \pm 2.82e-03

6.3. Molecular Property Prediction

Next, we evaluate LieAugmenter on molecular property prediction using QM9 dataset [Blum and Reymond, 2009, Rupp et al., 2012], which consists of small inorganic molecules represented as sets of atoms with 3D coordinates and atom-type features (e.g., atomic numbers). We focus on predicting the highest occupied molecular orbital energy (HOMO) and the lowest unoccupied molecular orbital energy (LUMO), two scalar targets that are invariant to global rigid motions of the atomic coordinates. In other words, rotating and translating all atoms by the same element of SE(3) does not change the HOMO/LUMO values. This setting is therefore well-suited for testing whether LieAugmenter can learn a *higher-dimensional* continuous symmetry model, since the Lie algebra basis of SE(3) is six-dimensional (three infinitesimal rotations and three infinitesimal translations).²

Following the experimental protocol in prior symmetry discovery and data augmentation evaluations on QM9 [Benton et al., 2020, Yang et al., 2023], we use LieConv [Finzi et al., 2020] with no equivariance (LieConv-Trivial) as the base model, such that any robustness to rigid motions arises from learned Lie-parameterized augmentations and the training objective rather than from architectural constraints. We compare the proposed LieAugmenter to alternative augmentation strategies, including (i) no augmentation, (ii) oracle SE(3) augmentations, and (iii) augmentations generated from symmetries discovered by Augerino and LieGAN.

Symmetry Discovery. To qualitatively assess symmetry recovery, we visualize the learned generators alongside a canonical Lie algebra basis of SE(3) in Figure 6. We see that the proposed LieAugmenter recovers generators that are consistent with the SE(3) structure across both targets. Note that bases of SE(3) are not unique: beyond permutations and sign flips, different linear combinations of generators can span the same Lie subalgebra. For this reason, we align learned generators to a canonical basis for visualization (for a more detailed description see Appendix D.4).

Predictive Performance and Proximity to Oracle Augmentation. Table 3 reports the mean absolute error (MAE) in meV for molecular property prediction. LieAugmenter achieves performance close to oracle SE(3) augmentation, with an oracle gap of 0.6 meV on HOMO and 0.9 meV on LUMO, while outperforming augmentations from the competing symmetry discovery methods. These results suggest that LieAugmenter can scale beyond one-dimensional symmetries, recover generators consistent with SE(3), and convert the discovered symmetry into improved performance and generalization on molecular regression tasks.

²QM9 models are also invariant to permutations of atom indices. This discrete symmetry is handled by the set architecture and is orthogonal to the continuous SE(3) symmetry studied here.

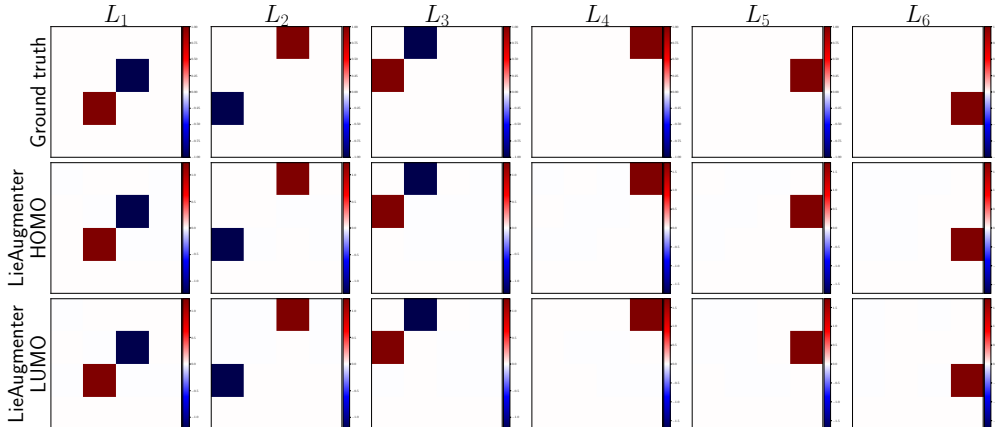


Figure 6: Comparison of canonical Lie algebra basis for SE(3) group (*top*) and the generators learned by LieAugmenter for HOMO (*middle*) and LUMO (*bottom*) on QM9. For interpretability, we match the learned generators to the closest canonical basis.

Table 3: MAE (in meV, lower is better) on QM9 dataset for HOMO and LUMO. *Oracle* SE(3) augmentation uses the ground-truth rigid-motion symmetry. We denote this oracle setting with $*$. Results marked with \dagger are taken from Benton et al. [2020], and those marked with \ddagger are from Yang et al. [2023].

	No aug.	Oracle aug.	Symmetry discovery		
	Trivial \dagger	SE(3) \dagger	Augerino \dagger	LieGAN \ddagger	LieAugmenter
HOMO	52.7	36.5*	<u>38.3</u>	43.5	37.1
LUMO	43.5	29.8*	<u>33.7</u>	36.4	30.7

6.4. Behavior in the Absence of Symmetry

The experiments above show that LieAugmenter can recover the underlying symmetry and improve predictive performance across datasets and tasks. Here we study the complementary case: data with no symmetry. Our goal is to test whether symmetry discovery methods learn misleading spurious transformations, or whether their outputs make it easy to diagnose that the dataset has no underlying symmetry.

We construct a synthetic regression problem that is learnable but has no nontrivial continuous equivariance as follows. We first construct an anisotropic, mean-shifted input distribution to reduce spurious symmetries in the marginal distribution: $x \sim \mathcal{N}(\mu, \Sigma)$, where $\mu = (0.2, -0.1, 0.3, -0.2, 0.15)$ and $\Sigma = \text{diag}(1, 2, 4, 8, 16)$. We then generate labels using a randomly initialized and frozen MLP $f^* : \mathbb{R}^5 \rightarrow \mathbb{R}$: $y = f^*(x) + \epsilon$, where $\epsilon \sim \mathcal{N}(0, \sigma^2)$ and $\sigma = 0.01$. With probability one over the draw of f^* , the resulting map remains learnable but has no nontrivial continuous symmetry.

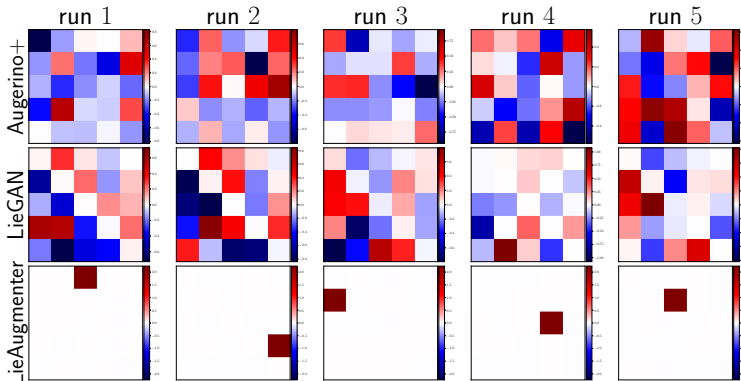


Figure 7: Learned Lie algebra bases across multiple runs on a synthetic dataset with no continuous symmetry. Baselines (Augerino+, LieGAN) exhibit noisy representations. LieAugmenter provides an interpretable signature for detecting the absence of symmetry.

Figure 7 summarizes the learned Lie algebra bases across multiple runs. Augerino+ and LieGAN learn arbitrary dense and noisy representations across multiple runs, which makes the learned transformations hard to interpret. In contrast, LieAugmenter produces sparse bases whose norm concentrates on a single entry, and the active entry changes across runs. This run-to-run entry variability indicates that there is no consistent continuous symmetry to recover, and it provides an interpretable empirical signature for detecting the lack of symmetry (see further details in Appendix C.2.2).

7. Conclusions

We introduce LieAugmenter, an end-to-end framework that jointly learns a prediction network and a Lie-parameterized augmentation generator for task-adaptive symmetry discovery. Our method relies on a multi-task objective consisting of supervised prediction, approximate equivariance, and regularization to avoid degeneracies and promote an interpretable generator basis. From a theoretical standpoint, we show identifiability conditions for the discovered symmetry, demonstrate that our method yields approximately symmetry-preserving networks with universal approximation properties, and connect approximate equivariance to robustness under transformation shifts. In addition, we demonstrate empirical advantages of LieAugmenter in symmetry discovery and predictive performance over competing methods on image classification, N -body dynamics prediction, and molecular property prediction, as well as providing an interpretable signature for detecting absence of symmetries.

Limitations and Future Work. A limitation of LieAugmenter is that augmentations are sampled via the matrix exponential, which restricts the reachable transformations to the identity component of the Lie subgroup generated by the learned generators. In future work, we plan to extend our framework to disconnected symmetries and non-compact Lie groups. We also plan to broaden our task-dependent soft-equivariant models to more general symmetry notions, e.g., nonlinear symmetries or structures beyond group actions.

Acknowledgments

We thank Valerie Engelmayer, Daniel Herbst, and Andreas Bergmeister for proofreading an earlier version of this manuscript. We also thank Jianke Yang for clarifying aspects of the experimental setup used in Yang et al. [2023]. This work was supported by an Alexander von Humboldt Professorship and a PhD fellowship from the Munich Center for Machine Learning.

References

- James Allingham, Bruno Mlodozeniec, Shreyas Padhy, Javier Antorán, David Krueger, Richard Turner, Eric Nalisnick, and José Miguel Hernández-Lobato. A generative model of symmetry transformations. *Advances in Neural Information Processing Systems*, 37:91091–91130, 2024.
- Khaled Alomar, Halil Ibrahim Aysel, and Xiaohao Cai. Data augmentation in classification and segmentation: A survey and new strategies. *Journal of Imaging*, 9(2):46, 2023.
- Joseph Aylett-Bullock, Simon Badger, and Ryan Moodie. Optimising simulations for diphoton production at hadron colliders using amplitude neural networks. *Journal of High Energy Physics*, 2021(8):1–30, 2021.
- Simon Badger and Joseph Bullock. Using neural networks for efficient evaluation of high multiplicity scattering amplitudes. *Journal of High Energy Physics*, 2020(6):1–26, 2020.
- Andrew Baker. *Matrix groups: An introduction to Lie group theory*. Springer Science & Business Media, 2003.
- Simon Batzner, Albert Musaelian, Lixin Sun, Mario Geiger, Jonathan P Mailoa, Mordechai Kornbluth, Nicola Molinari, Tess E Smidt, and Boris Kozinsky. E(3)-equivariant graph neural networks for data-efficient and accurate interatomic potentials. *Nature communications*, 13(1):2453, 2022.
- Gregory Benton, Marc Finzi, Pavel Izmailov, and Andrew G Wilson. Learning Invariances in Neural Networks from Training Data. In *Advances in Neural Information Processing Systems*, volume 33, pages 17605–17616. Curran Associates, Inc., 2020.
- Lorenz C Blum and Jean-Louis Reymond. 970 million druglike small molecules for virtual screening in the chemical universe database GDB-13. *Journal of the American Chemical Society*, 131(25):8732–8733, 2009.

- Michael M Bronstein, Joan Bruna, Yann LeCun, Arthur Szlam, and Pierre Vandergheynst. Geometric deep learning: going beyond euclidean data. *IEEE Signal Processing Magazine*, 34(4):18–42, 2017.
- Michael M. Bronstein, Joan Bruna, Taco Cohen, and Petar Veličković. Geometric Deep Learning: Grids, Groups, Graphs, Geodesics, and Gauges. *arXiv preprint arXiv:2104.13478*, 2021.
- Taco Cohen and Max Welling. Learning the irreducible representations of commutative Lie groups. In *International Conference on Machine Learning*, pages 1755–1763. PMLR, 2014.
- Taco Cohen and Max Welling. Group equivariant convolutional networks. In *International Conference on Machine Learning*, pages 2990–2999. PMLR, 2016.
- Taco Cohen, Maurice Weiler, Berkay Kicanaoglu, and Max Welling. Gauge equivariant convolutional networks and the icosahedral CNN. In *International Conference on Machine Learning*, pages 1321–1330. PMLR, 2019.
- Jonathan Crabbé and Mihaela van der Schaar. Evaluating the robustness of interpretability methods through explanation invariance and equivariance. *Advances in Neural Information Processing Systems*, 36: 71393–71429, 2023.
- Ekin D Cubuk, Barret Zoph, Dandelion Mane, Vijay Vasudevan, and Quoc V Le. Autoaugment: Learning augmentation strategies from data. In *Proceedings of the IEEE/CVF conference on computer vision and pattern recognition*, pages 113–123, 2019.
- George Cybenko. Approximation by superpositions of a sigmoidal function. *Mathematics of control, signals and systems*, 2(4):303–314, 1989.
- Daniel W Davies, Keith T Butler, Adam J Jackson, Andrew Morris, Jarvist M Frost, Jonathan M Skelton, and Aron Walsh. Computational screening of all stoichiometric inorganic materials. *Chem*, 1(4):617–627, 2016.
- Nima Dehmamy, Robin Walters, Yanchen Liu, Dashun Wang, and Rose Yu. Automatic symmetry discovery with Lie algebra convolutional network. *Advances in Neural Information Processing Systems*, 34:2503–2515, 2021.
- Li Deng. The MNIST Database of Handwritten Digit Images for Machine Learning Research [Best of the Web]. *IEEE Signal Processing Magazine*, 29(6):141–142, 2012. doi: 10.1109/MSP.2012.2211477.
- Krish Desai, Benjamin Nachman, and Jesse Thaler. SymmetryGAN: Symmetry Discovery with Deep Learning. *Physical Review D*, 105(9):096031, May 2022. ISSN 2470-0010, 2470-0029. doi: 10.1103/PhysRevD.105.096031.
- Alexey Dosovitskiy, Lucas Beyer, Alexander Kolesnikov, Dirk Weissenborn, Xiaohua Zhai, Thomas Unterthiner, Mostafa Dehghani, Matthias Minderer, Georg Heigold, Sylvain Gelly, Jakob Uszkoreit, and Neil Houlsby. An image is worth 16x16 words: Transformers for image recognition at scale. In *International Conference on Learning Representations*, 2021.
- Alexandre Agm Duval, Victor Schmidt, Alex Hernández-García, Santiago Miret, Fragkiskos D Malliaros, Yoshua Bengio, and David Rolnick. Faenet: Frame averaging equivariant GNN for materials modeling. In *International Conference on Machine Learning*, pages 9013–9033. PMLR, 2023.
- Nadav Dym, Hannah Lawrence, and Jonathan W Siegel. Equivariant Frames and the Impossibility of Continuous Canonicalization. In *International Conference on Machine Learning*, pages 12228–12267. PMLR, 2024.
- Bryn Elesedy and Sheheryar Zaidi. Provably strict generalisation benefit for equivariant models. In *International Conference on Machine Learning*, pages 2959–2969. PMLR, 2021.
- Ahmed A Elhag, T Konstantin Rusch, Francesco Di Giovanni, and Michael Bronstein. Relaxed Equivariance via Multitask Learning. *arXiv preprint arXiv:2410.17878*, 2024.
- Karin Erdmann and Mark J Wildon. *Introduction to Lie algebras*, volume 122. Springer, 2006.

- Luca Falorsi, Pim de Haan, Tim R Davidson, and Patrick Forré. Reparameterizing distributions on Lie groups. In *The 22nd International Conference on Artificial Intelligence and Statistics*, pages 3244–3253. PMLR, 2019.
- Luigi Favaro, Gerrit Gerhartz, Fred A Hamprecht, Peter Lippmann, Sebastian Pitz, Tilman Plehn, Huilin Qu, and Jonas Spinner. Lorentz-equivariance without limitations. *arXiv preprint arXiv:2508.14898*, 2025.
- Marc Finzi, Samuel Stanton, Pavel Izmailov, and Andrew Gordon Wilson. Generalizing convolutional neural networks for equivariance to Lie groups on arbitrary continuous data. In *International Conference on Machine Learning*, pages 3165–3176. PMLR, 2020.
- Marc Finzi, Max Welling, and Andrew Gordon Wilson. A practical method for constructing equivariant multilayer perceptrons for arbitrary matrix groups. In *International Conference on Machine Learning*, pages 3318–3328. PMLR, 2021.
- Fabian Fuchs, Daniel Worrall, Volker Fischer, and Max Welling. Se (3)-transformers: 3d roto-translation equivariant attention networks. *Advances in Neural Information Processing Systems*, 33:1970–1981, 2020.
- Jan Gerken, Oscar Carlsson, Hampus Linander, Fredrik Ohlsson, Christoffer Petersson, and Daniel Persson. Equivariance versus augmentation for spherical images. In *International Conference on Machine Learning*, pages 7404–7421. PMLR, 2022.
- Jan E Gerken and Pan Kessel. Emergent equivariance in deep ensembles. In *International Conference on Machine Learning*, pages 15438–15465. PMLR, 2024.
- Robert Gilmore. *Lie groups, Lie algebras, and some of their applications*. Courier Corporation, 2006.
- Abhinav Goel, Derek Lim, Hannah Lawrence, Stefanie Jegelka, and Ningyuan Huang. Any-subgroup equivariant networks via symmetry breaking. In *UniReps: 3rd Edition of the Workshop on Unifying Representations in Neural Models*, 2025.
- Rafael C Gonzalez. *Digital image processing*. Pearson education india, 2009.
- Samuel Greydanus, Misko Dzamba, and Jason Yosinski. Hamiltonian neural networks. *Advances in Neural Information Processing Systems*, 32, 2019.
- David J Gross. The role of symmetry in fundamental physics. *Proceedings of the National Academy of Sciences*, 93(25):14256–14259, 1996.
- Brian C Hall. Lie groups, Lie algebras, and representations. In *Quantum Theory for Mathematicians*, pages 333–366. Springer, 2013.
- Kurt Hornik, Maxwell Stinchcombe, and Halbert White. Multilayer feedforward networks are universal approximators. *Neural networks*, 2(5):359–366, 1989.
- Lexiang Hu, Yikang Li, and Zhouchen Lin. Explicit discovery of nonlinear symmetries from dynamic data. In *Forty-second International Conference on Machine Learning*, 2025a.
- Lexiang Hu, Yikang Li, and Zhouchen Lin. Symmetry discovery for different data types. *Neural Networks*, page 107481, 2025b.
- Ningyuan Huang, Ron Levie, and Soledad Villar. Approximately equivariant graph networks. *Advances in Neural Information Processing Systems*, 36:34627–34660, 2023.
- Max Jaderberg, Karen Simonyan, Andrew Zisserman, et al. Spatial transformer networks. *Advances in Neural Information Processing Systems*, 28, 2015.
- Sékou-Oumar Kaba, Arnab Kumar Mondal, Yan Zhang, Yoshua Bengio, and Siamak Ravanbakhsh. Equivariance with learned canonicalization functions. In *International Conference on Machine Learning*, pages 15546–15566. PMLR, 2023.
- Pavan Karjol, Vivek V Kashyap, Rohan Kashyap, et al. Learning Equivariant Functions via Quadratic Forms. *arXiv preprint arXiv:2509.22184*, 2025.

- Jakob Nikolas Kather, Niels Halama, and Alexander Marx. 100,000 histological images of human colorectal cancer and healthy tissue. 2018.
- Zekarias T Kefato, Sarunas Girdzijauskas, and Hannes Stärk. Jointly Learnable Data Augmentations for Self-Supervised GNNs. *arXiv preprint arXiv:2108.10420*, 2021.
- Sihyeon Kim, Sanghyeok Lee, Dasol Hwang, Jaewon Lee, Seong Jae Hwang, and Hyunwoo J Kim. Point cloud augmentation with weighted local transformations. In *Proceedings of the IEEE/CVF international conference on computer vision*, pages 548–557, 2021.
- Diederik P Kingma. Adam: A Method for Stochastic Optimization. *arXiv preprint arXiv:1412.6980*, 2014.
- Diederik P Kingma and Max Welling. Auto-Encoding Variational Bayes. *arXiv preprint arXiv:1312.6114*, 2013.
- Alexander A Kirillov. *An introduction to Lie groups and Lie algebras*, volume 113. Cambridge University Press, 2008.
- Gyeonghoon Ko, Hyunsu Kim, and Juho Lee. Learning infinitesimal generators of continuous symmetries from data. *Advances in Neural Information Processing Systems*, 37:85973–86003, 2024.
- Risi Kondor and Shubhendu Trivedi. On the generalization of equivariance and convolution in neural networks to the action of compact groups. In *International Conference on Machine Learning*, pages 2747–2755. PMLR, 2018.
- Masanori Koyama, Kenji Fukumizu, Kohei Hayashi, and Takeru Miyato. Neural Fourier Transform: A General Approach to Equivariant Representation Learning. In *The Twelfth International Conference on Learning Representations*, 2024.
- Sven Krippendorf and Marc Syvaeri. Detecting symmetries with neural networks. *Machine Learning: Science and Technology*, 2(1):015010, 2020.
- Alex Krizhevsky, Ilya Sutskever, and Geoffrey E Hinton. Imagenet classification with deep convolutional neural networks. *Advances in Neural Information Processing Systems*, 25, 2012.
- Hugo Larochelle, Dumitru Erhan, Aaron Courville, James Bergstra, and Yoshua Bengio. An empirical evaluation of deep architectures on problems with many factors of variation. In *Proceedings of the 24th international conference on Machine learning*, pages 473–480, 2007.
- Hannah Lawrence, Elyssa Hofgard, Vasco Portilheiro, Yuxuan Chen, Tess Smidt, and Robin Walters. To Augment or Not to Augment? Diagnosing Distributional Symmetry Breaking. *arXiv preprint arXiv:2510.01349*, 2025.
- Yann LeCun, Bernhard Boser, John S Denker, Donnie Henderson, Richard E Howard, Wayne Hubbard, and Lawrence D Jackel. Backpropagation applied to handwritten zip code recognition. *Neural computation*, 1(4):541–551, 1989.
- Moshe Leshno, Vladimir Ya. Lin, Allan Pinkus, and Shimon Schocken. Multilayer feedforward networks with a nonpolynomial activation function can approximate any function. *Neural Networks*, 6(6):861–867, 1993.
- Mario Lezcano-Casado and David Martinez-Rubio. Cheap orthogonal constraints in neural networks: A simple parametrization of the orthogonal and unitary group. In *International Conference on Machine Learning*, pages 3794–3803. PMLR, 2019.
- Yi-Lun Liao and Tess Smidt. Equiformer: Equivariant graph attention transformer for 3D atomistic graphs. In *The Eleventh International Conference on Learning Representations*, 2023.
- Ya-Wei Eileen Lin and Ron Levie. Adaptive canonicalization with application to invariant anisotropic geometric networks. *arXiv preprint arXiv:2509.24886*, 2025.
- Yuchao Lin, Jacob Helwig, Shurui Gui, and Shuiwang Ji. Equivariance via Minimal Frame Averaging for More Symmetries and Efficiency. In *International Conference on Machine Learning*, pages 30042–30079. PMLR, 2024.

- Ziming Liu and Max Tegmark. Machine learning hidden symmetries. *Physical Review Letters*, 128(18):180201, 2022.
- George Ma, Yifei Wang, Derek Lim, Stefanie Jegelka, and Yisen Wang. A canonicalization perspective on invariant and equivariant learning. *Advances in Neural Information Processing Systems*, 37:60936–60979, 2024.
- Lachlan E MacDonald, Sameera Ramasinghe, and Simon Lucey. Enabling equivariance for arbitrary Lie groups. In *Proceedings of the IEEE/CVF conference on computer vision and pattern recognition*, pages 8183–8192, 2022.
- Andrei Manolache, Luiz F. O. Chamon, and Mathias Niepert. Learning (Approximately) Equivariant Networks via Constrained Optimization. In *The Thirty-ninth Annual Conference on Neural Information Processing Systems*, 2025.
- Haggai Maron, Heli Ben-Hamu, Nadav Shamir, and Yaron Lipman. Invariant and equivariant graph networks. In *International Conference on Learning Representations*, 2019a.
- Haggai Maron, Ethan Fetaya, Nimrod Segol, and Yaron Lipman. On the universality of invariant networks. In *International Conference on Machine Learning*, pages 4363–4371. PMLR, 2019b.
- Karolis Martinkus, Jan Ludwiczak, Wei-Ching Liang, Julien Lafrance-Vanasse, Isidro Hotzel, Arvind Rajpal, Yan Wu, Kyunghyun Cho, Richard Bonneau, Vladimir Gligorijevic, et al. Abdifuser: full-atom generation of in-vitro functioning antibodies. *Advances in Neural Information Processing Systems*, 36:40729–40759, 2023.
- Ning Miao, Tom Rainforth, Emile Mathieu, Yann Dubois, Yee Whye Teh, Adam Foster, and Hyunjik Kim. Learning instance-specific augmentations by capturing local invariances. In *International Conference on Machine Learning*, pages 24720–24736. PMLR, 2023.
- Xu Miao and Rajesh PN Rao. Learning the Lie groups of visual invariance. *Neural computation*, 19(10):2665–2693, 2007.
- Thomas Mitchel, Michael J Taylor, and Vincent Sitzmann. Neural isometries: Taming transformations for equivariant ml. *Advances in Neural Information Processing Systems*, 37:7311–7338, 2024.
- Niloy J Mitra, Leonidas J Guibas, and Mark Pauly. Partial and approximate symmetry detection for 3d geometry. *ACM Transactions on Graphics (ToG)*, 25(3):560–568, 2006.
- Niloy J Mitra, Mark Pauly, Michael Wand, and Duygu Ceylan. Symmetry in 3D geometry: Extraction and applications. In *Computer graphics forum*, volume 32, pages 1–23. Wiley Online Library, 2013.
- Artem Moskalev, Anna Sepliarskaia, Ivan Sosnovik, and Arnold Smeulders. LieGG: Studying learned Lie group generators. *Advances in Neural Information Processing Systems*, 35:25212–25223, 2022.
- Martin Moskowitz and Richard Sacksteder. The exponential map and differential equations on real Lie groups. *Journal of Lie Theory*, 13(1):291–306, 2003.
- Alhassan Mumuni and Fuseini Mumuni. Data augmentation: A comprehensive survey of modern approaches. *Array*, 16:100258, 2022.
- Samuel E Otto, Nicholas Zolman, J Nathan Kutz, and Steven L Brunton. A unified framework to enforce, discover, and promote symmetry in machine learning. *Journal of Machine Learning Research*, 26(248):1–83, 2025.
- Jung Yeon Park, Yuxuan Chen, Floor Eijkelboom, Jan-Willem van de Meent, Lawson LS Wong, and Robin Walters. Discovering lie groups with flow matching. *arXiv preprint arXiv:2512.20043*, 2025.
- Mircea Petrache and Shubendu Trivedi. Approximation-generalization trade-offs under (approximate) group equivariance. *Advances in Neural Information Processing Systems*, 36:61936–61959, 2023.
- Robert Price. A useful theorem for nonlinear devices having gaussian inputs. *IRE Transactions on Information Theory*, 4(2):69–72, 2003.

- Omri Puny, Matan Atzmon, Edward J. Smith, Ishan Misra, Aditya Grover, Heli Ben-Hamu, and Yaron Lipman. Frame Averaging for Invariant and Equivariant Network Design. In *International Conference on Learning Representations*, 2022.
- Chen Qiu, Timo Pfroemer, Marius Kloft, Stephan Mandt, and Maja Rudolph. Neural transformation learning for deep anomaly detection beyond images. In *International Conference on Machine Learning*, pages 8703–8714. PMLR, 2021.
- Facundo Quiroga, Franco Ronchetti, Laura Lanzarini, and Aurelio F Bariviera. Revisiting data augmentation for rotational invariance in convolutional neural networks. In *Modelling and Simulation in Management Sciences: Proceedings of the International Conference on Modelling and Simulation in Management Sciences (MS-18)*, pages 127–141. Springer, 2020.
- Rajesh Rao and Daniel Ruderman. Learning Lie groups for invariant visual perception. *Advances in Neural Information Processing Systems*, 11, 1998.
- Christian P Robert, George Casella, and George Casella. *Monte Carlo statistical methods*, volume 2. Springer, 1999.
- Cédric Rommel, Thomas Moreau, and Alexandre Gramfort. Deep invariant networks with differentiable augmentation layers. *Advances in Neural Information Processing Systems*, 35:35672–35683, 2022.
- Matthias Rupp, Alexandre Tkatchenko, Klaus-Robert Müller, and O Anatole Von Lilienfeld. Fast and accurate modeling of molecular atomization energies with machine learning. *Physical review letters*, 108(5): 058301, 2012.
- Tobias Schmidt, Steffen Schneider, and Matthias Bethge. Equivariance by contrast: Identifiable equivariant embeddings from unlabeled finite group actions. In *The Thirty-ninth Annual Conference on Neural Information Processing Systems*, 2025.
- Kristof Schütt, Oliver Unke, and Michael Gastegger. Equivariant message passing for the prediction of tensorial properties and molecular spectra. In *International Conference on Machine Learning*, pages 9377–9388. PMLR, 2021.
- Ben Shaw, Abram Magner, and Kevin Moon. Symmetry discovery beyond affine transformations. *Advances in Neural Information Processing Systems*, 37:112889–112918, 2024.
- Connor Shorten and Taghi M Khoshgoftaar. A survey on image data augmentation for deep learning. *Journal of big data*, 6(1):1–48, 2019.
- Zakhar Shumaylov, Peter Zaika, James Rowbottom, Ferdia Sherry, Melanie Weber, and Carola-Bibiane Schönlieb. Lie Algebra Canonicalization: Equivariant Neural Operators under arbitrary Lie Groups. In *The Thirteenth International Conference on Learning Representations*, 2025.
- Tess E Smidt, Mario Geiger, and Benjamin Kurt Miller. Finding symmetry breaking order parameters with euclidean neural networks. *Physical Review Research*, 3(1):L012002, 2021.
- Jascha Sohl-Dickstein, Ching Ming Wang, and Bruno A Olshausen. An unsupervised algorithm for learning Lie group transformations. *arXiv preprint arXiv:1001.1027*, 2010.
- Jure Sokolic, Raja Giryes, Guillermo Sapiro, and Miguel Rodrigues. Generalization error of invariant classifiers. In *Artificial Intelligence and Statistics*, pages 1094–1103. PMLR, 2017.
- Joan Sola, Jeremie Deray, and Dinesh Atchuthan. A micro Lie theory for state estimation in robotics. *arXiv preprint arXiv:1812.01537*, 2018.
- Jonas Spinner, Victor Bresó, Pim De Haan, Tilman Plehn, Jesse Thaler, and Johann Brehmer. Lorentz-equivariant geometric algebra transformers for high-energy physics. *Advances in Neural Information Processing Systems*, 37:22178–22205, 2024.
- Behrooz Tahmasebi and Stefanie Jegelka. Sample Complexity Bounds for Estimating Probability Divergences under Invariances. In *International Conference on Machine Learning*, pages 47396–47417. PMLR, 2024.
- Behrooz Tahmasebi and Melanie Weber. Achieving Approximate Symmetry Is Exponentially Easier than Exact Symmetry. In *Topology, Algebra, and Geometry in Data Science*, 2025.

- Behrooz Tahmasebi, Melanie Weber, and Stefanie Jegelka. Data Augmentation: A Fourier analysis perspective. In *NeurIPS 2025 Workshop on Symmetry and Geometry in Neural Representations*, 2025.
- Mingxing Tan and Quoc Le. Efficientnet: Rethinking model scaling for convolutional neural networks. In *International Conference on Machine Learning*, pages 6105–6114. PMLR, 2019.
- Luke Taylor and Geoff Nitschke. Improving deep learning with generic data augmentation. In *2018 IEEE symposium series on computational intelligence (SSCI)*, pages 1542–1547. IEEE, 2018.
- Nathaniel Thomas, Tess Smidt, Steven Kearnes, Lusann Yang, Li Li, Kai Kohlhoff, and Patrick Riley. Tensor field networks: Rotation-and translation-equivariant neural networks for 3D point clouds. *arXiv preprint arXiv:1802.08219*, 2018.
- Antonio Torralba, Phillip Isola, and William T Freeman. *Foundations of computer vision*. MIT Press, 2024.
- Putri van der Linden, Alejandro García-Castellanos, Sharvaree Vadgama, Thijs Kuipers, and Erik Bekkers. Learning symmetries via weight-sharing with doubly stochastic tensors. *Advances in Neural Information Processing Systems*, 37:42738–42764, 2024.
- Tycho van der Ouderaa, David W Romero, and Mark van der Wilk. Relaxing equivariance constraints with non-stationary continuous filters. *Advances in Neural Information Processing Systems*, 35:33818–33830, 2022.
- Tycho van der Ouderaa, Alexander Immer, and Mark van der Wilk. Learning layer-wise equivariances automatically using gradients. *Advances in Neural Information Processing Systems*, 36:28365–28377, 2023.
- Tycho F van der Ouderaa, Mark van der Wilk, and Pim De Haan. Noether’s razor: Learning conserved quantities. *Advances in Neural Information Processing Systems*, 37:135943–135965, 2024.
- Elise Van der Pol, Daniel Worrall, Herke van Hoof, Frans Oliehoek, and Max Welling. Mdp homomorphic networks: Group symmetries in reinforcement learning. *Advances in Neural Information Processing Systems*, 33:4199–4210, 2020.
- Soledad Villar, David W Hogg, Kate Storey-Fisher, Weichi Yao, and Ben Blum-Smith. Scalars are universal: Equivariant machine learning, structured like classical physics. *Advances in Neural Information Processing Systems*, 34:28848–28863, 2021.
- Dian Wang, Jung Yeon Park, Neel Sortur, Lawson LS Wong, Robin Walters, and Robert Platt. The surprising effectiveness of equivariant models in domains with latent symmetry. *arXiv preprint arXiv:2211.09231*, 2022a.
- Rui Wang, Robin Walters, and Rose Yu. Approximately equivariant networks for imperfectly symmetric dynamics. In *International Conference on Machine Learning*, pages 23078–23091. PMLR, 2022b.
- Yipei Wang and Xiaoqian Wang. Self-interpretable model with transformation equivariant interpretation. *Advances in Neural Information Processing Systems*, 34:2359–2372, 2021.
- Maurice Weiler, Fred A Hamprecht, and Martin Storath. Learning steerable filters for rotation equivariant cnns. In *Proceedings of the IEEE Conference on Computer Vision and Pattern Recognition*, pages 849–858, 2018.
- Daniel E Worrall, Stephan J Garbin, Daniyar Turmukhambetov, and Gabriel J Brostow. Harmonic networks: Deep translation and rotation equivariance. In *Proceedings of the IEEE conference on computer vision and pattern recognition*, pages 5028–5037, 2017.
- Michael Wüstner. A connected Lie group equals the square of the exponential image. *Journal of Lie Theory*, 13(1):307–309, 2003.
- Mingle Xu, Sook Yoon, Alvaro Fuentes, and Dong Sun Park. A comprehensive survey of image augmentation techniques for deep learning. *Pattern Recognition*, 137:109347, 2023.
- Jianke Yang, Robin Walters, Nima Dehmamy, and Rose Yu. Generative Adversarial Symmetry Discovery. In *Proceedings of the 40th International Conference on Machine Learning*, pages 39488–39508. PMLR, July 2023.

- Jianke Yang, Nima Dehmamy, Robin Walters, and Rose Yu. Latent Space Symmetry Discovery. In *International Conference on Machine Learning*, pages 56047–56070. PMLR, 2024.
- Ernesto Zacur, Matias Bossa, and Salvador Olmos. Left-invariant riemannian geodesics on spatial transformation groups. *SIAM Journal on Imaging Sciences*, 7(3):1503–1557, 2014.
- Manzil Zaheer, Satwik Kottur, Siamak Ravanbakhsh, Barnabas Poczos, Russ R Salakhutdinov, and Alexander J Smola. Deep Sets. In *Advances in Neural Information Processing Systems*, volume 30. Curran Associates, Inc., 2017.
- Allan Zhou, Tom Knowles, and Chelsea Finn. Meta-learning Symmetries by Reparameterization. In *International Conference on Learning Representations*, 2021.

Appendix

The appendix is organized as follows:

- Appendix A includes notation used throughout the paper, explains our definition of the dimensionality of group generators for both vector and image data, and characterizes the class of symmetry groups that our method can recover.
- Appendix B provides a detailed discussion of prior work related to our approach. We cover equivariant machine learning, data augmentation and learned augmentation, symmetry discovery, and Lie group-based approaches to symmetry discovery.
- Appendix C includes the proofs of the theoretical properties of LieAugmenter presented in Section 5, including the Monte Carlo formulation of the equivariance objective, identifiability of the recovered symmetries, universal approximation properties, and the connection between approximate equivariance and robustness under transformation shifts. In addition, we provide additional theoretical analysis on a Fourier operator view of partial augmentation, the role of the additional regularization terms as a canonicalization principle, the detection of the absence of symmetry, and a convergence analysis.
- Appendix D provides the experimental details of our empirical results in Section 6. We describe additional details of the Lie group parameterization, the hyperparameter settings used across experiments, and the inference procedure. We also define the metrics used to evaluate symmetry discovery and equivariance error, and we summarize the experimental setups for image classification, N -body dynamics prediction, molecular property prediction, and for the experiment analyzing behavior in the absence of symmetry.
- Appendix E presents additional experimental results for LieAugmenter. We explore an alternative simplified inference strategy and show that the method remains robust, demonstrate empirical convergence, and provide an ablation study and hyperparameter analysis showing stability across a wide range of settings. We also evaluate sample efficiency. We also include further results for the N -body dynamics experiments, focusing on symmetry discovery with a less restrictive mask and without a mask. We additionally show strong performance on the more challenging scenario of considering and predicting additional timesteps. We provide a runtime analysis, along with further investigation of the behavior in the absence of symmetry. We also demonstrate that our approach can discover discrete symmetries, including discrete rotations and partial permutations. Finally, we showcase applications across multiple domains, including Lorentz symmetries in quantum field theory amplitude prediction and rotation symmetries in human colorectal cancer images.

A. Extended Background

Notation. For $v \in \mathbb{R}^d$, $\|v\|_1$, $\|v\|_2$, and $\|v\|_\infty$ denote the ℓ_1 , ℓ_2 , and ℓ_∞ norms. For a matrix $A \in \mathbb{R}^{p \times q}$, let $\|A\|_F$ be the Frobenius norm and $\langle A, B \rangle_F = \text{tr}(A^\top B)$ the Frobenius inner product. When using an entry-wise ℓ_1 penalty, we write $\|A\|_1 = \sum_{i,j} |A(i,j)|$. For a continuous function $f : \mathcal{X} \rightarrow \mathbb{R}^d$, we define the infinity norm over a topological space \mathcal{X} by $\|f\|_\infty = \sup_{x \in \mathcal{X}} |f(x)|$. If $\|f - g\|_\infty < \varepsilon$, we say that g uniformly approximates f up to error ε . For a probability distribution Q , $\text{supp}(Q)$ denotes its topological support.

A.1. Generator Dimension for Vector Data and Images

Our symmetry model samples Lie algebra elements of the form $A(w) = \sum_{i=1}^C w_i L_i$ and maps them to group elements via $g = \exp(A(w))$. The dimensionality of the generator matrices L_i is determined by the space in which the transformation is most naturally parameterized. For image data, a common choice is to parameterize transformations in a low-dimensional coordinate space (e.g., rotation, scaling, shear) and then apply the corresponding induced action to the high-dimensional pixel representation [Gonzalez, 2009, Torralba et al., 2024, Jaderberg et al., 2015, Mumuni and Mumuni, 2022]. We use d to denote this *transformation parameterization dimension* and distinguish it from n , the ambient dimension of the input representation $x \in \mathbb{R}^n$. In this setting, the generators satisfy $L_i \in \mathbb{R}^{d \times d}$, while their effect on inputs is realized through an induced representation acting on \mathbb{R}^n . This separation between a low-dimensional Lie algebra parameterization and an induced action on high-dimensional inputs follows common practice in Lie group reparameterization and symmetry discovery for images [Falorsi et al., 2019, Benton et al., 2020, Yang et al., 2023, Moskalev et al., 2022, Ko et al., 2024].

Vector-Valued Data: Generators in the Ambient Representation ($d = n$). For vector-valued inputs $x \in \mathbb{R}^n$, we represent the symmetry action directly in the ambient feature space. In this case, we take $d = n$ and learn generators $L_i \in \mathbb{R}^{n \times n}$. The action on inputs is realized as the standard matrix action on \mathbb{R}^n , yielding augmentations of the form

$$x \mapsto \rho_{\mathcal{X}}(g)x \equiv gx, \quad g = \exp \left[\sum_{i=1}^C w_i L_i \right] \in \mathbb{R}^{n \times n}. \quad (11)$$

This formulation allows the model to learn general linear symmetries acting directly on the feature representation.

Images: Generators in Coordinate Space (Homogeneous $d = 3$). For images, most continuous symmetries act on *pixel coordinates* rather than as arbitrary linear maps on vectorized pixel intensities. We write an image as $x \in \mathbb{R}^{H \times W \times C}$, and for notational convenience as a vector in \mathbb{R}^n with $n = HWC$. Transformations are parameterized in a low-dimensional coordinate space. We parameterize coordinate transformations in homogeneous coordinates with $d = 3$. A pixel coordinate $p = (u, v)^\top \in \mathbb{R}^2$ is embedded as $\tilde{p} = (u, v, 1)^\top \in \mathbb{R}^3$, and the sampled group element $g \in \mathbb{R}^{3 \times 3}$ acts linearly via $\tilde{p}' = g\tilde{p}$. The corresponding coordinate map is denoted $T_g : \mathbb{R}^2 \rightarrow \mathbb{R}^2$, and the induced action on image values is given by the pullback $(\rho_{\mathcal{X}}(g)x)(p) = x(T_g^{-1}(p))$. In practice, this action is implemented using differentiable grid warping and interpolation.³ Learning $L_i \in \mathbb{R}^{3 \times 3}$ corresponds to learning infinitesimal generators of the chosen coordinate transformation family, and $\rho_{\mathcal{X}}(g)$ is realized by warping the image grid according to T_g .

A.2. Recoverable Symmetry Groups

Here, we discuss which symmetry groups can be represented by our Lie-exponential sampler parameterization, which cases are not covered, and how the sampler can be extended to broaden coverage beyond these limitations.

Reachable Set under Single-Exponential Sampling. Let $Q_{L, \gamma}$ denote the distribution over group elements induced by the Lie algebra sampler Eq. (1). Our sampler draws a Lie algebra element $A(w) = \sum_{i=1}^C w_i L_i$ and maps it to a group element via a single matrix exponential $g = \exp(A(w))$. The induced distribution over transformations therefore satisfies $\text{supp}(Q_{L, \gamma}) \subseteq \exp(\text{span}\{L_1, \dots, L_C\})$. Since $t \mapsto \exp(tA)$ is a continuous path with $\exp(0) = \text{Id}$, every sampled g lies in the *identity component* of the Lie subgroup generated by the learned generators. Therefore, if the ground-truth symmetry group is disconnected, sampling a single exponential cannot reach components not containing the identity (e.g., reflection components). It is also important to distinguish the linear span $\text{span}\{L_1, \dots, L_C\}$ from the Lie algebra generated by $\{L_i\}$ under commutators (their Lie closure). Even if a small set of generators generates a full Lie algebra via commutators, single-exponential sampling only explores $\exp(\text{span}\{L_1, \dots, L_C\})$, i.e., exponentials of linear combinations. Thus, full recovery of a connected target group by a single exponential requires that $\text{span}\{L_1, \dots, L_C\}$ spans the target Lie algebra (up to a change of basis) and that the exponential map is surjective on the corresponding connected group.

Examples of Groups that Are Recoverable by a Single Exponential (under Correct Generators).

The conditions for reachable set are satisfied in many practically relevant continuous symmetry families. The following families are standard settings in which \exp is surjective (or even a global diffeomorphism), so the single-exponential sampler can in principle cover the entire connected group if $\text{span}\{L_1, \dots, L_C\}$ spans the appropriate Lie algebra: (i) translation \mathbb{R}^n and other abelian additive groups, (ii) positive scaling $\mathbb{R}_{>0}$ and products $\mathbb{R}_{>0}^k$ (e.g., global or channel-wise intensity scalings), (iii) tori $\mathbb{T}^k \cong \text{SO}(2)^k$ (e.g., phase or angle symmetries), (iv) connected and compact matrix groups, including $\text{SO}(n)$, $\text{U}(n)$, and $\text{SU}(n)$ (for which \exp is surjective) [Kirillov, 2008], (v) rigid motions groups $\text{SE}(n) = \text{SO}(n) \times \mathbb{R}^n$, which is commonly parameterized via exponential coordinates, and (vi) connected, simply connected nilpotent matrix groups (e.g., unipotent upper-triangular groups and the Heisenberg group) admit a global diffeomorphism. These cases cover many continuous augmentation families used in practice, including rotations, translations, rigid motions, and certain continuous photometric transformations [Gross, 1996, Gilmore, 2006, Thomas et al., 2018, Rao and Ruderman, 1998, Finzi et al., 2020, Falorsi et al., 2019, Sola et al., 2018, Kondor and Trivedi, 2018, Sohl-Dickstein et al.,

³For a fixed interpolation scheme, warping is linear in the pixel intensities, so $\rho_{\mathcal{X}}(g)$ can be viewed as a linear operator on \mathbb{R}^n . Due to discretization and resampling effects, this operator need not be exactly invertible for all g in practice. We therefore interpret $\rho_{\mathcal{X}}$ as an idealized representation of the underlying continuous transformation and its induced action on discrete image data.

2010, Cohen and Welling, 2014, Dehmamy et al., 2021, Miao and Rao, 2007, Shorten and Khoshgoftaar, 2019, Taylor and Nitschke, 2018, Kim et al., 2021, Alomar et al., 2023].

What Is Not Recoverable by a Single Exponential. There are two main ways single-exponential sampling can fail to recover a desired symmetry group. First, for disconnected groups, since the ground-truth symmetry group has multiple connected components, then $g = \exp(A(w))$ cannot leave the identity component. Therefore, the sampler cannot represent symmetries such as reflections, flips (and other discrete components), orthogonal group $O(n)$ (two components, $\det = \pm 1$), where the identity component is $SO(n)$, and full Euclidean group $E(n) = O(n) \times \mathbb{R}^n$, whose identity component is $SE(n)$. Second, even when the symmetry group is connected, the exponential map need not be surjective in general (notably for many non-compact Lie groups), so sampling a *single* exponential may not cover all elements of the identity component [Kirillov, 2008, Moskowicz and Sacksteder, 2003]. A standard connected counterexample is $SL(2, \mathbb{R})$, whose exponential image is a strict subset of the group. A further representational limitation is that, even when the target group is exponential, if C is too small or optimization converges to generators whose span $\text{span}\{L_1, \dots, L_C\}$ is a strict subspace of the target Lie algebra, then the single-exponential sampler can only recover a proper subgroup.

While our main experiments use a single-exponential sampler $g = \exp(\sum_i w_i L_i)$, there are standard extensions that broaden the representable symmetry families. First, one can sample a finite product of exponentials:

$$g = \prod_{r=1}^R \exp \left[\sum_{i=1}^C w_i^{(r)} L_i \right], \quad w^{(r)} \sim P(\gamma) \quad (12)$$

which remains differentiable and stays within the identity component [Wüstner, 2003, Kirillov, 2008]. Second, disconnected symmetries can be handled by a discrete mixture over connected components using the decomposition $G = \bigsqcup_{r \in \mathcal{R}} rG_0$, where G_0 is the identity component, \mathcal{R} is a discrete set of representatives for the connected components, and G/G_0 is discrete [Kirillov, 2008]. We leave a systematic study of these extensions to future work, since they introduce additional computational overhead and discrete optimization complexity (learning over components) beyond the scope of this paper.

B. Extended Related Work

The ubiquitous nature of symmetries in nature have led them to continuously be a predominant part of machine learning approaches. In particular, the three main ways in which symmetry is considered are: (i) the enforcement of known symmetries when training a model, (ii) the discovery of unknown symmetries from data and tasks, and (iii) the promotion of symmetries during training for a model that breaks pre-specified symmetries [Otto et al., 2025]. In this extended related work section, we present different examples of such approaches, with a special focus on the ones that are most related to our proposed method in that they discover unknown symmetries and softly promote them during training.

B.1. Equivariant Machine Learning

Many works have explored the design of equivariant models for groups known a priori, such as permutations in sets [Zaheer et al., 2017], translations [Krizhevsky et al., 2012], roto-translations [Fuchs et al., 2020], or local gauge transformations [Cohen et al., 2019]. Related to our proposed parameterization of symmetries is the use of Lie groups for the definition of networks equivariant to known continuous symmetries. For example, MacDonald et al. [2022] proposes a framework for the definition of architectures invariant to any pre-specified finite-dimensional Lie group, which includes previously overlooked warp transformations. The scalability of this approach is however limited by the high memory consumption of their convolutional layers.

Nevertheless, while harnessing symmetries as inductive biases to define equivariant architectures leads to many benefits, their highly constrained design for a priori specified symmetries is a challenging endeavor and limits their flexibility and applicability [Goel et al., 2025]. In particular, the associated architectural design requires the challenging derivation and implementation of group-specific equivariant layers, which precludes their direct application to other settings and domains with potentially different symmetries. This limitation has motivated a line of work that seeks to automatize the design of architectures equivariant to pre-specified symmetry groups, with methods such as EMLP [Finzi et al., 2021] and GCNN [Cohen and Welling, 2016]. Similarly, ASEN [Goel et al., 2025] is designed as an approach that can be simultaneously equivariant to different subgroups of a pre-defined base group by modulating auxiliary input features.

In addition, another limitation of equivariant architectures arises in their application to real-world data, which often deviates from strict mathematical symmetries due to, for instance, noisy or biased measurements

and symmetry-breaking effects [Manolache et al., 2025, Wang et al., 2022b]. In such cases, strictly enforcing equivariance can lead to a degradation of the training dynamics and predictive performance of the models. As a result, approximately equivariant networks emerge as a more fitting alternative for such scenarios, where they are still biased towards preserving the symmetry but are not strictly restricted to do so. Some examples include the constrained optimization approach ACE [Manolache et al., 2025], the relaxed weight-sharing and weight-tying strategy from Wang et al. [2022b], or the graph coarsening method for GNNs described in Huang et al. [2023]. Most related to our method is REMUL [Elhag et al., 2024], which frames learning equivariance as a weighted multi-task problem for unconstrained models.

Besides the introduction of architectural constraints, there are also various model-agnostic methods for realizing equivariant models to a priori known symmetries.

Frame averaging [Puny et al., 2022, Duval et al., 2023, Lin et al., 2024] seeks to achieve equivariance by averaging over a small input-dependent subset of the full group, which is known as a frame. This approach has been widely adopted, e.g., for material modeling [Duval et al., 2023] or antibody generation [Martinkus et al., 2023], but its applicability is restricted by its prohibitive computational cost for many other domains.

Canonicalization [Kaba et al., 2023, Ma et al., 2024], on the other hand, implements equivariance by defining a map from all equivalent inputs under the symmetry group to the same canonical form prior to their processing by the prediction network. In this way, any non-invariant base network can be made to produce invariant predictions in a simpler and more efficient manner. This approach, however, has some limitations, such as potentially resulting in architectures discontinuous with respect to the input [Dym et al., 2024, Lin and Levie, 2025]. Related to our work in its consideration of Lie groups is LieLAC [Shumaylov et al., 2025], which is designed to harness the action of the infinitesimal generators of the symmetry group, avoiding the need for full knowledge of the group structure.

B.2. Data Augmentation and Learned Augmentation

An integral part of our proposal consists of defining a data augmentation process that, rather than relying on predefined transformations, as is predominantly common in the literature [Shorten and Khoshgoftaar, 2019, Mumuni and Mumuni, 2022, Gerken et al., 2022, Quiroga et al., 2020, Xu et al., 2023], has learnable parameters that are trained jointly with the prediction model.

Learnable augmentations have already been explored in the context, for instance, of anomaly detection for time series [Qiu et al., 2021], or self-supervised GNNs [Kefato et al., 2021], showing that they are capable of providing additional flexibility and enhanced performance. However, in these previous works, the learnable augmentations are represented by black-box models, such as Multi-Layer Perceptrons (MLPs), limiting the interpretability of the generated augmentations. In contrast, our approach parameterizes the augmentations using Lie group theory, thus enabling simplified interpretability.

A more interpretable learnable augmentation approach is InstaAug [Miao et al., 2023] which learns an invariance module simultaneously with the end-to-end training of a downstream model. Differently from previous learnable augmentation approaches, that invariance module generates instance-specific augmentations by capturing local invariances. However, this approach relies on a parameterization over a distribution of pre-specified transformations, and so it also does not learn to generate augmentations for a priori fully unknown symmetries.

B.3. Symmetry Discovery and Lie Group-Based Approaches

In addition to LieGAN [Yang et al., 2023] and Augerino [Benton et al., 2020], which are the two models most related to our proposal, many other symmetry discovery methods with different restrictions on the symmetry search space and limitations have been proposed in recent years. The majority of these approaches share the usage of Lie groups for parameterizing the symmetries, which allows for wide applicability to many relevant tasks and also for simplified interpretability. In this section, we analyze some of the most relevant such approaches, which we categorize according to their underlying methodology, and provide a comparison of their main characteristics in Table 4.

B.3.1. Generative Methods

Many symmetry discovery approaches coincide in their modeling of the symmetry discovery process as a *generative method* that seeks to identify the transformations that preserve the data distribution. As previously explained, this type of models place strong and not always realistic assumptions on the uniformity of the

Table 4: Comparison of symmetry discovery approaches and our proposed LieAugmenter method based on their most relevant characteristics. While there are methods that are able to discover a wider class of symmetries, LieAugmenter provides widespread applicability and adaptability to a common and useful set of symmetries, while simultaneously producing approximately equivariant predictions. We group the methods according to their underlying approach and specify for each the type of symmetry generators, whether the discovered symmetry is explicitly represented, whether the approach produces approximately equivariant predictions jointly with the symmetry discovery, whether the model can learn task-dependent symmetries, and whether it has been shown to be applicable to discrete and continuous symmetries.

		Symmetry generators	Explicit	Equiv. predictions	Task-dependent	Discrete	Continuous
Generative	LieFlow [Park et al., 2025]	Pre-specified	×	×	×	✓	✓
	SGM [Allingham et al., 2024]	Pre-specified	×	×	×	✓	✓
	SymmetryGAN [Desai et al., 2022]	Linear	×	×	×	✓	✓
	LieGAN [Yang et al., 2023]	Affine	✓	×	×	✓	✓
	LaLiGAN [Yang et al., 2024]	Non-linear	×	×	×	✓	✓
Probing	LieGG [Moskalev et al., 2022]	Affine	✓	×	×	×	✓
	Shaw et al. [2024]	Vector fields	×	×	×	✓	✓
	LieNLSD [Hu et al., 2025a]	Non-linear	✓	×	×	×	✓
Neural ODEs	Ko et al. [2024]	Vector fields	×	×	✓	×	✓
Architectural	L-conv [Dehmamy et al., 2021]	Vector fields	×	✓	✓	×	✓
	WSCNN [van der Linden et al., 2024]	Regular representations	×	✓	✓	✓	×
Augmentations	Augerino [Benton et al., 2020]	Pre-specified	×	✓	✓	×	✓
	LieAugmenter (<i>Ours</i>)	Affine	✓	✓	✓	✓	✓

action of the group on the data, cannot detect task-specific symmetries, and also require the definition and training of a subsequent prediction network to make use of the discovered symmetries.

As an example, LieFlow [Park et al., 2025] defines symmetry discovery as a flow matching problem from a pre-specified supergroup to the subgroup that matches the true underlying symmetries of the data. This approach is applicable to both continuous and discrete symmetries, however its scalability to real-world datasets is still unexplored, and it displays a “last-minute mode convergence” behavior that limits its ability to discover complex symmetries.

Symmetry-aware Generative Model (SGM) [Allingham et al., 2024] is another approach that defines a generative model to capture approximate symmetries by learning the extent to which a broad pre-specified set of possible symmetries is present in the data. In particular, this method models a distribution over the data distribution by decomposing it into a distribution over prototypes and a distribution over parameters that control the transformations applied to each prototype. This two-step process depends, however, on the identification of a correct and unique prototype per sample, which might not always be possible for real-world data.

SymmetryGAN [Desai et al., 2022] learns symmetry transformations on the dataset distribution using a method based on generative adversarial networks (GANs). In particular, this method defines symmetries in terms of inertial reference densities of the data, in such a way that it requires the generator network to preserve not only the PDF of the input, but also the PDF of the defined inertial density. An important limitation of this approach, however, is that it can only discover one group element per training round and requires additional terms and techniques to extend its applicability to finding subgroups or fully identifying the group.

LaLiGAN [Yang et al., 2024] is an extension of the approach described in LieGAN to non-linear symmetries. This method learns to map the data to a latent space where the symmetry becomes linear through the combination of an autoencoder model and a GAN network trained on the latent embeddings. Just like LieGAN [Yang et al., 2023], this approach shares with our method the inclusion of regularization terms in the loss function to encourage desirable properties for the discovered symmetry. In any case, while this approach is able to learn a wider class of symmetries, it is still restricted to the assumption of compact Lie groups and various restrictive conditions on the orbit space of the group actions. Moreover, the discovered symmetries are explicitly represented only in terms of their linear action on the latent space, but not directly for their effect on the input space.

Therefore, given that our approach already considers a large class of useful and common symmetries and that beyond non-linear symmetries there is still a larger family of symmetries that remains undiscoverable by this type of generative approaches, we believe that the question of greater importance lies in addressing their other common limitations that we previously highlighted. In particular, we view the necessity of training an additional network to make use of the symmetry, the assumptions on the data distribution, and the lack of adaptability to the task as more critical restrictions for the usefulness and applicability of these symmetry

discovery techniques. As a result, those are the factors that we addressed with our proposed method and we leave the exploration of potential extensions to larger classes of symmetries to future work.

B.3.2. Probing Trained Networks

In contrast to approaches that discover symmetries in an unsupervised manner directly from the data, we also find a line of work that studies the problem of identifying symmetries from previously trained unconstrained prediction models [Krippendorf and Syvaeri, 2020, Moskalev et al., 2022, Hu et al., 2025b]. These methods share the limitation that they assume that the prediction network needs to learn to make (approximately) equivariant predictions in order to perform well on the considered task, which might not be necessarily the case in the overparameterized regime and under limited data.

As an example, LieGG [Moskalev et al., 2022] finds a Lie algebra basis of the data symmetries learned by a neural network from the polarization matrix of the discriminator function of the dataset, thus providing straightforward and explicit interpretability of the learned symmetry.

Similarly, Shaw et al. [2024] explores another method for the detection of symmetries from previously defined machine learning functions for the considered dataset. Despite its applicability to continuous symmetries beyond affine transformations, it lacks explicit interpretability into the learned symmetries and, thus, requires their subsequent extraction and analysis.

Recently, some works have also attempted to discover a larger class of symmetries, with special focus on non-linear ones. For instance, LieNLS [Hu et al., 2025a] is designed to determine the number of infinitesimal generators and their explicit representation from a pre-specified function library. In particular, this approach consists of two separate and decoupled stages: training a neural network and then discovering symmetries from it. In addition, its scalability and lack of applicability to discrete symmetries are important limitations.

B.3.3. Neural ODEs

In order to relax the restrictions over the class of symmetries that can be discovered (e.g., pre-specified supergroups, affine transformations, etc.), Ko et al. [2024] introduce an approach based on Neural Ordinary Differential Equations (Neural ODEs) that models one-parameter Lie groups. However, this approach requires to carefully select numerical differentiation and interpolation methods to ensure stability of the training and it comes with an associated high computational cost due to the integration with ODEs. Moreover, it can only be applied to domains with proper validity scores, which are selected based on characteristics of the data and target task. This method also does not directly produce predictions, needing an additional network to apply the discovered symmetries.

B.3.4. Learnable Architectural Constraints

There are also some works that attempt to discover symmetry through *learnable architectural constraints*. The resulting approaches learn to generate equivariant predictions that are potentially more exact than those obtained by data augmentation-based methods, but this comes at the cost of additional computational complexity, less flexible architectures, and a restricted class of discoverable symmetries.

For instance, L-conv [Dehmamy et al., 2021] proposes a building block for group equivariant networks that is based on using localized kernels constructed from a learnable Lie algebra basis. However, this method suffers from high computational complexity due to the computation of exponential maps in every layer of their architecture, and is also not well-suited for dealing with approximate and inexact symmetries.

Similarly, Weight Sharing Convolutional Neural Networks (WSCNNs) [van der Linden et al., 2024] learn a weight-sharing scheme from data in the form of a collection of learnable doubly stochastic matrices, which can implement regular group convolutions for strongly symmetric datasets. The associated computational requirements, however, prevent their application to large groups or high-resolution data, and the need for task-specific regularization also limits their applicability.

In addition, other methods have been proposed with the goal of streamlining the discovery of highly specific families of symmetries. As an example, Karjol et al. [2025] proposes G-Ortho-Nets as an approach for the discovery of orthogonal groups, which preserve a specific quadratic form, and their joint incorporation into equivariant models. While restricted to such a narrow class of symmetries, this method has the advantage of simultaneously learning a prediction network during training in contrast to the previously presented two-step approaches. Similarly, Noether’s razor [van der Ouderaa et al., 2024] parameterizes symmetries as learnable quadratic conserved quantities and discovers them from training data through approximate Bayesian model

selection. This approach requires some post-processing based on the singular value decomposition of the learned generators to identify the discovered symmetries, but also has the advantage of jointly learning a prediction model.

B.3.5. Latent Space Disentanglement

Another line of work explores the related problem of learning a latent space where the embeddings are equivariant to the action of a pre-specified group.

Equivariance by Contrast (EbC) [Schmidt et al., 2025], for instance, applies contrastive learning to train an encoder-only method on a dataset of paired samples $(y, g \cdot y)$, showing that the resulting embeddings present high-fidelity equivariance.

Similarly, there is also a set of related works that correspond to unsupervised representation learning of latent spaces that disentangle the action of a potentially unknown group on the original input space to facilitate the subsequent application of simpler equivariant models that operate on that pretrained latent space [Koyama et al., 2024, Mitchel et al., 2024]. These works, however, are not designed to produce interpretable representations of the possibly unknown group or to directly generate approximately equivariant predictions, and, thus, strongly differ from the problems that our method aims to address.

C. Theoretical Properties of LieAugmenter

We present the theoretical results and proofs for LieAugmenter. To support these proofs, we also provide several additional propositions and lemmas, which are numbered separately for clarity. In addition, we provide an extended theoretical analysis on the ability of when and why the augmenter learns the correct symmetry, including bounds and considerations on the number of augmentations required. We further analyze the role of our regularizers, interpreting them as a form of canonicalization that promotes an interpretable generator. Finally, we present a theoretical justification for detecting the absence of symmetry when no nontrivial symmetry is present in the data.

Population Objectives. The (unknown) continuous symmetry is a connected matrix Lie group G with representations $\rho_X : G \rightarrow \text{GL}(n)$ and $\rho_Y : G \rightarrow \text{GL}(m)$ acting on $\mathcal{X} \subseteq \mathbb{R}^n$ and $\mathcal{Y} \subseteq \mathbb{R}^m$. A function $f : \mathcal{X} \rightarrow \mathcal{Y}$ is called G -equivariant if $f(\rho_X(g)x) = \rho_Y(g)f(x)$, $\forall g \in G, \forall x \in \mathcal{X}$. LieAugmenter learns generators $L = \{L_i \in \mathbb{R}^{n \times n}\}_{i=1}^C$ and a coefficient distribution $P(\gamma)$ on $w \in \mathbb{R}^C$, sampling $g = \exp(\sum_{i=1}^C w_i L_i)$, $w \sim P(\gamma)$, as in Eq. (1). Let $Q_{L,\gamma}$ denote the distribution over group elements induced by the Lie algebra sampler Eq. (1). Define the learned Lie algebra subspace and its generated connected subgroup: $\widehat{\mathfrak{g}}(L) := \text{span}\{L_1, \dots, L_C\}$, $\widehat{G}(L) :=$ the connected subgroup generated by $\widehat{\mathfrak{g}}(L)$. Let $(X, Y) \sim P$. Define $\mathcal{L}_{\text{emp}}^{\text{pop}}(\Psi) := \mathbb{E}[\|Y - \Psi(X)\|_2^2]$, $\mathcal{L}_{\text{equiv}}^{\text{pop}}(\Psi, L, \gamma) := \mathbb{E}[\mathbb{E}_{g \sim Q_{L,\gamma}}[\|\Psi(\rho_X(g)X) - \rho_Y(g)Y\|_1]]$, and $\mathcal{L}_{\text{main}}^{\text{pop}} := \alpha \mathcal{L}_{\text{emp}}^{\text{pop}} + \beta \mathcal{L}_{\text{equiv}}^{\text{pop}}$. We study the population quantities and connect them to the finite- K empirical objective in Eq. (5) and Eq. (9).

C.1. Proof of Lemma 5.1

LieAugmenter constructs K augmentations per sample by drawing $g \sim Q_{L,\gamma}$. Therefore, $\mathcal{L}_{\text{equiv}}$ in Eq. (4) is a Monte Carlo estimate of $\mathcal{L}_{\text{equiv}}^{\text{pop}}$. We formalize the unbiasedness and explain why increasing K stabilizes the symmetry-learning signal in the next lemma.

Lemma 5.1. Fix $(x, y) \in \mathcal{X} \times \mathcal{Y}$ and parameters (Ψ, L, γ) . Let $g_1, \dots, g_K \stackrel{\text{i.i.d.}}{\sim} Q_{L,\gamma}$ and define

$$\widehat{\ell}_{\text{equiv}}(x, y) := \frac{1}{K} \sum_{j=1}^K \|\Psi(\rho_X(g_j)x) - \rho_Y(g_j)y\|_1. \quad (13)$$

Assuming $\mathbb{E}_{g \sim Q_{L,\gamma}}[\|\Psi(\rho_X(g)x) - \rho_Y(g)y\|_1] < \infty$, we have $\mathbb{E}[\widehat{\ell}_{\text{equiv}}(x, y)] = \mathbb{E}_{g \sim Q_{L,\gamma}}[\|\Psi(\rho_X(g)x) - \rho_Y(g)y\|_1]$. Moreover, if $\sigma^2(x, y) := \text{Var}_{g \sim Q_{L,\gamma}}(\|\Psi(\rho_X(g)x) - \rho_Y(g)y\|_1) < \infty$, then $\text{Var}(\widehat{\ell}_{\text{equiv}}(x, y)) = \frac{\sigma^2(x, y)}{K}$.

Proof. Let $Z_j := \|\Psi(\rho_X(g_j)x) - \rho_Y(g_j)y\|_1$. By i.i.d. sampling and linearity of expectation, we have

$$\mathbb{E}[\widehat{\ell}_{\text{equiv}}(x, y)] = \frac{1}{K} \sum_{j=1}^K \mathbb{E}[Z_j] = \mathbb{E}[Z_1] = \mathbb{E}_{g \sim Q_{L,\gamma}}[\|\Psi(\rho_X(g)x) - \rho_Y(g)y\|_1], \quad (14)$$

which gives unbiasedness. For the variance, independence gives

$$\text{Var}(\widehat{\ell}_{\text{equiv}}(x, y)) = \text{Var}\left(\frac{1}{K} \sum_{j=1}^K Z_j\right) = \frac{1}{K^2} \sum_{j=1}^K \text{Var}(Z_j) = \frac{1}{K^2} \cdot K \sigma^2(x, y) = \frac{\sigma^2(x, y)}{K}. \quad (15)$$

□

Remark C.1. Let $\{Z_j := \|\Psi(\rho_X(g_j)x) - \rho_Y(g_j)y\|_1\}_{j=1}^K$ be independent random variables such that $0 \leq Z_j \leq B$ are almost surely, using Hoeffding's inequality yields $\mathbb{P}(|\widehat{\ell}_{\text{equiv}}(x, y) - \mathbb{E}[Z]| \geq \varepsilon) \leq 2 \exp(-2K\varepsilon^2/B^2)$ for every $\varepsilon > 0$.

C.1.1. A Fourier-Operator View of Partial Augmentation

Our equivariance loss draws K sampled group elements per example, which can be viewed as a form of partial data augmentation. That is, instead of averaging over the entire group, we average over a random subset of size K at each training step. This perspective is closely related to recent Fourier analysis results from Tahmasebi et al. [2025]. We briefly summarize the main ideas of their work below and refer to Tahmasebi et al. [2025] for full details.

Let G be a compact group and let $\rho : G \rightarrow U(r)$ be a unitary representation acting on an r -dimensional subspace. Given a distribution μ on G , we define the averaged representation by $D_\mu = \mathbb{E}_{g \sim \mu}[\rho(g)] \in \mathbb{R}^{r \times r}$. Given i.i.d. samples $g_1, \dots, g_K \sim \mu$, we then define the empirical average as $D_K = \frac{1}{K} \sum_{j=1}^K \rho(g_j)$. By the relation between the population operator and empirical operator, we have the following lemma for the concentration of the empirical augmentation operator.

Lemma C.2. Let $g_1, \dots, g_K \sim \mu$ be i.i.d. and let $\rho : G \rightarrow U(r)$ be unitary. Then, for any $\delta \in (0, 1)$, with probability at least $1 - \delta$, we have $\|D_K - D_\mu\|_{\text{op}} \leq C \sqrt{\frac{\log(r/\delta)}{K}}$ for some $C > 0$.

Now, specifically, we consider μ as the Haar measure on G and define the invariant subspace by $V^G := \{v \in \mathbb{R}^r : \rho(g)v = v \ \forall g \in G\}$ with dimension r_{inv} . Then, D_μ is the orthogonal projector onto V^G . Therefore, in an orthonormal basis aligned with $V^G \oplus (V^G)^\perp$, $D_\mu = \text{diag}(I_{r_{\text{inv}}}, 0)$. Let \widetilde{D}_K be the restriction of D_K to the non-invariant subspace in this basis. We have $\|\widetilde{D}_K\|_{\text{op}} = \|D_K - D_\mu\|_{\text{op}} \leq C \sqrt{\frac{\log(r/\delta)}{K}}$ with probability at least $1 - \delta$ for some $C > 0$. Hence, partial augmentation with K random group elements suppresses non-invariant Fourier modes at a rate $\|\widetilde{D}_K\|_{\text{op}}^2 = (\log r/K)$. In settings where the relevant representation space has dimension $r = O(d^k)$ (e.g., spherical harmonics up to degree k on \mathbb{S}^{d-1}), we have $\log r = O(k \log d)$, and hence $\|\widetilde{D}_K\|_{\text{op}}^2 = O(\frac{k \log d}{K})$ with high probability. Thus, the number of augmentations needed to approximate full group-averaging grows only logarithmically with the ambient dimension and polynomially with the effective Fourier degree. The connection to LieAugmenter is as follows. For fixed augmentation generator parameters (L, γ) , LieAugmenter samples K transformation augmentations per example from $Q_{L, \gamma}$ and optimizes a Monte Carlo approximation of a group-averaged equivariance objective. When the augmentation distribution is (approximately) supported on a compact subgroup and the prediction network effectively operates in an r -dimensional representation subspace, the resulting empirical augmentation operator concentrates at rate $\widetilde{O}(1/\sqrt{K})$ (up to $\sqrt{\log r}$ factors) following by the results from Tahmasebi et al. [2025], which further provides a spectral justification for small K in practice. Empirically, we find that a small number of samples per example (e.g., $K = 10$) already yields strong performance (see Section 6 and Appendix E). Appendix E further provides a sensitivity analysis over K , showing that our method is stable across a range of augmentations.

C.2. Proof of Theorem 5.2

We now turn to the symmetry discovery mechanism. Intuitively, if a sampled transformation does not preserve the task labels, then enforcing label-consistency under that transformation creates a systematic discrepancy and increases the population equivariance loss $\mathcal{L}_{\text{equiv}}^{\text{pop}}$. The supervised term fixes the predictor to the ground-truth target, and the equivariance term then selects transformations that act as symmetries of that target. This leads to an identifiability statement for the learned connected subgroup $\widehat{G}(L)$, up to the usual non-uniqueness of a basis for the learned Lie algebra subspace.

Consider without loss of generality the following conditions. We assume $Y = f^*(X)$ almost surely. In addition, suppose $\mathcal{L}_{\text{equiv}}^{\text{pop}}(f^*, L, \gamma) = 0$. We assume the supervised population objective $\mathcal{L}_{\text{emp}}^{\text{pop}}(\Psi)$ has a unique

minimizer f^* over the predictor class. We assume $\text{supp}(P(\gamma))$ contains an open neighborhood of $0 \in \mathbb{R}^C$ so $\text{supp}(Q_{L,\gamma})$ contains a neighborhood of the identity in $\widehat{G}(L)$ generated by $\widehat{\mathfrak{g}}(L) = \text{span}\{L_1, \dots, L_C\}$. When stating conditions for exact recovery, we assume the connected symmetry group of f^* (under the given representations) is exactly G .

Lemma C.3. *Assume $Y = f^*(X)$ almost surely. Suppose $\Psi = f^*$ and $\mathcal{L}_{\text{equiv}}^{\text{POP}}(f^*, L, \gamma) = 0$. Then for every $g \in \text{supp}(Q_{L,\gamma})$,*

$$f^*(\rho_X(g)x) = \rho_Y(g)f^*(x) \quad \text{for } P_X\text{-almost every } x \in \mathcal{X}. \quad (16)$$

Proof. For fixed g , define $\phi(g) := \mathbb{E}_X[\|f^*(\rho_X(g)X) - \rho_Y(g)f^*(X)\|_1]$. The integrand is nonnegative, so $\mathcal{L}_{\text{equiv}}^{\text{POP}}(f^*, L, \gamma) = 0$ implies $\phi(g) = 0$ for $Q_{L,\gamma}$ -almost every g . Now take any $g_0 \in \text{supp}(Q_{L,\gamma})$. If $\phi(g_0) > 0$, then under the standard continuity of the group actions and the norm, ϕ is lower semicontinuous, so there exists a neighborhood U of g_0 such that $\phi(g) > 0$ for all $g \in U$. Since g_0 lies in the support of $Q_{L,\gamma}$, we have $Q_{L,\gamma}(U) > 0$, which contradicts $\phi(g) = 0$ for $Q_{L,\gamma}$ -almost every g . Therefore $\phi(g) = 0$ for all $g \in \text{supp}(Q_{L,\gamma})$, which is equivalent to the stated equivariance identity holding for P_X -almost every x . \square

Lemma C.4. *Let be a connected topological group and let $S \subseteq H$ be a subgroup. If S contains a nonempty open neighborhood of the identity in H , then $S = H$.*

Proof. If $U \subseteq S$ is an open neighborhood of the identity, then for any $s \in S$ the translate sU is open and contained in S , so S is an open subgroup of H . A connected topological group has no proper nontrivial open subgroups, because the (open) cosets would partition H into disjoint open sets. Hence $S = H$. \square

Theorem 5.2. *Assume $Y = f^*(X)$ almost surely and that f^* is the unique minimizer of $\mathcal{L}_{\text{emp}}^{\text{POP}}(\Psi)$ over the predictor class. Assume $\mathcal{L}_{\text{equiv}}^{\text{POP}}(f^*, L) = 0$ and that $P(\gamma)$ has support containing a neighborhood of $0 \in \mathbb{R}^C$, so that $\text{supp}(Q_{L,\gamma})$ contains a neighborhood of the identity element in $\widehat{G}(L)$. Then, for $\alpha > 0$, $\beta > 0$:*

1. $\Psi^* = f^*$ almost surely.
2. Every element of the learned connected subgroup $\widehat{G}(L^*)$ is a symmetry of f^* , i.e., $\widehat{G}(L^*) \subseteq G$.

If in addition the connected symmetry group of f^ is exactly G and $\dim(\widehat{G}(L^*)) = \dim(G)$, then $\widehat{G}(L^*) = G$ and $\widehat{\mathfrak{g}}(L^*) = \mathfrak{g}$ (the true Lie algebra). The generator $\{L_i^*\}$ is identifiable only up to invertible changes of basis spanning the same subspace.*

Proof. We proceed in two steps.

1. The supervised population objective $\mathcal{L}_{\text{emp}}^{\text{POP}}(\Psi)$ is uniquely minimized by f^* . Since $\alpha > 0$ and $\beta > 0$, any global minimizer of $\mathcal{L}_{\text{main}}^{\text{POP}}$ must also minimize the supervised term, which forces $\Psi^*(x) = f^*(x)$ for P_X -almost every x .
2. With $\Psi^* = f^*$ (in the P_X -almost-everywhere sense), consider the choice $L = 0$. This yields only the identity transformation and therefore $\mathcal{L}_{\text{equiv}}^{\text{POP}}(f^*, 0, \gamma) = 0$. Hence any global minimizer must satisfy $\mathcal{L}_{\text{equiv}}^{\text{POP}}(f^*, L^*, \gamma^*) = 0$. Lemma C.3 then implies that every $g \in \text{supp}(Q_{L^*,\gamma^*})$ acts as a symmetry of f^* on the data distribution. Moreover, $\text{supp}(Q_{L^*,\gamma^*})$ contains an open neighborhood of the identity inside $\widehat{G}(L^*)$. Let $S := \{g \in \widehat{G}(L^*) : f^*(\rho_X(g)x) = \rho_Y(g)f^*(x) \text{ for } P_X\text{-almost every } x\}$. The set S is a subgroup of $\widehat{G}(L^*)$, and it contains a neighborhood of the identity. Lemma C.4 gives $S = \widehat{G}(L^*)$, so every element of $\widehat{G}(L^*)$ is a symmetry of f^* , which is exactly $\widehat{G}(L^*) \subseteq G$. If in addition the connected symmetry group of f^* is exactly G and $\dim(\widehat{G}(L^*)) = \dim(G)$, then the inclusion of connected Lie groups with equal dimension implies equality, so $\widehat{G}(L^*) = G$ and $\widehat{\mathfrak{g}}(L^*) = \mathfrak{g}$. The remaining ambiguity is the standard one: any invertible linear recombination of the generators produces a different basis for the same subspace $\widehat{\mathfrak{g}}(L^*)$ and generates the same connected subgroup.

\square

Lemma C.5. Let $B \in \text{GL}(C)$ and define new generators $L'_i := \sum_{j=1}^C B_{ji} L_j$. For any $w \in \mathbb{R}^C$ define $w' := B^{-1}w$. Then $\sum_i w_i L_i = \sum_i w'_i L'_i$ and hence $\exp(\sum_i w_i L_i) = \exp(\sum_i w'_i L'_i)$. Therefore, if the distribution of w' is the pushforward of the distribution of w under B^{-1} , the induced distribution $Q_{L,\gamma}$ over group elements is unchanged.

Proof. By construction, $\sum_i w'_i L'_i = \sum_i w'_i \sum_j B_{ji} L_j = \sum_j (\sum_i B_{ji} w'_i) L_j = \sum_j w_j L_j$ since $w = Bw'$. Applying the matrix exponential, we have $\exp(\sum_i w_i L_i) = \exp(\sum_i w'_i L'_i)$. \square

Theorem 5.2 provides a population-level explanation of why LieAugmenter performs symmetry discovery. The supervised term recovers the target f^* , and the equivariance term then filters the learned transformations so that the connected subgroup generated by $\{L_i^*\}$ is consistent with the true symmetry structure of the task.

C.2.1. Regularizers induce canonicalization and regularized identifiability

Our regularizers in Eq. (9) are designed to break this degeneracy and promote a non-trivial, interpretable basis. We formalize this statement as follows.

Proposition C.6. Let $\mathcal{L}_{\text{main}}^{\text{POP}}(\Psi, L, \gamma) = \alpha \mathcal{L}_{\text{emp}}^{\text{POP}}(\Psi) + \beta \mathcal{L}_{\text{equiv}}^{\text{POP}}(\Psi, L, \gamma)$ with $\alpha, \beta > 0$, and define the canonicalization functional

$$\mathcal{C}(L, \gamma) := \lambda \ell_{\text{areg}}^{\text{POP}}(L, \gamma) + \eta \ell_{\text{bcreg}}(L) + \nu \ell_{\text{bsreg}}(L), \text{ where } \lambda, \eta, \nu \geq 0. \quad (17)$$

Assume $Y = f^*(X)$ almost surely, and that f^* is the unique minimizer of $\mathcal{L}_{\text{emp}}^{\text{POP}}$ over the predictor class. Suppose $\mathcal{L}_{\text{equiv}}^{\text{POP}}(f^*, L) = 0$ without loss of generality. Assume additionally a gauge fixing condition preventing rescaling degeneracies between (L, γ) (e.g., $\|L_i\|_F = 1$ for all i). Let $\mathcal{S} := \arg \min_{\Psi, L, \gamma} (\Psi, L, \gamma)$ denote the set of global minimizers of the main population objective, and define the set of symmetry-consistent symmetry parameters $\mathcal{S}_G := \{(L, \gamma) : (f^*, L, \gamma) \in \mathcal{S}\}$. For $\tau > 0$, consider the canonicalized (regularized) population objective $\mathcal{L}_{\tau}^{\text{POP}}(\Psi, L, \gamma) := \mathcal{L}_{\text{main}}^{\text{POP}}(\Psi, L, \gamma) + \tau \mathcal{C}(L, \gamma)$ and let $(\Psi_{\tau}, L_{\tau}, \gamma_{\tau})$ be any global minimizer of $\mathcal{L}_{\tau}^{\text{POP}}$. Then,

1. Let $C^* := \inf_{(L, \gamma) \in \mathcal{S}_G} \mathcal{C}(L, \gamma)$. Then, $\mathcal{L}_{\text{main}}^{\text{POP}}(\Psi_{\tau}, L_{\tau}, \gamma_{\tau}) \leq \tau C^*$ and $\lim_{\tau \rightarrow 0} \mathcal{L}_{\text{main}}^{\text{POP}}(\Psi_{\tau}, L_{\tau}, \gamma_{\tau}) = 0$.
2. Any accumulation point $(\bar{\Psi}, \bar{L}, \bar{\gamma})$ of $\{(\Psi_{\tau}, L_{\tau}, \gamma_{\tau})\}_{\tau \rightarrow 0}$ belongs to \mathcal{S} . Thus, under the assumptions of Theorem 5.2 for the main objective, such limit points satisfy $\bar{\Psi} = f^*$ almost surely and the learned connected subgroup satisfies $\hat{G}(\bar{L}) \subseteq G^*$.
3. Every accumulation point $(\bar{\Psi}, \bar{L}, \bar{\gamma}) \in \mathcal{S}$ additionally minimizes the canonicalization functional over \mathcal{S}_G , i.e.,

$$(\bar{L}, \bar{\gamma}) \in \arg \min_{(L, \gamma) \in \mathcal{S}_G} \mathcal{C}(L, \gamma). \quad (18)$$

If this minimizer is unique up to a prescribed equivalence (e.g., signed permutation of generators), then $(\bar{L}, \bar{\gamma})$ is identifiable up to that equivalence.

Proof. We proceed in three steps.

1. Let $(L^{\dagger}, \gamma^{\dagger}) \in \mathcal{S}_G$ be such that $\mathcal{C}(L^{\dagger}, \gamma^{\dagger}) \leq C^* + \epsilon$ for some $\epsilon > 0$. Since $(f^*, L^{\dagger}, \gamma^{\dagger}) \in \mathcal{S}$, we have $\mathcal{L}_{\text{main}}^{\text{POP}}(f^*, L^{\dagger}, \gamma^{\dagger}) = 0$, hence $\inf_{\Psi, L, \gamma} \mathcal{L}_{\tau}^{\text{POP}}(\Psi, L, \gamma) \leq \mathcal{L}_{\tau}^{\text{POP}}(f^*, L^{\dagger}, \gamma^{\dagger}) = \tau \mathcal{C}(L^{\dagger}, \gamma^{\dagger}) \leq \tau(C^* + \epsilon)$. By optimality of $(\Psi_{\tau}, L_{\tau}, \gamma_{\tau})$ and nonnegativity of $\mathcal{L}_{\text{main}}^{\text{POP}}$, we have $\mathcal{L}_{\text{main}}^{\text{POP}}(\Psi_{\tau}, L_{\tau}, \gamma_{\tau}) \leq \mathcal{L}_{\tau}^{\text{POP}}(\Psi_{\tau}, L_{\tau}, \gamma_{\tau}) \leq \tau(C^* + \epsilon)$, and letting $\epsilon \rightarrow 0$ yields item (1).
2. Take any sequence $\tau_k \rightarrow 0$ along which $(\Psi_{\tau_k}, L_{\tau_k}, \gamma_{\tau_k}) \rightarrow (\bar{\Psi}, \bar{L}, \bar{\gamma})$, where the existence of accumulation points follows from compactness and coercivity implied by the gauge fixing. Item (1) gives $\mathcal{L}_{\text{main}}^{\text{POP}}(\Psi_{\tau_k}, L_{\tau_k}, \gamma_{\tau_k}) \rightarrow 0$. By continuity of $\mathcal{L}_{\text{main}}^{\text{POP}}$, $\mathcal{L}_{\text{main}}^{\text{POP}}(\bar{\Psi}, \bar{L}, \bar{\gamma}) = 0$, hence $(\bar{\Psi}, \bar{L}, \bar{\gamma}) \in \mathcal{S}$. The stated symmetry-consistent conclusions then follow by Theorem 5.2.

3. Rewrite optimality as $\mathcal{L}_{\text{main}}^{\text{POP}}(\Psi_\tau, L_\tau, \gamma_\tau) + \tau\mathcal{C}(L_\tau, \gamma_\tau) \leq \tau\mathcal{C}(L^\dagger, \gamma^\dagger)$. Divide by τ and use nonnegativity of $\mathcal{L}_{\text{main}}^{\text{POP}}$ to obtain $\mathcal{C}(L_\tau, \gamma_\tau) \leq \mathcal{C}(L^\dagger, \gamma^\dagger)$ for all $(L^\dagger, \gamma^\dagger) \in \mathcal{S}_G$. Letting $\tau \rightarrow 0$ along τ_k and taking limits yields $\mathcal{C}(\bar{L}, \bar{\gamma}) \leq \mathcal{C}(L^\dagger, \gamma^\dagger)$ for all $(L^\dagger, \gamma^\dagger) \in \mathcal{S}_G$, proving the minimization claim. Uniqueness yields identifiability up to the specified equivalence. \square

The main population objective typically admits a *family* of symmetry-consistent solutions in (L, γ) (e.g., corresponding to different subgroups of G and different generator bases), so the symmetry parameters are not uniquely determined by $\mathcal{L}_{\text{main}}^{\text{POP}}$ alone. Proposition C.6 formalizes the role of the regularizers as a *canonicalization principle*: as the regularization strength τ decreases, global minimizers of the canonicalized objective approach main-optimal solutions, while simultaneously selecting a canonical representative within the symmetry-consistent solution set by minimizing $\mathcal{C}(L, \gamma)$. Under a uniqueness condition for this canonical representative (after gauge fixing), the learned generators become identifiable up to the remaining unavoidable equivalences (e.g., signed permutation).

C.2.2. Detecting the Absence of Symmetry

LieAugmenter is designed to discover task symmetries by minimizing an equivariance deviation under learned augmentation. However, in some applications, the target mapping admits no non-trivial continuous symmetry. In this case, a desirable behavior of symmetry discovery methods is that the learned augmentation collapses to the identity, thereby avoiding spurious symmetry discovery. To the best of our knowledge, this no-symmetry regime has not been explicitly investigated in existing Lie-group-based symmetry discovery approaches. In contrast, we explicitly consider this setting and assess whether the learned augmentations remain non-trivial only when supported by the task.

Note that in practical implementations, we include non-triviality regularization (e.g., ℓ_{areg} in Eq. (9)), which discourages identity transformations. We therefore analyze two complementary cases: (i) a setting in which identity collapse is permitted, allowing the augmenter to revert to the identity when no meaningful continuous symmetry is present, and (ii) a setting in which non-triviality is enforced, in which case the augmenter is driven to learn the simplest admissible transformation that still satisfies the regularized objective.

We assume without loss of generality noiseless supervision $Y = f^*(X)$ almost surely. For $g \in G$, the population equivariance violation of the ground-truth map is defined as

$$\Delta(g) = \mathbb{E}[\ell_{\text{task}}(f^*(\rho_X(g)X), \rho_Y(g)f^*(X))] \geq 0, \quad (19)$$

where ℓ_{task} is the supervised loss. We say that f^* has no non-trivial connected symmetry (locally around the identity) if

$$\Delta(g) = 0 \iff g = \text{Id} \quad (20)$$

for all g in a neighborhood of the identity.

Lemma C.7. *Let $\alpha, \beta > 0$ and we assume $Y = f^*(X)$ almost surely. We further assume f^* is the unique minimizer of $\mathcal{L}_{\text{emp}}^{\text{POP}}(\Psi) = \mathbb{E}[\ell_{\text{task}}(\Psi(X), Y)]$ over the prediction network class, and assume the no-symmetry condition Eq. (20). Suppose the sampling family $P(\gamma)$ can realize (or arbitrarily approximate) a point mass at $w = 0$ (hence $g = \text{Id}$). Consider the population main objective (without regularization), $\mathcal{L}_{\text{main}}^{\text{POP}} = \alpha\mathcal{L}_{\text{emp}}^{\text{POP}} + \beta\mathcal{L}_{\text{equiv}}^{\text{POP}}$. Then any global minimizer (Ψ^*, L^*, γ^*) satisfies (i) $\Psi^* = f^*$ almost surely and (ii) Q_{L^*, γ^*} is supported on the identity, i.e., $g = \text{Id}$ almost surely for $g \sim Q_{L^*, \gamma^*}$.*

Proof. By definition,

$$\mathcal{L}_{\text{main}}^{\text{POP}}(\Psi, L, \gamma) = \alpha\mathbb{E}[\ell_{\text{task}}(\Psi(X), Y)] + \beta\mathbb{E}_{g \sim Q_{L, \gamma}}\mathbb{E}[\ell_{\text{task}}(\Psi(\rho_X(g)X), \rho_Y(g)Y)]. \quad (21)$$

Since $Y = f^*(X)$ almost surely and $\alpha > 0$, any global minimizer must minimize $\mathcal{L}_{\text{emp}}^{\text{POP}}$. By uniqueness, $\Psi^* = f^*$ almost surely. Now fix $\Psi = f^*$. The equivariance term becomes

$$\mathcal{L}_{\text{equiv}}^{\text{POP}}(f^*, L, \gamma) = \mathbb{E}_{g \sim Q_{L, \gamma}}[\Delta(g)], \quad (22)$$

where $\Delta(g) \geq 0$ is defined in Eq. (19). Hence, $\mathcal{L}_{\text{equiv}}^{\text{POP}}(f^*, L, \gamma) = 0$ if and only if $\Delta(g) = 0$ holds $Q_{L, \gamma}$ -almost surely. Under Eq. (20), $\Delta(g) = 0$ implies $g = e$ (in a neighborhood of the identity), and since the sampling can realize $w = 0$ (hence $g = \text{Id}$), the minimal attainable value of the equivariance term is 0 and it is achieved only when $Q_{L, \gamma}$ is supported on Id. Because $\beta > 0$, any global minimizer must attain this minimum, so $g = \text{Id}$ almost surely under Q_{L^*, γ^*} . \square

Lemma C.7 provides a “no symmetry” statement that when identity collapse is permitted, the optimal learned augmentations collapse to the identity (vanishing Lie algebra element).

In the full LieAugmenter objective in Eq. (9), the non-triviality regularizer ℓ_{areg} discourages near-identity augmentations. When the task has no symmetry, this creates a trade-off: the equivariance loss prefers identity, while ℓ_{areg} prefers non-trivial transformations. In this setting, the learned augmentation generators canonicalize the solution on the least complex non-identity transformation that balances these competing terms, i.e., the simplest transformation consistent with the regularized objective. In our method, we model enforced non-triviality by constraining the expected Lie algebra energy to be non-zero. Let $A(w) = \sum_{i=1}^C w_i L_i$ and we use the Frobenius-normalization of generators as $L'_i = \frac{\sqrt{D}}{\|L_i\|_F} L_i$. We consider the following constrained problem

$$\min_{L, \gamma} \mathcal{L}_{\text{equiv}}^{\text{POP}}(f^*, L, \gamma) + \nu \sum_{i=1}^C \|L_i\|_1 \quad (23)$$

such that $\mathbb{E}_{w \sim P(\gamma)}[\|A(w)\|_F^2] = \sigma^2$ for some fixed $\sigma > 0$ and $\nu > 0$, where $\|\cdot\|_1$ is the entrywise ℓ_1 norm. The phenomenon of random single-entry generators is most pronounced when the task provides no strong directional preference. We capture this via a local isotropy condition around identity: there exist $\kappa > 0$ and $r_0 > 0$ such that, for all A with $\|A\|_F \leq r_0$,

$$\Delta(\exp(A)) = \kappa \|A\|_F^2. \quad (24)$$

Equivalently, the second-order sensitivity of the equivariance violation at identity is proportional to the identity operator in the chosen basis.

Lemma C.8. *For any matrix M , $\|M\|_1 \geq \|M\|_F$, with equality if and only if M has at most one non-zero entry.*

Proposition C.9. *Assume the no-symmetry condition Eq. (20) and the local isotropy condition Eq. (24). Assume the generator parametrization enforces $\|L_i\|_F = 1$ for any active generator, while unused generators can be set to 0. Assume $\sigma > 0$ is small enough that $\|A(w)\|_F \leq r_0$ almost surely under $w \sim P(\gamma)$ at optimality. Then there exists an optimal solution (L^*, γ^*) of Eq. (23) with: (i) there is an index i^* such that w_{i^*} is non-degenerate and $w_j = 0$ almost surely for all $j \neq i^*$, (ii) L_{i^*} has exactly one non-zero entry (up to sign), i.e., $L_{i^*} = \pm E_{pq}$ for some canonical basis matrix E_{pq} , and consequently, (iii) $A(w) = w_{i^*} L_{i^*}$ injects randomness into a single matrix entry.*

Proof. Under Eq. (24) and the assumption $\|A(w)\|_F \leq r_0$ almost surely,

$$\mathcal{L}_{\text{equiv}}^{\text{POP}}(f^*, L, \gamma) = \mathbb{E}_{w \sim P(\gamma)}[\Delta(\exp(A(w)))] = \kappa \mathbb{E}_{w \sim P(\gamma)}[\|A(w)\|_F^2]. \quad (25)$$

By the constraint in Eq. (23), this equals $\kappa \sigma^2$ for all feasible (L, γ) . Therefore, the optimization reduces to minimizing the regularizer $\nu \sum_i \|L_i\|_1$ over feasible solutions.

Let M be the number of active generators (i.e., those used with non-zero coefficient variance). For each active generator, $\|L_i\|_F = 1$ and Lemma C.8 gives $\|L_i\|_1 \geq 1$. Therefore, $\sum_{i=1}^C \|L_i\|_1 \geq M$. This lower bound is achieved by choosing exactly one active generator L_{i^*} and making it one-sparse, i.e., $L_{i^*} = \pm E_{pq}$, which satisfies $\|L_{i^*}\|_F = 1$ and $\|L_{i^*}\|_1 = 1$. Feasibility of the energy constraint is achieved by setting all coefficients except w_{i^*} to zero almost surely and choosing $P(\gamma^*)$ such that $\mathbb{E}[w_{i^*}^2] = \sigma^2$, then $\mathbb{E}\|A(w)\|_F^2 = \mathbb{E}[w_{i^*}^2] \|L_{i^*}\|_F^2 = \sigma^2$. Thus there exists a feasible solution attaining the minimal regularizer value, and it is optimal. \square

Proposition C.9 characterizes an optimal structure, i.e., single-entry concentration, but it also implies a large set of equivalent optima.

Corollary C.10. *Under the assumptions of Proposition C.9, any choice of (p, q) and sign \pm yields an optimal one-sparse generator $L_{i^*} = \pm E_{pq}$ (with an appropriate $P(\gamma)$ satisfying $\mathbb{E}[w_{i^*}^2] = \sigma^2$). Hence the set of global optima contains at least $2d^2$ distinct single-entry solutions, and the location (p, q) is not identifiable.*

Proof. All canonical basis matrices satisfy $\|E_{pq}\|_F = 1$ and $\|E_{pq}\|_1 = 1$. By Proposition C.9, the objective value is $\kappa \sigma^2 + \nu$ for any such choice, and does not depend on (p, q) or sign. \square

Corollary C.10 explains the empirical observation in Section 6.4. In no-symmetry tasks with enforced non-triviality, the learned generator norm concentrates on a single entry whose location changes across random seeds. Different runs can converge to different (equally optimal) single-entry solutions. In contrast, when a true continuous symmetry exists, the learned generators exhibit stable, structured patterns across seeds, reflecting identifiable directions preferred by the equivariance objective.

C.3. Proof of Proposition 5.3

We now examine whether adding the equivariance term restricts the expressive power of the predictor class. We work under the following conditions. We assume the input domain $\mathcal{X} \subset \mathbb{R}^n$ is compact and closed under the input action, i.e., $\rho_{\mathcal{X}}(g)\mathcal{X} \subseteq \mathcal{X}$ for all g in the support of $Q_{L,\gamma}$. We assume the target function $f^* : \mathcal{X} \rightarrow \mathcal{Y}$ is continuous and G -equivariant $\forall g \in \text{supp}(Q_{L,\gamma})$. For approximation, we assume the hypothesis class used for Ψ is dense in $C(\mathcal{X}, \mathcal{Y})$ under the uniform norm. For example, standard multilayer perceptrons Ψ satisfy universal approximation results on compact domains under standard activation assumptions [Hornik et al., 1989, Cybenko, 1989, Leshno et al., 1993]. When relating approximation error to self-consistency, we additionally assume the output action is uniformly bounded over the support of the learned augmentation distribution,

$$M_Y(L, \gamma) := \sup_{g \in \text{supp}(Q_{L,\gamma})} \|\rho_{\mathcal{Y}}(g)\|_{\text{op}} < \infty. \quad (26)$$

Finally, we assume symmetry-consistent sampling $\text{supp}(Q_{L,\gamma}) \subseteq G$.

We first state that uniform approximation of an equivariant target immediately controls the population *label-consistency* equivariance loss.

Lemma C.11. *Assume \mathcal{X} is compact and $\rho_{\mathcal{X}}(g)\mathcal{X} \subseteq \mathcal{X}$ for all $g \in \text{supp}(Q_{L,\gamma})$ and all $x \in \mathcal{X}$. Suppose the target function $f^* : \mathcal{X} \rightarrow \mathcal{Y}$ is continuous and equivariant $\forall g \in \text{supp}(Q_{L,\gamma})$. Assume a model $Y = f^*(X)$ almost surely. If Ψ satisfies $\sup_{x \in \mathcal{X}} |\Psi(x) - f^*(x)| < \varepsilon$, then*

$$\mathcal{L}_{\text{equiv}}^{\text{POP}}(\Psi, L, \gamma) < \varepsilon. \quad (27)$$

Proof. Fix $g \in \text{supp}(Q_{L,\gamma}) \subseteq G$ and $x \in \mathcal{X}$. Using realizability and equivariance of f^* ,

$$\begin{aligned} \|\Psi(\rho_{\mathcal{X}}(g)x) - \rho_{\mathcal{Y}}(g)f^*(x)\|_1 &\leq \|\Psi(\rho_{\mathcal{X}}(g)x) - f^*(\rho_{\mathcal{X}}(g)x)\|_1 + \|f^*(\rho_{\mathcal{X}}(g)x) - \rho_{\mathcal{Y}}(g)f^*(x)\|_1 \\ &= \|\Psi(\rho_{\mathcal{X}}(g)x) - f^*(\rho_{\mathcal{X}}(g)x)\|_1 < \varepsilon, \end{aligned}$$

where the last inequality uses $\rho_{\mathcal{X}}(g)x \in \mathcal{X}$. Taking expectations over (X, Y) and $g \sim Q_{L,\gamma}$ yields the claim. \square

Next, we show that the same approximation guarantee also controls a population *self-consistency* discrepancy, provided the output action is uniformly bounded on the sampled transformations.

Lemma C.12. *Assume \mathcal{X} is compact and $\rho_{\mathcal{X}}(g)\mathcal{X} \subseteq \mathcal{X}$ for all $g \in \text{supp}(Q_{L,\gamma})$ and all $x \in \mathcal{X}$. Suppose the target function $f^* : \mathcal{X} \rightarrow \mathcal{Y}$ is continuous and equivariant $\forall g \in \text{supp}(Q_{L,\gamma})$. Suppose the output action is uniformly bounded over sampled transforms: $M_Y(L, \gamma) := \sup_{g \in \text{supp}(Q_{L,\gamma})} \|\rho_{\mathcal{Y}}(g)\|_{\text{op}} < \infty$. Let Ψ satisfy $\sup_{x \in \mathcal{X}} |\Psi(x) - f^*(x)| < \varepsilon$. Define the population self-consistency discrepancy*

$$\mathcal{E}_{\text{self}}^{\text{POP}}(\Psi, L, \gamma) := \mathbb{E}[\mathbb{E}_{g \sim Q_{L,\gamma}}[\|\Psi(\rho_{\mathcal{X}}(g)X) - \rho_{\mathcal{Y}}(g)\Psi(X)\|_1]]. \quad (28)$$

Then, $\mathcal{E}_{\text{self}}^{\text{POP}}(\Psi, L, \gamma) \leq (1 + M_Y(L, \gamma))\varepsilon$.

Proof. Fix $g \in \text{supp}(Q_{L,\gamma}) \subseteq G$ and $x \in \mathcal{X}$. Add and subtract the equivariant target:

$$\begin{aligned} \|\Psi(\rho_{\mathcal{X}}(g)x) - \rho_{\mathcal{Y}}(g)\Psi(x)\|_1 &\leq \|\Psi(\rho_{\mathcal{X}}(g)x) - f^*(\rho_{\mathcal{X}}(g)x)\|_1 \\ &\quad + \|f^*(\rho_{\mathcal{X}}(g)x) - \rho_{\mathcal{Y}}(g)f^*(x)\|_1 \\ &\quad + \|\rho_{\mathcal{Y}}(g)(f^*(x) - \Psi(x))\|_1. \end{aligned}$$

The first term is at most ε since $\rho_{\mathcal{X}}(g)x \in \mathcal{X}$. The middle term is 0 by equivariance of f^* . The last term is bounded by $\|\rho_{\mathcal{Y}}(g)(f^*(x) - \Psi(x))\|_1 \leq \|\rho_{\mathcal{Y}}(g)\|_{\text{op}} \|f^*(x) - \Psi(x)\|_1 \leq M_Y(L, \gamma)\varepsilon$. Taking expectations over X and g yields the result. \square

We now combine the universal approximation property with the results above to obtain a direct implication: if the ground-truth target is equivariant, then symmetry-agnostic predictors can approximate it arbitrarily well, and therefore can achieve arbitrarily small label-consistency equivariance loss under symmetry-consistent transformations.

Proposition 5.3. *Assume \mathcal{X} is compact and $\rho_{\mathcal{X}}(g)\mathcal{X} \subseteq \mathcal{X}$ for all $g \in \text{supp}(Q_{L,\gamma})$ and all $x \in \mathcal{X}$. Assume a model $Y = f^*(X)$ where f^* is continuous and equivariant $\forall g \in \text{supp}(Q_{L,\gamma})$. Then for any $\varepsilon > 0$ there exists a (symmetry-agnostic) predictor Ψ in the hypothesis class such that*

$$\sup_{x \in \mathcal{X}} |\Psi(x) - f^*(x)| < \varepsilon \text{ and } \mathcal{L}_{\text{equiv}}^{\text{POP}}(\Psi, L, \gamma) < \varepsilon. \quad (29)$$

If further $M_Y(L, \gamma) := \sup_{g \in \text{supp}(Q_{L,\gamma})} \|\rho_Y(g)\|_{\text{op}} < \infty$, then $\mathcal{E}_{\text{self}}^{\text{POP}}(\Psi, L, \gamma) \leq (1 + M_Y(L, \gamma))\varepsilon$.

Proof. By universal approximation theorem [Hornik et al., 1989, Cybenko, 1989, Leshno et al., 1993], for any $\varepsilon > 0$ there exists a network Ψ in the hypothesis class such that $\sup_{x \in \mathcal{X}} |\Psi(x) - f^*(x)| < \varepsilon$. The remaining claims follow from Lemmas C.11 and C.12. \square

We show that if the target is equivariant, then symmetry-agnostic predictors can approximate it arbitrarily well, and consequently can achieve arbitrarily small *label-consistency* equivariance loss under symmetry-consistent transformations.

Remark C.13. *It is a standard technique to assume that $\mathcal{X} \subset \mathbb{R}^n$ is compact and $\rho_{\mathcal{X}}(g)\mathcal{X} \subseteq \mathcal{X}$, since it is used to i) cite uniform approximation on compact domains and (ii) make sure that transformed inputs remain within the domain on which Ψ is approximating. In the proof above, this assumption is used only to guarantee that $\rho_{\mathcal{X}}(g)x \in \mathcal{X}$ whenever $x \in \mathcal{X}$ and g is a transformation against which the equivariance deviation is evaluated.*

It is important to note that LieAugmenter does not require invariance for all $g \in G$ in practice. It only promotes consistency for transformations sampled via Eq. (1), i.e., $g \sim Q_{L,\gamma}$. Accordingly, the closure condition can be weakened to $\rho_{\mathcal{X}}(g)\mathcal{X} \subseteq \mathcal{X}$ for all $g \in \text{supp}(Q_{L,\gamma})$, or, equivalently, to invariance over a compact subset $G_0 \subseteq G$ on which $Q_{L,\gamma}$ concentrates (e.g., induced by restricting the coefficient samples $w \sim P(\gamma)$ to a bounded range).

C.4. Proof of Proposition 5.4

We now connect the approximate equivariance to out-of-distribution (OOD) generalization under transformation shift. Here the test distribution is obtained by applying a group element to both inputs and labels. Under such shifts, the key quantity that governs robustness is a self-consistency discrepancy of the predictor, $\|\Psi(\rho_{\mathcal{X}}(g)X) - \rho_Y(g)\Psi(X)\|_1$, which measures whether applying the transformation before or after prediction leads to consistent outputs. Since LieAugmenter directly optimizes the *label-consistency* term in $\mathcal{L}_{\text{equiv}}^{\text{POP}}$, we first relate these two discrepancies.

Let $(X, Y) \sim P$ be the training distribution. For $g \in G$, define the shifted distribution $P^{(g)}$ by $(X', Y') = (\rho_{\mathcal{X}}(g)X, \rho_Y(g)Y)$. Let $\ell : \mathcal{Y} \times \mathcal{Y} \rightarrow \mathbb{R}_+$ be the task loss and define the risk $\mathcal{R}_P(\Psi) := \mathbb{E}_{(X,Y) \sim P}[\ell(\Psi(X), Y)]$.

Lemma C.14. *Suppose $M_Y(L, \gamma) := \sup_{g \in \text{supp}(Q_{L,\gamma})} \|\rho_Y(g)\|_{\text{op}} < \infty$. Then the self-consistency discrepancy in*

Eq. (28) satisfies

$$\mathcal{E}_{\text{self}}^{\text{POP}}(\Psi, L, \gamma) \leq \mathcal{L}_{\text{equiv}}^{\text{POP}}(\Psi, L, \gamma) + M_Y(L, \gamma) \mathbb{E}[\|Y - \Psi(X)\|_1]. \quad (30)$$

Proof. For any g and any (X, Y) , by the triangle inequality, we have

$$\begin{aligned} \|\Psi(\rho_{\mathcal{X}}(g)X) - \rho_Y(g)\Psi(X)\|_1 &\leq \|\Psi(\rho_{\mathcal{X}}(g)X) - \rho_Y(g)Y\|_1 + \|\rho_Y(g)(Y - \Psi(X))\|_1 \\ &\leq \|\Psi(\rho_{\mathcal{X}}(g)X) - \rho_Y(g)Y\|_1 + \|\rho_Y(g)\|_{\text{op}}\|Y - \Psi(X)\|_1. \end{aligned}$$

Taking expectations over $(X, Y) \sim P$ and $g \sim Q_{L,\gamma}$, and using $\|\rho_Y(g)\|_{\text{op}} \leq M_Y(L, \gamma)$ on the support of $Q_{L,\gamma}$, we have $\mathcal{E}_{\text{self}}^{\text{POP}}(\Psi, L, \gamma) \leq \mathcal{L}_{\text{equiv}}^{\text{POP}}(\Psi, L, \gamma) + M_Y(L, \gamma) \mathbb{E}[\|Y - \Psi(X)\|_1]$. \square

Remark C.15. *If $\mathcal{Y} \subseteq \mathbb{R}^m$, the norm equivalence and Cauchy-Schwarz inequality imply $\mathbb{E}\|Y - \Psi(X)\|_1 \leq \sqrt{m}(\mathbb{E}\|Y - \Psi(X)\|_2^2)^{1/2} = \sqrt{m}(\mathcal{L}_{\text{emp}}^{\text{POP}}(\Psi))^{1/2}$. This shows that small supervised population loss controls the ℓ_1 prediction error term in Lemma C.14.*

We now state a risk bound under the transformation shift. The assumptions on the task loss ℓ are standard: we require invariance under the label action and Lipschitz continuity in the prediction argument.

Proposition 5.4. Assume that the task loss ℓ satisfies: (i) $\ell(\rho_{\mathcal{Y}}(g)a, \rho_{\mathcal{Y}}(g)b) = \ell(a, b) \forall a, b \in \mathcal{Y}, g \in G$, and (ii) there exists $L_\ell > 0$ s.t. $|\ell(u, y) - \ell(v, y)| \leq L_\ell \|u - v\|_1 \forall u, v, y \in \mathcal{Y}$. Then for any network Ψ and any $g \in G$,

$$\mathcal{R}_{P^{(g)}}(\Psi) \leq \mathcal{R}_P(\Psi) + L_\ell \mathbb{E}[\|\Psi(\rho_{\mathcal{X}}(g)X) - \rho_{\mathcal{Y}}(g)\Psi(X)\|_1]. \quad (31)$$

In addition, if Ψ is exactly G -equivariant, then $\mathcal{R}_{P^{(g)}}(\Psi) = \mathcal{R}_P(\Psi)$.

Proof. By the definition of $P^{(g)}$, we have $\mathcal{R}_{P^{(g)}}(\Psi) = \mathbb{E}_{(X, Y) \sim P}[\ell(\Psi(\rho_{\mathcal{X}}(g)X), \rho_{\mathcal{Y}}(g)Y)]$. Add and subtract $\rho_{\mathcal{Y}}(g)\Psi(X)$ in the first argument and apply Lipschitzness, we obtain

$$\ell(\Psi(\rho_{\mathcal{X}}(g)X), \rho_{\mathcal{Y}}(g)Y) \leq \ell(\rho_{\mathcal{Y}}(g)\Psi(X), \rho_{\mathcal{Y}}(g)Y) + L_\ell \|\Psi(\rho_{\mathcal{X}}(g)X) - \rho_{\mathcal{Y}}(g)\Psi(X)\|_1. \quad (32)$$

By label-action invariance, we have $\ell(\rho_{\mathcal{Y}}(g)\Psi(X), \rho_{\mathcal{Y}}(g)Y) = \ell(\Psi(X), Y)$. Taking expectations over $(X, Y) \sim P$ gives $\mathcal{R}_{P^{(g)}}(\Psi) \leq \mathcal{R}_P(\Psi) + L_\ell \mathbb{E}[\|\Psi(\rho_{\mathcal{X}}(g)X) - \rho_{\mathcal{Y}}(g)\Psi(X)\|_1]$. \square

Lemma C.14 and Proposition 5.4 link the training objectives to robustness under transformation shift. Proposition 5.4 shows that the excess risk under $P^{(g)}$ is controlled by a self-consistency term at g , and Lemma C.14 bounds the corresponding population self-consistency discrepancy using the label-consistency equivariance loss and the supervised prediction error. In addition, averaging Proposition 5.4 over $g \sim Q_{L, \gamma}$ yields

$$\mathbb{E}_{g \sim Q_{L, \gamma}}[\mathcal{R}_{P^{(g)}}(\Psi)] \leq \mathcal{R}_P(\Psi) + L_\ell \mathcal{E}_{\text{self}}^{\text{POP}}(\Psi, L, \gamma), \quad (33)$$

and substituting Eq. (30) provides an explicit bound in terms of the two quantities optimized by LieAugmenter.

C.5. Convergence Analysis

We now provide a standard convergence guarantee for stochastic gradient methods [Kingma, 2014] applied to the reparameterized objective. Since our objective contains non-smooth components (e.g., $\|\cdot\|_1$ and absolute values in the regularizers), we state the result for a differentiable surrogate $\mathcal{L}_{\text{total}}^{(\tau)}$ obtained by replacing $|z|$ with a smooth approximation such as $|z|_\tau := \sqrt{z^2 + \tau^2}$ and $\|v\|_1$ with $\|v\|_{1, \tau} := \sum_k |v_k|_\tau$ for $\tau > 0$. This yields a differentiable objective with the same minimizers in the limit $\tau \rightarrow 0$ under mild conditions.

Let $\theta := (\theta_\Psi, L, \gamma)$ denote all trainable parameters. For a fixed dataset $\mathcal{D} = \{(x_i, y_i)\}_{i=1}^N$, the expected (smoothed) training objective is defined by

$$F_\tau(\theta) = \mathbb{E}_{i \sim \text{Unif}([N])} \mathbb{E}_\varepsilon[\ell_\tau(\theta; i, \varepsilon)], \quad (34)$$

where ε is base noise for the reparameterization, $w = r(\varepsilon; \gamma)$, and $g(\varepsilon; L, \gamma) = \exp(\sum_{c=1}^C w_c L_c)$. The per-sample loss ℓ_τ corresponds to one datapoint and one sampled group element (or one sampled set of K elements).

Lemma C.16. Assume $\ell_\tau(\theta; i, \varepsilon)$ is differentiable in θ and that ∇_θ can be interchanged with \mathbb{E}_ε in Eq. (34). Let $\hat{g}(\theta)$ denote the gradient estimator obtained by sampling a minibatch \mathcal{B} of size B and K independent noises $\varepsilon_{i,1}, \dots, \varepsilon_{i,K}$ per $i \in \mathcal{B}$

$$\hat{g}(\theta) = \frac{1}{B} \sum_{i \in \mathcal{B}} \frac{1}{K} \sum_{k=1}^K \nabla_\theta \ell_\tau(\theta; i, \varepsilon_{i,k}). \quad (35)$$

Then $\mathbb{E}[\hat{g}(\theta)] = \nabla F_\tau(\theta)$, where the expectation is over the minibatch sampling and reparameterization noise.

Proof. By linearity of expectation and the interchange assumption, $\nabla F_\tau(\theta) = \mathbb{E}_i \mathbb{E}_\varepsilon[\nabla_\theta \ell_\tau(\theta; i, \varepsilon)]$. Since \mathcal{B} is sampled uniformly and $\varepsilon_{i,k}$ are i.i.d., $\mathbb{E}[\hat{g}(\theta)] = \mathbb{E}_i \mathbb{E}_\varepsilon[\nabla_\theta \ell_\tau(\theta; i, \varepsilon)] = \nabla F_\tau(\theta)$. \square

Lemma C.17. Assume there exists $\sigma^2 < \infty$ such that for all θ ,

$$\mathbb{E}_{i, \varepsilon}[\|\nabla_\theta \ell_\tau(\theta; i, \varepsilon) - \nabla F_\tau(\theta)\|_2^2] \leq \sigma^2. \quad (36)$$

Then the estimator $\hat{g}(\theta)$ in Lemma C.16 satisfies $\mathbb{E}[\|\hat{g}(\theta) - \nabla F_\tau(\theta)\|_2^2] \leq \frac{\sigma^2}{BK}$.

Proof. $\hat{g}(\theta)$ is the average of BK independent, mean-zero noise terms $\nabla_\theta \ell_\tau(\theta; i, \varepsilon) - \nabla F_\tau(\theta)$ (conditionally on θ). Thus, the variance of an average of independent terms scales inversely with the number of terms. \square

Proposition C.18. Assume F_τ is lower bounded by F_{inf} and has L -Lipschitz gradient: $\|\nabla F_\tau(u) - \nabla F_\tau(v)\|_2 \leq L\|u - v\|_2$ for all u, v . Run SGD with constant step size $\eta \leq 1/L$: $\theta_{t+1} = \theta_t - \eta \hat{g}(\theta_t)$, where $\hat{g}(\theta_t)$ is the unbiased estimator in Lemma C.16 with variance controlled as in Lemma C.17. Then for any $T \geq 1$,

$$\frac{1}{T} \sum_{t=0}^{T-1} \mathbb{E}[\|\nabla F_\tau(\theta_t)\|_2^2] \leq \frac{2(F_\tau(\theta_0) - F_{\text{inf}})}{\eta T} + \eta \frac{L\sigma^2}{BK}. \quad (37)$$

Specifically, choosing $\eta = \min\{1/L, \sqrt{2BK(F_\tau(\theta_0) - F_{\text{inf}})/(L\sigma^2 T)}\}$ gives $\min_{0 \leq t < T} \mathbb{E}[\|\nabla F_\tau(\theta_t)\|_2^2] = O\left(\sqrt{\frac{1}{BK T}}\right)$.

Proof. By L -smoothness, for any t , we have $F_\tau(\theta_{t+1}) \leq F_\tau(\theta_t) + \langle \nabla F_\tau(\theta_t), \theta_{t+1} - \theta_t \rangle + \frac{L}{2} \|\theta_{t+1} - \theta_t\|_2^2$. By substituting $\theta_{t+1} - \theta_t = -\eta \hat{g}(\theta_t)$, we have $F_\tau(\theta_{t+1}) \leq F_\tau(\theta_t) - \eta \langle \nabla F_\tau(\theta_t), \hat{g}(\theta_t) \rangle + \frac{L\eta^2}{2} \|\hat{g}(\theta_t)\|_2^2$. Now, we take the expectation conditional on θ_t and use unbiasedness $\mathbb{E}[\hat{g}(\theta_t) \mid \theta_t] = \nabla F_\tau(\theta_t)$ to have $\mathbb{E}[F_\tau(\theta_{t+1}) \mid \theta_t] \leq F_\tau(\theta_t) - \eta \|\nabla F_\tau(\theta_t)\|_2^2 + \frac{L\eta^2}{2} \mathbb{E}[\|\hat{g}(\theta_t)\|_2^2 \mid \theta_t]$. By decomposition $\mathbb{E}[\|\hat{g}\|_2^2] = \|\nabla F_\tau(\theta_t)\|_2^2 + \mathbb{E}\|\hat{g} - \nabla F_\tau(\theta_t)\|_2^2$ and applying Lemma C.17, we have $\mathbb{E}[F_\tau(\theta_{t+1}) \mid \theta_t] \leq F_\tau(\theta_t) - \eta(1 - \frac{L\eta}{2})\|\nabla F_\tau(\theta_t)\|_2^2 + \frac{L\eta^2}{2} \cdot \frac{\sigma^2}{BK}$. Since $\eta \leq 1/L$, we have $1 - \frac{L\eta}{2} \geq \frac{1}{2}$. By taking the total expectation and summing over $t = 0, \dots, T-1$, it gives $\mathbb{E}[F_\tau(\theta_T)] \leq F_\tau(\theta_0) - \frac{\eta}{2} \sum_{t=0}^{T-1} \mathbb{E}\|\nabla F_\tau(\theta_t)\|_2^2 + \frac{L\eta^2 T}{2} \cdot \frac{\sigma^2}{BK}$. \square

Proposition C.18 shows that the stochastic optimization of the (smoothed) LieAugmenter objective converges to an approximate stationary point. The gradient variance decreases as $1/(BK)$ (Lemma C.17), so using more augmentations per sample reduces optimization noise in the same way as increasing the minibatch size, at the expected computational cost per iteration. Empirically, we corroborate this convergence behavior in Appendix E.2.

D. Experimental Details

In this section, we provide additional experimental details and setup supporting the empirical results in Section 6.

We utilized different GPUs for each of our experiments in order to adapt to the demands that their increasing complexity imposed. Specifically, the synthetic dataset without continuous symmetries was run on an NVIDIA GeForce GTX 1060 Mobile GPU, the RotatedMNIST and N -body dynamics experiments were run on an NVIDIA A100, and the QM9 experiment was run on an NVIDIA H100.

All experiments were implemented using PyTorch and executed using CUDA version 12.2.

D.1. Sampling Strategy and Lie Algebra Basis Initialization

While the parameter γ for the sampling distribution $P(\gamma)$ could in principle be learned, in our experiments we adopt a simplified setting with fixed γ and uniform sampling $P(\gamma) = \mathcal{U}[-\gamma, \gamma]$, aiming to avoid any unwanted bias towards sampling a specific subset of group elements. Even under this simplification, we observe that our method already yields strong empirical performance (see Section 6 and Appendix E). In addition, we conduct a sensitivity analysis of γ in Appendix E.3, demonstrating that our method remains largely robust to changes in the specified value. Finally, note that our framework can seamlessly support alternative sampling distributions, which is useful in settings such as discrete symmetry discovery (Appendix E.8). Extending the framework to a learnable γ is a natural next step, and we leave it to future work.

We initialize all the parameters of the Lie algebra basis to a small constant value (1e-2). This provides an uninformative prior over possible structures and reduces sensitivity to potentially favorable, or adversarial, random initializations. During training, we additionally enforce a fixed Frobenius norm by re-scaling each basis element as

$$L'_i = \frac{\sqrt{D}}{\|L_i\|_F} L_i. \quad (38)$$

This normalization keeps the basis at a constant scale, improving optimization stability. The scale factor depends on the basis dimensionality and thus encourages more consistent representations across bases of different dimensions.

D.2. Hyperparameter Configuration

To enable a fair comparison with the considered baselines, we run all competing methods using the same hyperparameter settings reported in their papers or provided in the corresponding public implementations. We also follow the training schedule from those sources, including the same number of epochs and batch size. As a result, the reported performance of LieAugmenter may be slightly conservative and could potentially be improved with additional tuning of the training schedule. We also do not perform an exhaustive, fine-grained search over the hyperparameters that are specific to our approach. More generally, hyperparameter tuning remains an important and widely used technique across many fields, and a more systematic search could further improve performance. In this work, however, our primary goal is not to maximize results through extensive tuning, but to introduce LieAugmenter and demonstrate its effectiveness within a reasonable range of hyperparameter values that aligns with the existing experimental protocols.

Table 5 summarizes the number of epochs, batch size, and hyperparameter values for LieAugmenter used across all experiments. In addition, we used the Adam optimizer with a learning rate of 1e-3 in all experiments, keeping the rest of its default hyperparameter values.

Table 5: Number of epochs, batch size, and hyperparameter values for LieAugmenter in each of the experiments. We use * to denote that the value of η is irrelevant for certain experiments due to the Lie algebra basis having $C = 1$, which means that $\ell_{\text{bcreg}} = 0$.

	Epochs	Batch size	α	β	λ	η	ν	γ	K	C
Image Classification	15	64	1.0	7.0	1e-1	0*	1e-2	3.0	10	1
N -Body Dynamics	100	64	1.0	10.0	1.0	0*	1e-3	2.0	10	1
Molecular Property Prediction	500	125	1.0	3.0	1e-1	1.0	1e-3	3.0	3	6
Absence of Symmetry	25	64	1.0	1.0	1e-1	0*	1e-1	5.0	10	1

D.3. Inference

At inference time, we compute final predictions by

$$\hat{y}_i = \frac{1}{K+1} \left(\hat{y}_{i,1} + \sum_{j=1}^K \rho_{\mathcal{Y}}(g_{i,j}^{-1}) \hat{y}_{i,j+1} \right), \quad (39)$$

where $\rho_{\mathcal{Y}}(g_{i,j}^{-1})$ denotes the induced action on the output space: for equivariant tasks it corresponds to applying $g_{i,j}^{-1}$ to the prediction, while for invariant tasks it reduces to the identity. This inverse transformation is well-defined because the labels admit a corresponding group action, and because the equivariance loss in our training objective encourages the model to produce outputs that are consistent with the learned transformations.

We also explore a simplified alternative inference strategy in Appendix E.1, which allows for faster but less robust predictions.

D.4. Evaluation Metrics for Symmetry Discovery and Equivariance

Symmetry Discovery Metrics. To quantitatively evaluate the symmetry discovery results for LieAugmenter and the baseline methods, we compare the learned Lie algebra basis to a canonical ground-truth basis using two complementary metrics. First, we report the absolute cosine similarity, which is a scale-invariant measure of the directional alignment of the basis to the ground truth. Second, we report the absolute Frobenius projection of the learned basis \hat{L} to the ground truth L^* , given by $\frac{\langle \hat{L}, L^* \rangle_F}{\|L^*\|_F^2}$, which captures the scale alignment of the bases.

Note that direction is typically more critical for correctness in symmetry discovery, since it determines whether the learned generators span the right tangent directions of the group action. However, the scale of the learned bases can have a significant effect on the diversity of augmentations that can be sampled using the described reparameterization technique with a fixed distribution. Therefore, these two metrics combine to provide a global insight into both the correctness of the learned Lie algebra bases and their potential direct usefulness for downstream tasks.

For visualization, we match each learned generator to the closest canonical basis element and optionally flip its sign so that the matched pair has a positive Frobenius inner product. This improves interpretability

when comparing against the ground truth. Importantly, permuting generators or flipping their signs does not change the induced augmentation distribution under the symmetric coefficient sampling used in our method (see Section 3 and Appendix A).

Equivariance Error. We assess equivariance by measuring the consistency of model predictions under transformations sampled from the ground-truth symmetry group. Specifically, we compute

$$\frac{1}{N} \sum_{i=1}^N \left\| \frac{1}{K} \sum_{j=1}^K \rho_{\mathcal{Y}}(g_j)(\Psi(x_i)) - \frac{1}{K} \sum_{j=1}^K \Psi(\rho_{\mathcal{X}}(g_j)(x_i)) \right\|_1, \quad (40)$$

which contrasts transform-then-predict with predict-then-transform, averaged over K sampled group elements and N data points. To provide a more detailed characterization, we additionally report an alternative equivariance-error metric in Appendix E.12.

D.5. Image Classification

In this experiment, we used the prediction network as a CNN with four convolutional filters and two interleaved max-pooling layers. Following Cohen and Welling [2016], we also consider a group-equivariant CNN (GCNN) that is invariant to the $p4$ group, i.e., the set of planar translations composed with rotations by multiples of 90 degrees about any grid-aligned center. Its underlying implementation is defined analogously to our base CNN model in terms of the number and type of layers, in order to facilitate the comparison. We note, however, that this invariance is enforced architecturally (hard-coded) and is restricted to a small discrete subgroup of the underlying continuous rotation group, which can limit performance when the true variability is continuous.

We construct a RotatedMNIST dataset by applying random rotations to MNIST images [Deng, 2012]. We maintain the default train-test splits of MNIST in the resulting dataset, but also create a validation set with 10% of the training set samples. Thus, the final dataset consists of 54,000 training samples, 6,000 validation samples, and 10,000 test samples.

Regarding the results for this experiment, it is worth emphasizing an additional challenge in the out-of-distribution (OOD) setting beyond reduced data diversity. Specifically, restricting the rotation range can increase the effective overlap between certain classes (e.g., digits 6 and 9) making them harder to distinguish. This can lead to a somewhat counterintuitive outcome: a model that learns a more faithful symmetry (e.g., LieAugmenter) may still incur higher test-time confusion between these classes than a model that relies on an imperfect or coarser symmetry assumption (e.g., LieGAN-based augmentations), simply because the latter may not fully align samples in a way that amplifies the ambiguity. Moreover, in our end-to-end setting, symmetry discovery and prediction are learned jointly. When the relevant symmetry is difficult to recover, the model may benefit from longer training to fully realize the gains from the learned augmentations (even if this is still typically less costly than sequentially training separate discovery and prediction stages used by some baselines). These factors help explain part of the performance gap between the in-distribution (ID) and OOD results reported in Table 1. The effect is particularly evident in the class-wise error patterns, which we visualize via confusion matrices in Figure 8.

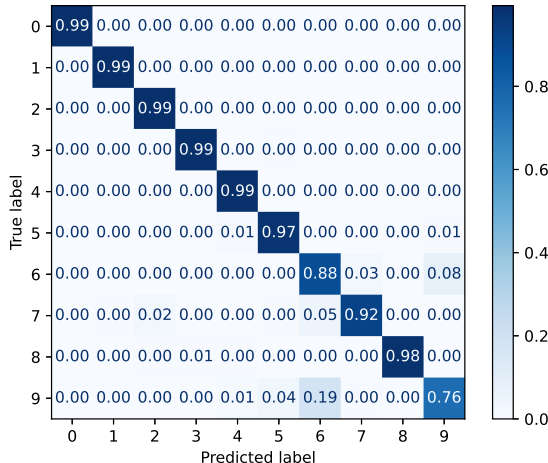


Figure 8: Confusion matrix for the test predictions of LieAugmenter in the OOD setting of the RotatedMNIST dataset.

D.6. N-Body Dynamics Prediction

For this experiment, we used a multilayer perceptron (MLP) as the prediction network for LieAugmenter and all augmentation-based baselines. The MLP comprises four fully connected layers with ReLU activations. We follow the dataset construction and splits of Yang et al. [2023], using 14,652 training samples and 14,220 test

samples. We also provide additional experiments on the N -body dynamic prediction in Appendix E.5, which covers a more challenging setup for 3-timestep prediction as well as the no mask variant.

D.7. Molecular Property Prediction

In this experiment, we again use the standard QM9 train/validation/test split [Blum and Reymond, 2009, Rupp et al., 2012], consisting of 100,000 training samples, 17,748 validation samples, and 13,083 test samples.

We note that the results reported by Benton et al. [2020] and Yang et al. [2023] were obtained under a slightly different training protocol. For example, using a batch size of 75 and employing a learning rate scheduling strategy. Despite these differences, we expect the reported numbers to remain broadly comparable.

D.8. Behavior in the Absence of Symmetry

For this final synthetic experiment, we generate 50,000 training samples, 10,000 validation samples, and 10,000 test samples. The frozen MLP f^* consists of two hidden layers of width 64 with tanh activations, and we randomly sample its weights i.i.d. from a continuous distribution $\mathcal{N}(0, \sigma)$ with $\sigma = 0.01$.

D.9. Scope and Future Work Beyond Linear Actions and the Exponential Map

Our current implementation assumes that the group acts linearly on inputs and outputs via a representation. This assumption is in line with Lie-based symmetry discovery and equivariant learning methods. It makes the learned symmetries easy to interpret and compare. Importantly, it is a modeling choice rather than a fundamental restriction of the framework.

One natural extension is to handle projective group actions. For example, $SL(3, \mathbb{R})$ acting on the plane, $SL(2, \mathbb{C})$ acting on the Riemann sphere. In such cases, an embedding layer could lift inputs to homogeneous coordinates, where the group action becomes linear. LieAugmenter could then be applied in the lifted space, with an additional projection step to map outputs back to the original domain. This would support projective actions with relatively minor pre- and post-processing, while keeping our core symmetry-learning mechanism unchanged. More general non-linear actions without an explicit linearization step would likely require further architectural design and analysis, which we leave for future work.

Another direction is to consider alternative exponential maps that might mitigate some limitations of the current design. The Riemannian exponential is a natural candidate, and on certain manifolds it can have favorable global properties (e.g., surjectivity in some settings). However, these properties are not guaranteed in general, and the Riemannian exponential does not necessarily preserve the algebraic structure we rely on. For matrix Lie groups, when the metric is bi-invariant, the Riemannian exponential agrees with the Lie (matrix) exponential under the standard identification at the identity (see Appendix C in Lezcano-Casado and Martnez-Rubio [2019]). More broadly, closed-form Riemannian exponentials are only available for particular groups and choices of invariant metrics [Zacur et al., 2014]. This makes it less straightforward to use for symmetry discovery in our setting, since it can depend on geometric assumptions about the group that may not be known a priori.

That being said, exploring alternative exponential maps would require a careful treatment of both their algebraic and computational implications. In this work, our focus is on proposing task-adaptive symmetry discovery, i.e., learning symmetries end-to-end in a way that is directly driven by the downstream objective, under the standard and interpretable setting of linear group actions with the Lie (matrix) exponential. Extending this task-adaptive formulation to broader classes of group actions and alternative exponential constructions is an interesting direction to explore in future work.

E. Additional Experiments

In this section, we present additional experimental results that further demonstrate the effectiveness of our method across a broader range of settings, spanning different datasets, symmetry structures, and model classes.

Specifically, we study an alternative inference procedure and find that performance remains robust. We provide evidence of empirical convergence, along with an ablation study and a hyperparameter sensitivity analysis indicating stable behavior across a wide range of configurations. We also evaluate sample efficiency.

We further extend the N -body experiments by considering symmetry discovery without a mask, as well as different masked variants, and we additionally report results for three timestep prediction. We include a runtime analysis and examine model behavior in settings where no meaningful symmetry is present.

Finally, we demonstrate that the proposed framework can also recover discrete symmetries, including discrete rotations and partial permutations, and we showcase applications across multiple domains, including Lorentz symmetries in quantum field theory amplitude prediction and human colorectal cancer data.

E.1. Exploring Alternative Inference Strategy

We study a faster inference variant in which no augmentations are generated at test time. In this setting, we feed only the original inputs through the prediction network and output its direct prediction. This option can be preferable in applications where inference latency is a primary constraint.

To evaluate the impact of this choice, we rerun the RotatedMNIST image classification and apply the no-test-augmentation strategy to LieAugmenter and the fixed augmentation strategies with oracle and LieGAN symmetries. As shown in Tables 6 and 16, accuracy decreases slightly compared to the aggregation-based inference used in the main results (Table 1), while the overall test-time cost is correspondingly reduced (Table 15).

Table 6: RotatedMNIST results for in-distribution (ID) and out-of-distribution (OOD) evaluation following the alternative inference strategy. We report classification accuracy (higher is better) and equivariance error (lower is better) for CNN models trained (i) with *Oracle* rotation augmentation (ground-truth symmetry), (ii) with LieGAN augmentations, and (iii) with LieAugmenter (*Ours*). All values are reported as mean \pm std over three random seeds.

	Oracle augmentation		Symmetry discovery	
	Rotation	LieGAN Aug.	LieAugmenter (Ours)	
ID Acc. (%) (\uparrow)	98.45 \pm 0.11	97.84 \pm 0.13	98.55 \pm 0.08	
ID Equiv. Error (\downarrow)	3.91 \pm 0.23	4.92 \pm 0.74	3.72 \pm 0.15	
OOD Acc. (%) (\uparrow)	98.35 \pm 0.11	84.97 \pm 0.43	93.40 \pm 2.46	
OOD Equiv. Error (\downarrow)	4.03 \pm 0.17	6.80 \pm 0.85	3.40 \pm 0.47	

E.2. Empirical Convergence

In order to complement the previous analysis of the convergence of our reparameterized objective presented in Appendix C.5, we carry out an empirical exploration of convergence in our experiments, seeking to provide greater insight and evidence of the applicability of our proposed approach in practice. We report the train and validation loss curves as well as the corresponding separate evolution of the main loss terms of the train loss (i.e., objective/empirical loss and equivariance loss) during training for RotatedMNIST (Figure 9) and QM9 (Figure 10). We see that all losses quickly decrease and start converging despite the complexity of the associated optimization problem.

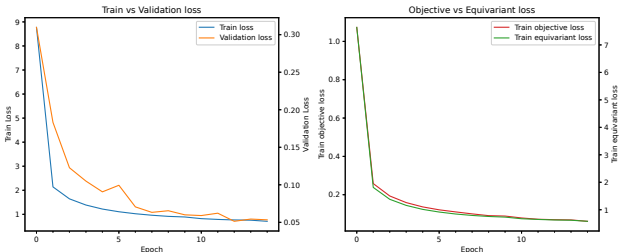


Figure 9: Loss curves of LieAugmenter for RotatedMNIST dataset. (Left) Train and validation losses. (Right) Objective and equivariance losses.

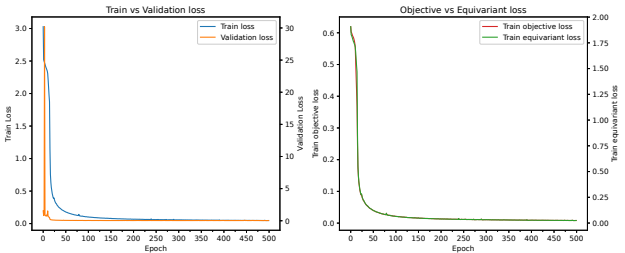


Figure 10: Loss curves for LUMO task of the QM9 dataset. (Left) Train and validation losses. (Right) Objective and equivariance losses.

E.3. Ablation Study and Hyperparameter Analysis

We conduct a set of ablations over LieAugmenter’s loss weights and key hyperparameters to assess how each component affects performance. For this analysis, we focus on RotatedMNIST, since it has the lowest runtime among our symmetry-based benchmarks and therefore supports a more extensive sweep.

Note that α is not a strictly necessary weight coefficient, given that setting $\alpha = \beta$ would be approximately equivalent to merging the empirical prediction loss \mathcal{L}_{emp} into the equivariance loss \mathcal{L}_{equiv} by changing the averaging over augmentations to also include the original sample. Nevertheless, we consider a separate weight to enhance the flexibility of our method and provide a more rigorous analysis of its impact on the performance.

From Figure 11 (left), we observe that the performance of our model is quite robust to changes in the values of the weights for the different terms of the loss function except for β , i.e., the weight for the \mathcal{L}_{equiv} term. In particular, decreasing the value of β leads to a degraded performance, as expected, since the LieAugmenter will not receive a strong enough learning signal to properly learn the correct symmetry. In addition, in Figure 11 (right), we see that the number of sampled augmentations per input sample can also considerably affect the performance of the model, although not so drastically. In particular, increasing the number of augmentations generally leads to an improved performance, as we could expect, but after a certain point, the performance starts decreasing and becomes more variable across runs. A plausible explanation is that when the number of augmented instances becomes large relative to the batch size, optimization becomes dominated by augmented samples, effectively down-weighting the original data and making training less stable.

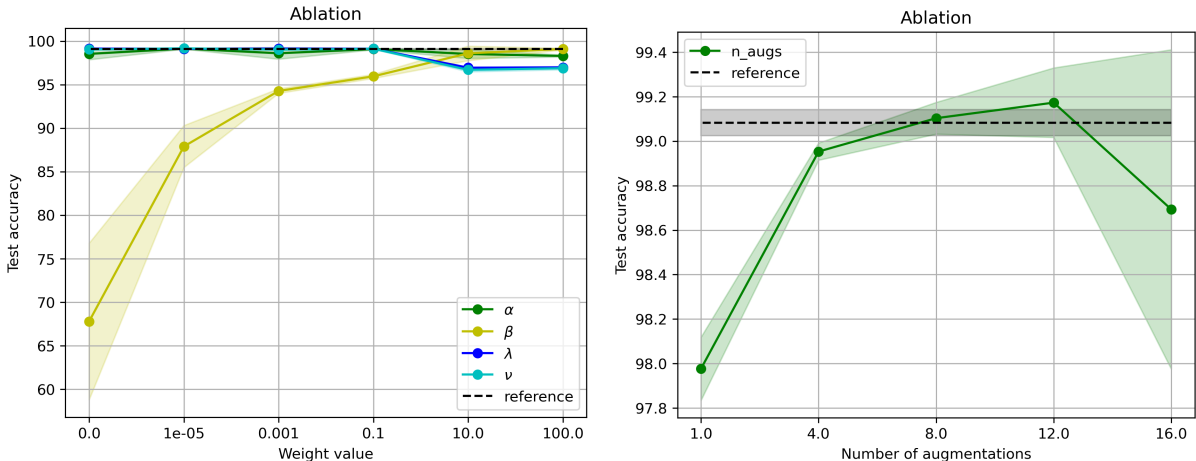


Figure 11: Ablation results for the accuracy metric in the RotatedMNIST dataset for varying values for the weight terms of the loss function (left) and the number of augmentations per sample (right). The reference results correspond to the hyperparameters considered in the main experiments. All results are reported as the mean and standard deviation over three runs with different random seeds.

In Figure 12, we can find the corresponding results for the ablation analysis focusing on the cosine similarity of the learned Lie algebra basis to the ground truth instead of the performance metric. For the weight terms of the loss function, we can see that modifying α (the weight of \mathcal{L}_{obj}) has little effect on the symmetry discovery process. Modifying λ and ν also has little impact below a threshold of 0.1, but when those terms are increased too much, they lead to a degraded symmetry discovery performance, as the difference of the augmentations from the original data (λ) or the sparsity of the learned basis (ν) become too prominent in the loss. Furthermore, β also has a relevant impact on the symmetry discovery process, where we observe that higher values of that weight help the performance of the model. Lastly, the number of augmentations per sample has little impact on the symmetry discovery process for values below 16, but at that point the performance degrades, possibly for the same reason that we hypothesized for the performance metric.

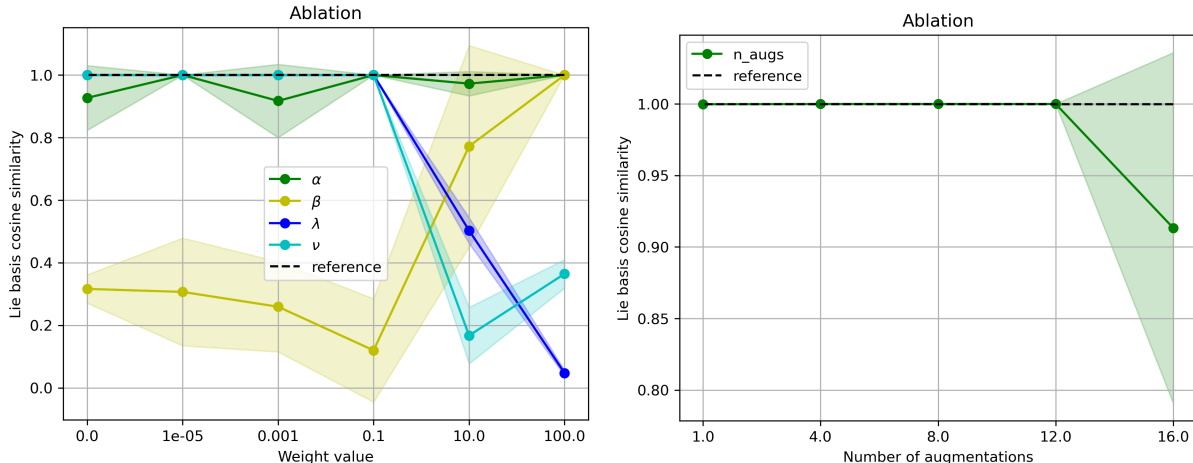


Figure 12: Ablation results for the cosine similarity of the learned Lie algebra basis to the ground truth in the RotatedMNIST dataset for varying values for the weight terms of the loss function (left) and the number of augmentations per sample (right). The reference results correspond to the hyperparameters considered in the main experiments. All results are reported as the mean and standard deviation over three runs with different random seeds.

Next, we also explore the effect of the chosen range γ for the uniform sampling of coefficients for the linear combination of elements of the Lie algebra basis, which is then mapped to a group element. This is a hyperparameter that we did not extensively tune in our experiments, and its values were chosen mainly seeking to encourage the sampling of diverse elements of the group while not being excessively large to avoid distortions in the uniformity of the sampling (e.g., for rotation groups the sampled elements would “wrap around” for larger ranges, thus distorting the effective sampling density of the group elements).

In order to verify our intuition and solidify our explanation in that regard, we run an additional ablation experiment for the γ hyperparameter using the RotatedMNIST dataset, the results of which are shown in Table 7. In these results, we would start observing the “wrap around” effect starting at $\gamma = 5.0$ if the model were to learn the ground truth symmetry, which may explain the decrease in performance and cosine similarity for that and the larger values of this hyperparameter. In the case of $\gamma = 13.0$, we hypothesize that the slight increase in the performance and similarity of the basis is due to the fact that learning the ground truth Lie algebra basis would lead to rotations approximately in the range $[-2\pi, 2\pi]$, thus circumventing the issue.

Finally, we also explore the symmetry discovery performance of LieAugmenter under a misspecified Lie algebra basis cardinality C in Figure 13. As we can see, under the slight misspecification of setting $C = 2$, we observe redundancy across the different elements of the learned basis, which shows that our model is able to robustly discover the correct basis. In the more extreme cases of setting $C = 4$ or $C = 6$, we start observing a slight degradation in the discovered basis, which is somewhat noisier. In addition, while some elements in the basis are inverses of one another, their linear combination would still lead to a valid rotation augmentation. Therefore, while knowing the correct (or a close approximation) of the basis cardinality a priori helps the symmetry discovery performance of the model, we have shown that it can be robust in scenarios where that knowledge may not be available.

Table 7: Results for the ablation of γ . We report the mean and standard deviation for both metrics across three runs using different random seeds. The accuracies are expressed as percentages.

γ	Test accuracy	Cosine similarity basis
1.0	97.73±0.17	0.9999±0.0001
2.0	98.04±0.22	1.0000±0.0000
3.0	99.08±0.06	0.9997±0.0002
5.0	95.97±3.24	0.7860±0.3026
8.0	93.11±3.79	0.5706±0.3571
9.0	94.93±4.94	0.6783±0.4549
10.0	92.56±4.19	0.6273±0.2656
11.0	89.28±2.96	0.3709±0.2551
12.0	96.74±2.14	0.6881±0.4381
13.0	96.98±0.72	0.9812±0.0178
14.0	93.32±2.99	0.7236±0.2095
15.0	91.89±2.20	0.5346±0.0607
16.0	93.52±0.91	0.2104±0.1597
17.0	90.28±3.33	0.2779±0.1739
21.0	89.00±4.13	0.0006±0.0006

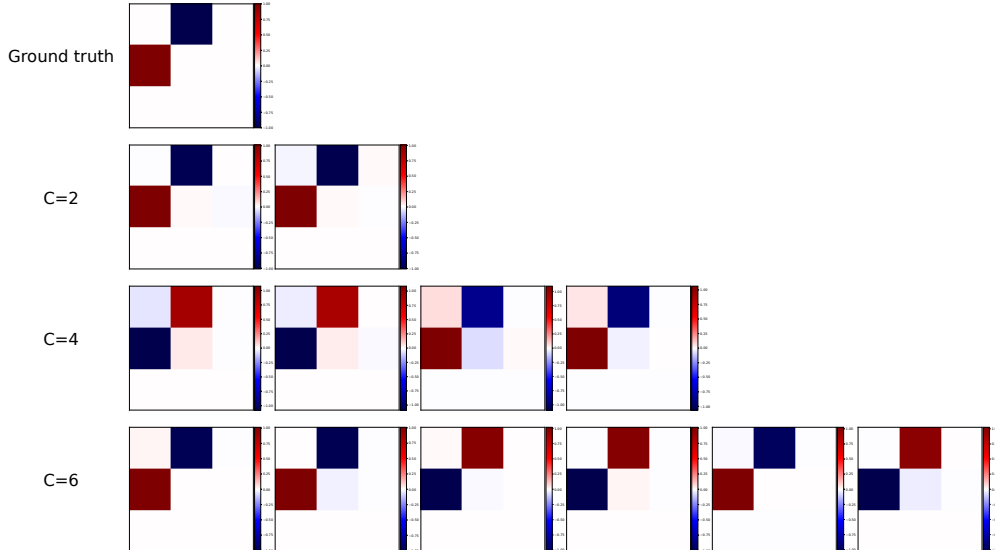


Figure 13: LieAugmenter is able to correctly discover a representation of the underlying symmetry even when the cardinality of the Lie algebra basis is misspecified in the RotatedMNIST dataset.

E.4. Sample efficiency

We explore the sample efficiency of LieAugmenter when compared to the other considered prediction approaches by measuring their test performance when trained with a varying number of samples in the training set. As we can see in Figure 14, LieAugmenter matches the performance of the CNN trained with ground truth augmentations up to training with 50% of the data, after which its performance decreases but remains higher than that of the other baselines.

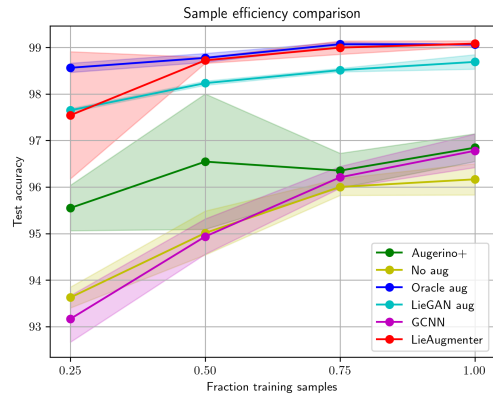


Figure 14: Comparison of the sample efficiency for the equivariant-architecture baseline (GCNN, $p4$) and CNN models trained (i) without augmentation (No aug), (ii) with ground truth rotation augmentation (Oracle aug), (iii) with symmetry-discovery baselines (Augerino+ and LieGAN aug), and (iv) with LieAugmenter (*Ours*), which are trained with different fractions of the total training set samples of the RotatedMNIST dataset.

E.5. N -Body Dynamics Prediction

In this section, we provide a deeper exploration of the performance of LieAugmenter and the baseline methods for the task of N -body dynamics prediction. On one hand, we analyze the symmetry discovery behavior under more relaxed assumptions regarding the search space for the symmetry in the form of different masks for the learnable Lie algebra basis. On the other hand, we study the more challenging scenario of having access to deeper time horizon for both the inputs and the predictions, in particular consisting of three timesteps per sample, instead of the single timestep considered in our main results.

E.5.1. 1-Timestep Prediction

As described in the paper, previous symmetry discovery methods considered some auxiliary knowledge about this task in order to restrict the search space for the symmetry. In particular, such prior assumptions led to the definition of a 2×2 block diagonal mask that restricts which entries of the parameterized Lie algebra basis are learnable.

We denote that mask as Mask_2 and study the effect of considering more relaxed prior assumptions on the symmetry search space. First, we consider a mask that allows interactions between only positions and only momenta across the different bodies (Mask_4). In addition, we explore the effect of removing all prior constraints on the search space (Mask_0). We add the same numerical suffixes to LieAugmenter and the baseline models to indicate which mask is applied in each case.

Symmetry Discovery. Figure 15 shows a visualization of the different masks, as well as the learned Lie algebra basis by each of the models in the in-distribution and out-of-distribution scenarios. As we can observe, when relaxing the constraints on the symmetry search space, LieAugmenter learns a Lie algebra basis that differs from the canonical ground truth that is identified under the Mask_2 setup. However, we can show that for the physical parameters considered in the definition of this dataset, that basis actually corresponds to an alternative representation of the rotational symmetry defined by the ground truth. Please refer to Appendix E.5.3 for further details. As a result, we can conclude that LieAugmenter successfully recovers the correct symmetry under all constraint masks and also the lack thereof in both in-distribution and out-of-distribution scenarios.

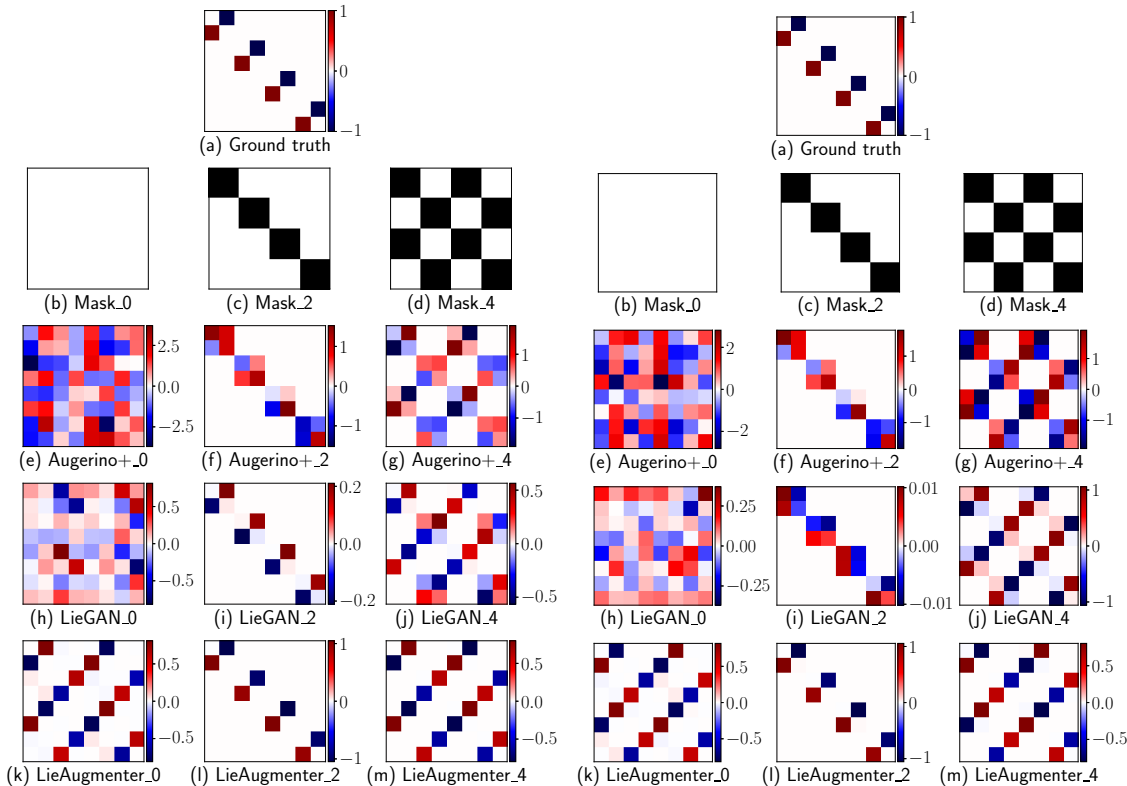


Figure 15: Ground-truth Lie algebra basis, masks of learnable entries, and bases learned by baseline symmetry discovery methods and LieAugmenter for 2-body dynamics prediction with one input and one output timestep. Results are shown for the ID (*left*) and OOD settings (*right*).

Predictive Performance. Similarly, we extend our previous performance analysis by including the models that incorporate the symmetry discovery results obtained with different masks. In addition, we also add the results for an equivariant model, EMLP [Finzi et al., 2021], which is defined to be equivariant with respect to the ground truth Lie algebra basis. Table 8 reports the MSE and equivariance error of the different approaches in the ID and OOD settings. As we can observe, regardless of the mask, LieAugmenter achieves

the best performance only (closely) behind the equivariant model, but still surpassing the methods that consider oracle augmentation and augmentation based on discovered symmetries. In addition, note that LieAugmenter is considerably faster to train than the equivariant model (requiring almost a third of the training time), as we present in Table 17.

Table 8: 2-body dynamics results for ID and OOD evaluations under different masks restrictions on the symmetry search space for one input and output timestep. We report MSE and equivariance error for an equivariant architecture (EMLP) and for MLP models trained (i) without augmentation (*Trivial*), (ii) with *Oracle* rotation augmentation (ground-truth symmetry), (iii) with symmetry-discovery baselines (Augerino+ and LieGAN Aug.), and (iv) with LieAugmenter (*Ours*). All values are reported as mean \pm std over three random seeds.

		In-distribution		Out-of-distribution	
		MSE (\downarrow)	Equiv. Error (\downarrow)	MSE (\downarrow)	Equiv. Error (\downarrow)
Equiv. architecture	EMLP	1.74e-06 \pm 1.50e-06	5.32e-05 \pm 1.16e-05	4.64e-06 \pm 4.86e-06	5.27e-05 \pm 1.10e-05
Data augmentation	Trivial	5.16e-03 \pm 2.79e-03	2.48e-02 \pm 7.37e-03	1.86e-02 \pm 3.74e-03	3.33e-02 \pm 2.56e-03
	Oracle	2.13e-05 \pm 1.56e-05	3.03e-03 \pm 1.03e-03	3.03e-05 \pm 8.81e-06	3.70e-03 \pm 1.14e-03
Symmetry discovery	Augerino+_0	5.28e+00 \pm 4.23e-01	1.90e-01 \pm 1.92e-03	3.26e+00 \pm 7.30e-01	1.94e-01 \pm 4.15e-03
	LieGAN_0 aug	3.23e-03 \pm 6.25e-04	1.91e-02 \pm 1.47e-03	1.15e-02 \pm 3.00e-03	2.84e-02 \pm 3.04e-03
	LieAugmenter_0	1.39e-05 \pm 6.08e-07	2.78e-03 \pm 4.88e-04	2.38e-05 \pm 9.04e-06	2.59e-03 \pm 9.89e-05
	Augerino+_2	9.67e+03 \pm 1.37e+04	2.37e-01 \pm 7.53e-02	1.48e+05 \pm 2.09e+05	1.95e-01 \pm 9.23e-03
	LieGAN_2 aug	1.10e-03 \pm 6.98e-04	1.48e-02 \pm 4.80e-03	8.94e-03 \pm 9.31e-04	2.73e-02 \pm 1.10e-03
	LieAugmenter_2	1.30e-05 \pm 5.58e-06	3.28e-03 \pm 9.36e-04	3.73e-05 \pm 2.97e-05	5.96e-03 \pm 2.82e-03
	Augerino+_4	1.79e+00 \pm 2.77e-02	1.87e-01 \pm 2.92e-04	1.55e+00 \pm 8.59e-03	1.86e-01 \pm 5.90e-04
	LieGAN_4 aug	2.85e-05 \pm 1.19e-05	3.02e-03 \pm 5.08e-04	5.12e-05 \pm 8.47e-06	2.78e-03 \pm 3.62e-04
	LieAugmenter_4	1.45e-05 \pm 6.15e-06	3.15e-03 \pm 9.78e-04	1.61e-05 \pm 1.22e-06	3.13e-03 \pm 2.79e-04

E.5.2. 3-Timestep Prediction

In this section, we follow the same analysis as in the previous one but we study the more challenging task of predicting three future timesteps from three past observations of the trajectory of the bodies.

Symmetry Discovery. Figure 16 shows a visualization of the ground truth Lie algebra basis and masks, together with the bases learned by LieAugmenter and each of the baseline symmetry discovery approaches. As we can observe, once again, LieAugmenter provides a strong and robust performance across both the ID and OOD settings irrespective of the applied mask, learning either the canonical representation of the basis or the alternative one that we saw previously.

Predictive Performance. Table 9 reports the MSE and equivariance error of the different approaches in the ID and OOD settings. Regardless of the mask, LieAugmenter again achieves the best performance only (closely) behind the equivariant model, but still surpassing the methods that consider oracle augmentation and augmentation based on discovered symmetries. As previously noted, we remark the faster training speed of LieAugmenter over the equivariant model (requiring almost a third of the training time), as we present in Table 17.

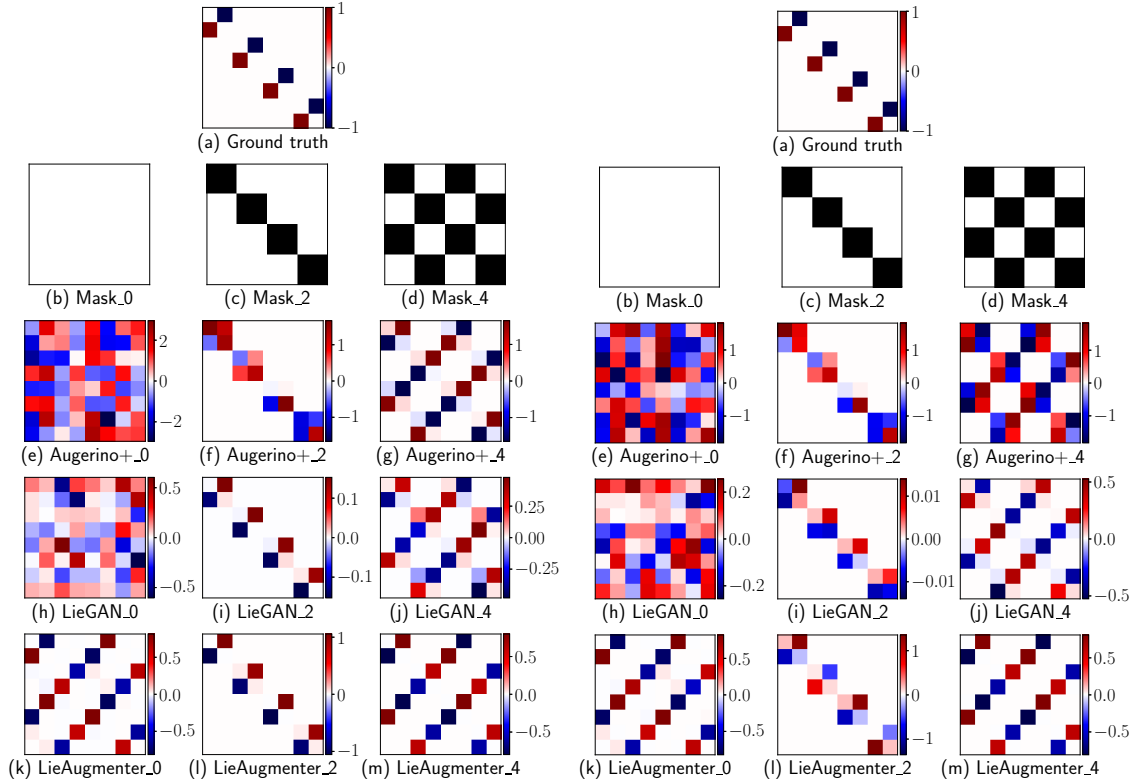


Figure 16: Ground-truth Lie algebra basis, masks of learnable entries, and bases learned by baseline symmetry discovery methods and LieAugmenter for 2-body dynamics prediction with three input and three output timesteps. Results are shown for the ID (*left*) and OOD settings (*right*).

Table 9: 2-body dynamics results for ID and OOD evaluation under different masks restrictions on the symmetry search space for three input and output timesteps. We report MSE and equivariance error for an equivariant architecture (EMLP) and for MLP models trained (i) without augmentation (*Trivial*), (ii) with *Oracle* rotation augmentation (ground-truth symmetry), (iii) with symmetry-discovery baselines (Augerino+ and LieGAN Aug.), and (iv) with LieAugmenter (*Ours*). All values are reported as mean \pm std over three random seeds.

		In-distribution		Out-of-distribution	
		MSE (\downarrow)	Equiv. Error (\downarrow)	MSE (\downarrow)	Equiv. Error (\downarrow)
Equiv. architecture	EMLP	4.54e-06 \pm 2.20e-06	2.91e-05 \pm 4.71e-06	6.30e-06 \pm 3.68e-06	2.90e-05 \pm 4.79e-06
Data augmentation	Trivial	9.62e-03 \pm 4.32e-03	3.58e-02 \pm 7.57e-03	1.45e-02 \pm 1.30e-03	3.51e-02 \pm 1.39e-03
	Oracle	3.96e-05 \pm 1.75e-05	5.08e-03 \pm 1.19e-03	4.92e-05 \pm 2.25e-05	3.88e-03 \pm 6.66e-04
Symmetry discovery	Augerino+_0	4.03e+00 \pm 3.49e-01	1.91e-01 \pm 2.17e-03	2.68e+00 \pm 4.94e-01	1.98e-01 \pm 9.13e-03
	LieGAN_0 aug	8.83e-03 \pm 2.72e-03	3.59e-02 \pm 5.83e-03	1.88e-02 \pm 4.80e-03	4.15e-02 \pm 5.98e-03
	LieAugmenter_0	5.98e-05 \pm 2.17e-05	4.07e-03 \pm 1.50e-03	1.59e-04 \pm 1.93e-04	4.90e-03 \pm 1.88e-03
	Augerino+_2	8.70e+00 \pm 1.00e+01	1.96e-01 \pm 8.81e-03	1.09e+01 \pm 1.33e+01	1.87e-01 \pm 8.77e-03
	LieGAN_2 aug	2.71e-03 \pm 2.39e-04	2.26e-02 \pm 1.16e-03	1.83e-02 \pm 4.37e-03	4.05e-02 \pm 3.98e-03
	LieAugmenter_2	1.75e-05 \pm 6.22e-06	4.58e-03 \pm 4.07e-04	3.67e-04 \pm 1.10e-04	7.97e-03 \pm 1.45e-03
	Augerino+_4	1.72e+00 \pm 1.03e-01	1.88e-01 \pm 1.83e-03	1.64e+00 \pm 7.75e-02	1.88e-01 \pm 2.73e-03
	LieGAN_4 aug	8.86e-05 \pm 7.58e-05	4.24e-03 \pm 1.10e-03	7.94e-05 \pm 2.55e-05	4.78e-03 \pm 7.64e-04
	LieAugmenter_4	2.85e-05 \pm 3.92e-06	3.97e-03 \pm 6.82e-04	5.32e-05 \pm 1.28e-05	4.22e-03 \pm 1.75e-04

E.5.3. Alternative representation of the rotation symmetry

Throughout our experiments with this 2-body dynamics dataset, we have observed what we have claimed to be an alternative representation of the correct symmetry in the context of the specific values for the physical parameters of this dataset. In that sense, following Yang et al. [2023], we present the derivation that confirms that claim.

Firstly, we can write this alternative representation of the Lie algebra basis in the following way to highlight its structure after removing the slightly noisy entries:

$$R = \begin{bmatrix} 0 & -1 \\ 1 & 0 \end{bmatrix}$$

$$L = \begin{bmatrix} R & 0 & -R & 0 \\ 0 & R & 0 & -R \\ -R & 0 & R & 0 \\ 0 & -R & 0 & R \end{bmatrix}$$

Then, we can express the result of applying the matrix exponential to a weighted version of that basis as follows:

$$\exp(wL) = I + \begin{bmatrix} G(w) & 0 & -G(w) & 0 \\ 0 & G(w) & 0 & -G(w) \\ -G(w) & 0 & G(w) & 0 \\ 0 & -G(w) & 0 & G(w) \end{bmatrix}$$

$$G(w) = \sum_{n=0}^{\infty} \frac{(-1)^n 2^{2n} w^{2n+1}}{(2n+1)!} R + \sum_{n=1}^{\infty} \frac{(-1)^n 2^{2n-1} w^{2n}}{(2n)!} I$$

As a result, we can define its action on the input data as follows:

$$\exp(wL) \begin{bmatrix} \mathbf{q}_1 \\ \mathbf{p}_1 \\ \mathbf{q}_2 \\ \mathbf{p}_2 \end{bmatrix} = \text{diag}(I + 2G(w)) \begin{bmatrix} \mathbf{q}_1 \\ \mathbf{p}_1 \\ \mathbf{q}_2 \\ \mathbf{p}_2 \end{bmatrix},$$

where we have used our knowledge about the dataset, i.e., the origin is at the center of mass, and we have $m_1 = m_2$, $\mathbf{q}_1 = -\mathbf{q}_2$, and $\mathbf{p}_1 = -\mathbf{p}_2$.

Lastly, we can notice the following relation between the resulting expression and the ground truth rotation symmetry:

$$I + 2G(w) = \sum_{n=0}^{\infty} \frac{(-1)^n 2^{2n+1} w^{2n+1}}{(2n+1)!} R + \sum_{n=0}^{\infty} \frac{(-1)^n 2^{2n} w^{2n}}{(2n)!} I$$

$$= \begin{bmatrix} \cos 2w & -\sin 2w \\ \sin 2w & \cos 2w \end{bmatrix}$$

E.6. Behavior in the Absence of Symmetry

In this section, we complement our analysis of the behavior of LieAugmenter and symmetry discovery baselines in the absence of symmetries in the data.

First, we compute two metrics that quantify how close to the identity the learned symmetry is for each of the considered methods and present the results in Table 10. In this way, we seek to more closely analyze whether the previously visualized Lie algebra bases actually encode any behavior similar to the expected identity transformations. From the results, we can observe that Augerino+ learns augmentations that significantly differ from the identity, and that LieGAN learns augmentations that are closest to the identity but still considerably differ from it. For LieAugmenter, the augmentations are similarly close to the identity as for LieGAN, and the high variability of the results matches our previous analysis of the visualizations of the learned Lie algebra basis.

Secondly, we present the performance of LieAugmenter and different augmentation approaches in Table 11, aiming to verify that our method does not lead to a degradation of the performance even when there is no continuous symmetry to discover in the data. As we can observe, the performance of LieAugmenter is indeed similar to that provided by the other augmentation approaches, and even slightly better. This indicates that our proposed method can still be successfully applied despite our goal of discovering underlying symmetries not being supported by the data.

Table 10: Evaluation of the proximity of the learned augmentations to the identity in a dataset without continuous symmetries for LieAugmenter and baseline symmetry discovery approaches.

	$\mathbb{E}_{x,g} [\ \rho\chi(g)x - x\ _2]$	$\mathbb{E} [\ g - I\ _F]$
Augerino+	262.8388±199.6667	176.3353±192.0428
LieGAN	6.9031±0.0805	3.4250±0.1813
LieAugmenter	10.6570±4.4892	5.5936±0.0123

Table 11: Evaluation of the predictive performance in a dataset without continuous symmetries. We report MSE for MLP models trained (i) without augmentation (*Trivial*), (ii) with *Oracle* augmentation (identity transformations), (iii) with symmetry-discovery baselines (Augerino+ and LieGAN Aug.), and (iv) with LieAugmenter. All values are reported as mean ± std over three random seeds.

		MSE (↓)
Data augmentation	No aug.	2.29e-04±1.86e-04
	Oracle aug.	6.31e-04±4.24e-04
Symmetry discovery	Augerino+	2.22e-04±1.12e-04
	LieGAN Aug.	6.30e-04±4.31e-04
	LieAugmenter	1.99e-04 ±7.23e-05

E.7. Rotations in Colorectal Cancer Detection from Images

As another more complex experiment for analyzing the performance of our proposal, we consider the task of human colorectal cancer (CRC) detection from stained histological images of human tissues. In particular, we consider the datasets NCT-CRC-HE-100K for training and CRC-VAL-HE-7K for testing [Kather et al., 2018], each containing 100,000 and 7,000 samples, respectively, of histological slices of human colorectal cancer and normal tissue, represented as 224x224 RGB images. Rotational invariance has been shown to be particularly important for this classification task [Gerken and Kessel, 2024].

The main goal of this experiment is to explore the applicability of our approach to a more complex and relevant computer vision scenario, where the images are larger and in color. In addition, we also seek to study the effect of applying LieAugmenter to more complex architectures besides simple CNNs and MLPs, e.g., Vision Transformer (ViT) [Dosovitskiy et al., 2021] and EfficientNet [Tan and Le, 2019].

Note that in this experiment, we do not seek to attain the highest possible performance for the considered models in this dataset, but rather to observe the effect of applying LieAugmenter in contrast to using trivial and ground truth augmentations on each of the base models. As a result, we do not tune the hyperparameters, which we set similarly to previous experiments: $\alpha = 1.0$, $\beta = 7.0$, $\lambda = 0.1$, $\eta = 0.0$, $\nu = 0.01$, $\gamma = 3.0$, and $K = 10$. We train all models for 25 epochs with a batch size of 64.

Symmetry Discovery. In terms of symmetry discovery, we follow the same procedure as for the RotatedMNIST dataset and set the cardinality of the Lie algebra basis to $C = 1$ while searching over the six-dimensional space of 2D affine transformations, which are defined to act on the pixel coordinates of the images. With that definition, LieAugmenter is able to learn the correct symmetry for all of the considered architectures, as shown in Figure 17.

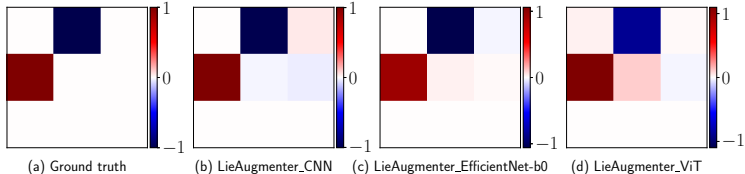


Figure 17: Ground-truth Lie algebra basis, and bases learned by LieAugmenter trained with CNN, EfficientNet-b0, and ViT as prediction networks for the CRC dataset.

Predictive Performance. As we can see in the results in Table 12, LieAugmenter provides an equal or better performance than using ground truth augmentations for all three prediction networks. This observation coincides with and reinforces our previous results, demonstrating once more the benefits and ease of applicability of our approach.

Table 12: CRC results for the evaluation of the CNN, EfficientNet-b0, and Vision Transformer models trained (i) without augmentation (No aug.), (ii) with ground truth augmentations (Oracle aug.), and (iii) LieAugmenter. We report accuracy and equivariance error as mean \pm std over three random seeds.

Prediction network	Method	Accuracy (%) (\uparrow)	Equiv. Error (\downarrow)
CNN	No aug.	84.87 \pm 4.44	2.95 \pm 0.15
	Oracle aug.	85.27 \pm 3.34	1.75 \pm 0.29
	LieAugmenter	89.42 \pm 0.89	1.86 \pm 0.21
EfficientNet-b0	No aug.	93.04 \pm 1.18	2.55 \pm 0.24
	Oracle aug.	93.35 \pm 1.93	1.49 \pm 0.14
	LieAugmenter	92.74 \pm 2.55	1.21 \pm 0.10
Vision Transformer	No aug.	75.69 \pm 3.90	2.02 \pm 0.42
	Oracle aug.	81.16 \pm 2.67	1.09 \pm 0.07
	LieAugmenter	85.63 \pm 2.93	0.82 \pm 0.15

E.8. Discovering Discrete Symmetries

Next, we also explore the ability of LieAugmenter to identify the correct Lie group when the symmetry of the data corresponds to discrete subgroups of a Lie group instead of continuous groups, as we studied in the main experiments. To that effect, we construct two synthetic regression datasets based on some scenarios explored in Yang et al. [2023].

For both of these datasets, we set the following hyperparameter values for our model: $\alpha = 1.0$, $\beta = 5.0$, $\lambda = 0.1$, $\eta = 0.0$, $\nu = 0.001$, $\gamma = 3.0$, and $K = 10$. Once more, η has no effect on this particular scenario, because the cardinality of the bases is $C = 1$. We generate 54,000 samples for the training set, 6,000 for the validation set, and 10,000 for the test set. The prediction network for LieAugmenter and the different augmentation approaches is defined in both problems as a simple MLP, consisting of four layers and ReLU activations.

In order to attempt to model the discrete nature of the studied groups, we modify the sampling strategy of the coefficients of the linear combination of the elements of the Lie algebra basis by sampling from a uniform integer grid instead of a uniform distribution. We would expect such modification to possibly lead to slight predictive performance improvements, but it could also degrade the quality of the symmetry discovery results due to the restricted nature of the generated augmentations.

Since prior knowledge about the discrete or continuous nature of the underlying group is not always readily available, we also explore the performance of LieAugmenter with the previous uniform sampling strategy to show its robustness to such a possible misspecification. We distinguish the results by the nomenclature ‘LieAugmenter (discrete)’ and ‘LieAugmenter (continuous)’. Overall, we observe that both sampling strategies provide similarly strong performance (especially for symmetry discovery), with the discrete formulation providing slightly higher task performance in our experiments.

E.8.1. Discrete Rotations

As the first synthetic dataset, we consider the synthetic regression problem given by $f(x, y, z) = z/(1 + \arctan \frac{y}{x} \bmod \frac{2\pi}{k})$, which is invariant to rotations of multiples of $2\pi/k$ in the xy plane, thus corresponding to a discrete cyclic subgroup of $SO(2)$ with size k . Specifically, we consider the case where $k = 6$ and $x, y, z \sim \mathcal{N}(0, I)$.

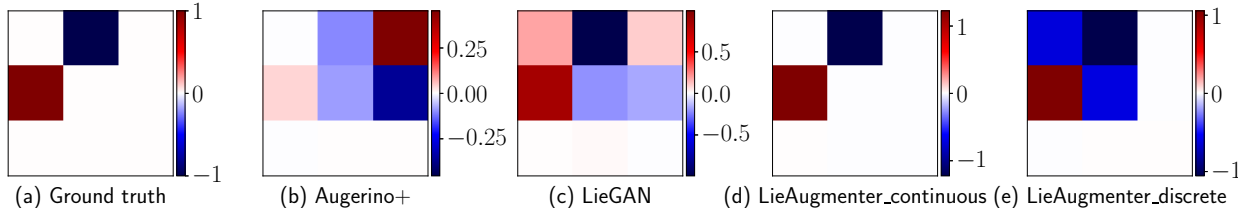


Figure 18: Ground-truth Lie algebra basis, and bases learned by the different sampling strategies for LieAugmenter and baseline symmetry discovery methods in the discrete rotation dataset. The sign of the bases is aligned to simplify their interpretation, since it is irrelevant for their correctness.

Symmetry Discovery. From Figures 18 and Figure 19, we can see that LieAugmenter is capable of correctly learning a Lie algebra basis for the $SO(2)$ supergroup of the underlying discrete rotation symmetry irrespectively of the discreteness of the distribution selected for sampling. It seems, however, that discretely sampling from a uniform integer grid leads to a slightly worse recovery of the basis, as we had expected.

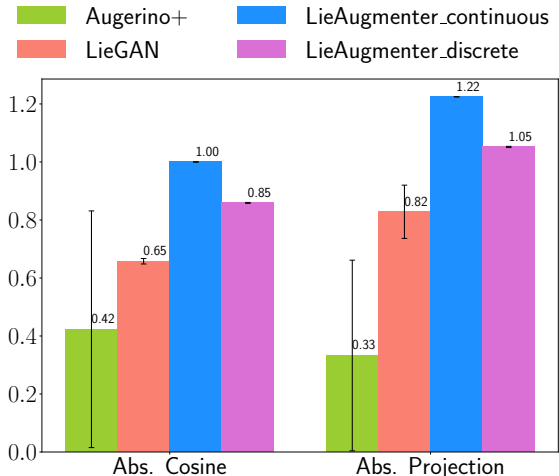


Figure 19: Absolute cosine similarity and absolute Frobenius projection for Lie algebra basis recovery on the discrete rotation dataset (mean \pm std over three random seeds).

Predictive Performance. Table 13 reports the MSE and equivariance error of the different prediction approaches. We can observe that the discrete sampling version of LieAugmenter provides the strongest performance, with an error that is notably much lower than the one from applying our standard continuous sampling strategy. This result thus indicates that despite more accurately recovering the correct subgroup of the underlying symmetry, enforcing invariance in a manner that does not exactly match the nature of such symmetry can be detrimental to the performance. As a result, this motivates a future exploration of the possibility of making the sampling distribution learnable to dynamically adapt to the characteristics of the considered data.

Table 13: Discrete rotation evaluation results. We report MSE and equivariance error for MLP models trained (i) without augmentation, (ii) with *Oracle* rotation augmentation (ground-truth symmetry), (iii) with symmetry-discovery baselines (Augerino+ and LieGAN augmentation), and (iv) with the discrete and continuous sampling strategies for LieAugmenter (*Ours*). All values are reported as mean \pm std over three random seeds.

		MSE (\downarrow)	Equiv. Error (\downarrow)
Data augmentation	No augmentation	$4.06e-03 \pm 3.02e-04$	$9.57e-02 \pm 1.54e-03$
	Oracle augmentation	$2.10e-02 \pm 1.19e-03$	$2.31e-03 \pm 2.36e-04$
Symmetry discovery	Augerino+	$2.09e-02 \pm 5.56e-04$	$1.08e-02 \pm 4.22e-03$
	LieGAN augmentation	$2.10e-02 \pm 1.10e-03$	$3.28e-03 \pm 3.45e-04$
	LieAugmenter (continuous)	$2.12e-02 \pm 1.24e-03$	$2.46e-03 \pm 3.29e-04$
	LieAugmenter (discrete)	$3.36e-03 \pm 4.56e-04$	$3.09e-02 \pm 1.80e-03$

E.8.2. Partial Permutations

Next, we seek to show that LieAugmenter is able to learn discrete symmetry groups beyond those concerning rotations. In particular, we consider the function $f(x) = x_1 + x_2 + x_3 + x_4^2 - x_5^2$, $x \in \mathbb{R}^5$ with $x \sim \mathcal{U}[-100, 100]$. This function is invariant to partial permutations, with the output remaining the same if we permute the first three dimensions of the input, but changing if we permute the last two.

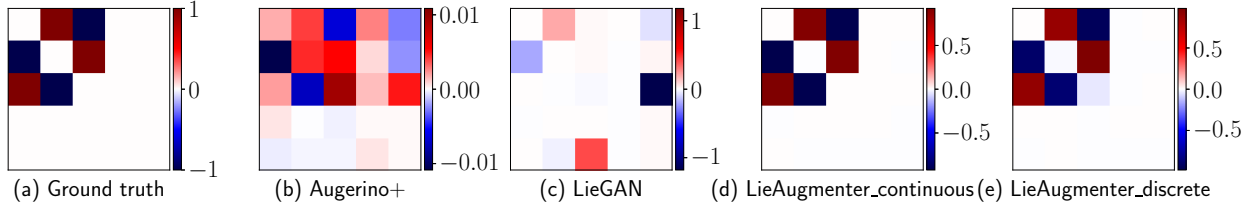


Figure 20: Ground-truth Lie algebra basis, and bases learned by the different sampling strategies for LieAugmenter and baseline symmetry discovery methods in the partial permutation dataset. The sign of the bases is aligned to simplify their interpretation, since it is irrelevant for their correctness.

Symmetry Discovery. From Figures 20 and Figure 21, we can see that LieAugmenter is capable of correctly learning a Lie algebra basis for the underlying discrete partial permutation symmetry irrespectively of the discreteness of the distribution selected for sampling.

Although LieGAN underperforms in our runs, the original work introducing the method [Yang et al., 2023] reports successful recovery of this symmetry. Our implementation follows the available description and code as closely as possible, but we did not match the reported performance for this particular setting.

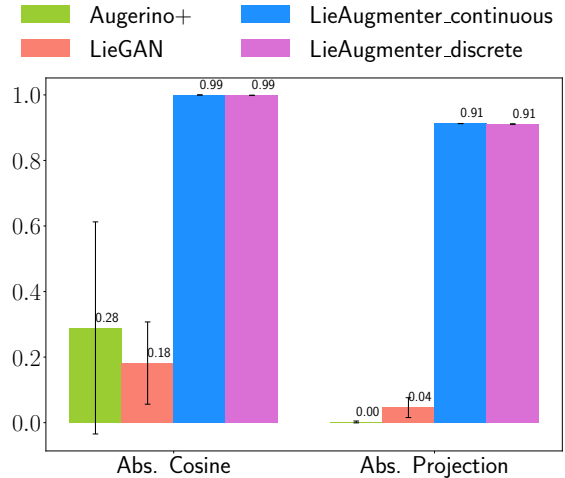


Figure 21: Absolute cosine similarity and absolute Frobenius projection for Lie algebra basis recovery on the partial permutation dataset (mean \pm std over three random seeds).

Predictive Performance. From the results in Table 14, we can observe that once more the discrete sampling strategy for LieAugmenter provides the strongest results, outperforming the continuous approach to sampling. However, differently from the previous discrete rotation experiment, in this case the performance difference is much smaller, which suggests that our standard continuous sampling setting can still perform quite robustly not only in terms of symmetry discovery but also for the generation of predictions despite the misalignment with the level of discreteness of the symmetry that underlies the data.

Table 14: Partial permutation evaluation results. We report MSE and equivariance error for MLP models trained (i) without augmentation, (ii) with *Oracle* rotation augmentation (ground-truth symmetry), (iii) with symmetry-discovery baselines (Augerino+ and LieGAN augmentation), and (iv) with the discrete and continuous sampling strategies for LieAugmenter (*Ours*). All values are reported as mean \pm std over three random seeds.

		MSE (\downarrow)	Equiv. Error (\downarrow)
Data augmentation	No augmentation	1.97e+03 \pm 1.20e+03	1.23e+01 \pm 3.21e+00
	Oracle augmentation	1.69e+03 \pm 8.44e+02	1.41e+01 \pm 2.06e+00
Symmetry discovery	Augerino+	3.38e+03 \pm 8.96e+02	2.52e+01 \pm 4.52e+00
	LieGAN augmentation	1.24e+04 \pm 2.90e+03	1.05e+01 \pm 2.12e+00
	LieAugmenter (continuous)	1.77e+03 \pm 3.57e+02	1.37e+01 \pm 4.55e+00
	LieAugmenter (discrete)	1.49e+03 \pm 6.55e+01	1.19e+01 \pm 2.76e+00

E.9. Lorentz Symmetries in Quantum Field Theory Amplitude Predictions

As an additional experiment, we study the applicability of LieAugmenter to the task of defining a neural surrogate for quantum field theoretical amplitudes [Spinner et al., 2024, Aylett-Bullock et al., 2021, Badger and Bullock, 2020]. This is a problem of great importance in the physics community due to it being central to

the theoretical predictions that LHC measurements are compared to. In particular, these amplitudes describe the unnormalized probability of interactions of fundamental particles as a function of their four-momenta, which are exactly Lorentz-invariant. Following [Spinner et al. \[2024\]](#), we study the setting $q\bar{q} \rightarrow Z + ng$, i.e., the production of a Z boson with $n = 1, \dots, 4$ additional gluons from a quark-antiquark pair. In particular, we focus on the scenario where $n = 2$ and we generate and split the dataset as in that work.

We train LieAugmenter using the baseline Transformer model defined in [Spinner et al. \[2024\]](#) as the prediction network, and with a learnable Lie algebra basis of cardinality $C = 6$ corresponding to that of the restricted Lorentz group $SO^+(1, 3)$, i.e., the connected identity component of the Lorentz group. From [Figure 22](#), we can observe that LieAugmenter is able to approximately learn the correct group. Even though some of the elements of the learned Lie algebra basis (especially those corresponding to boosts) are not exactly equivalent to their ground truth counterparts, we believe that this is more of a side-effect caused by the symmetries that exist in this particular dataset rather than a partial imprecision of our method.

Interestingly, that observation of certain generators of the group being more strongly represented in the data aligns with the particular characteristics of many LHC applications, where often symmetry is only realized to a subset of the full Lorentz group [\[Favaro et al., 2025\]](#). In particular, detector effects and the beam axis direction reduce the symmetry group to $SO(2)_{\text{beam}}$, i.e., rotations around the beam axis. For the specific dataset we consider, the beam for the collision is aligned to the z-axis, so we could expect the generator of rotations on the xy plane to be the one most strongly recovered, and we observe that to be the case in [Figure 22](#).

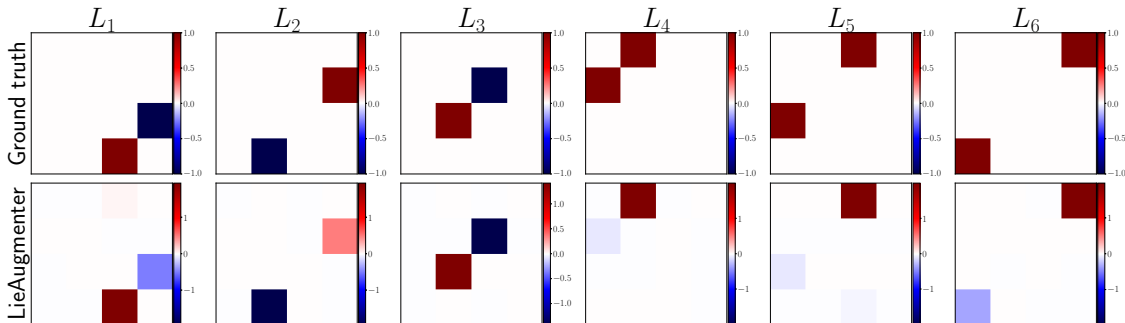


Figure 22: Comparison of canonical ground truth Lie algebra basis for $SO^+(1, 3)$ group (*top*) and the generators learned by LieAugmenter (*bottom*) on the QFT amplitude regression task. For interpretability, we match the learned generators to the closest canonical basis.

Due to the existence of those symmetry breaking effects in the dataset, a model trained with data augmentation from the full $SO^+(1, 3)$ group would not generally be able to achieve optimal performance in this task. As a result, the flexibility and task-adaptiveness of LieAugmenter allows for a more effective data augmentation approach in this scenario. We verify this expectation through the prediction performance shown in [Figure 23](#), where we compare L-GATr [\[Spinner et al., 2024\]](#), which is equivariant to the full Lorentz group, with Transformer prediction networks trained with and without data augmentation from the $SO^+(1, 3)$ group, as well as using our LieAugmenter approach. As we can observe, the performance of LieAugmenter is indeed better than that of the Transformer trained with data augmentation, and it is close to the one obtained with the Transformer without data augmentation and L-GATr despite it simultaneously discovering the symmetry group.

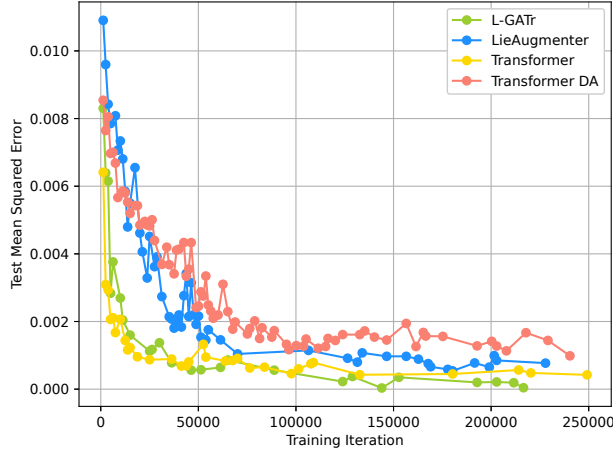


Figure 23: Test MSE during training for the equivariant model L-GATr, a Transformer prediction network trained with and without data augmentation as well using our LieAugmenter method in the QFT amplitude regression dataset.

E.10. Illustration of Augmented Samples

In order to provide increased interpretability into the way the symmetries learned by LieAugmenter act on the data in order to create the augmentations, we present a visualization of augmented samples generated by our model for RotatedMNIST (Figure 24), N -body dynamics (Figure 25), and CRC (Figure 26).

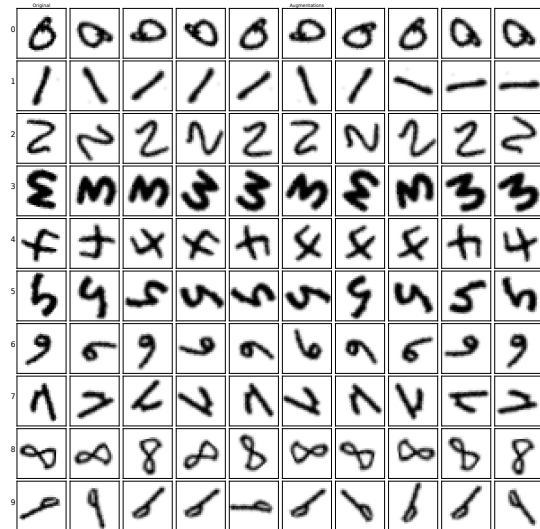


Figure 24: Example of augmentations generated by LieAugmenter for the RotatedMNIST dataset. The first column shows the original samples, and the subsequent ones correspond to the generated augmentations.

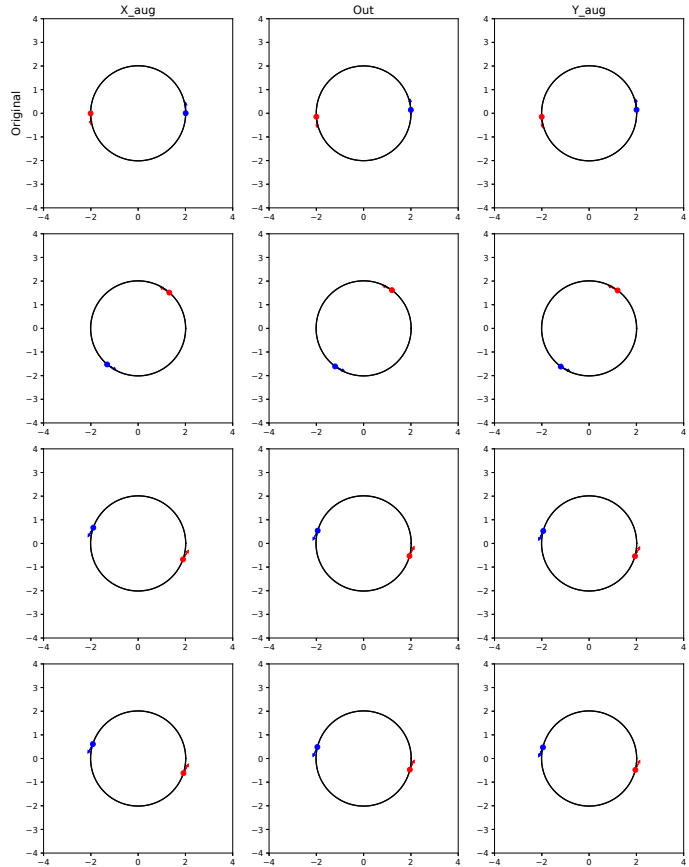


Figure 25: Example of augmentations generated by LieAugmenter for the 2-body dataset. The top row shows (from left to right) the original input sample, the output of the model for that sample, and the target prediction. The rows below show different augmented versions.

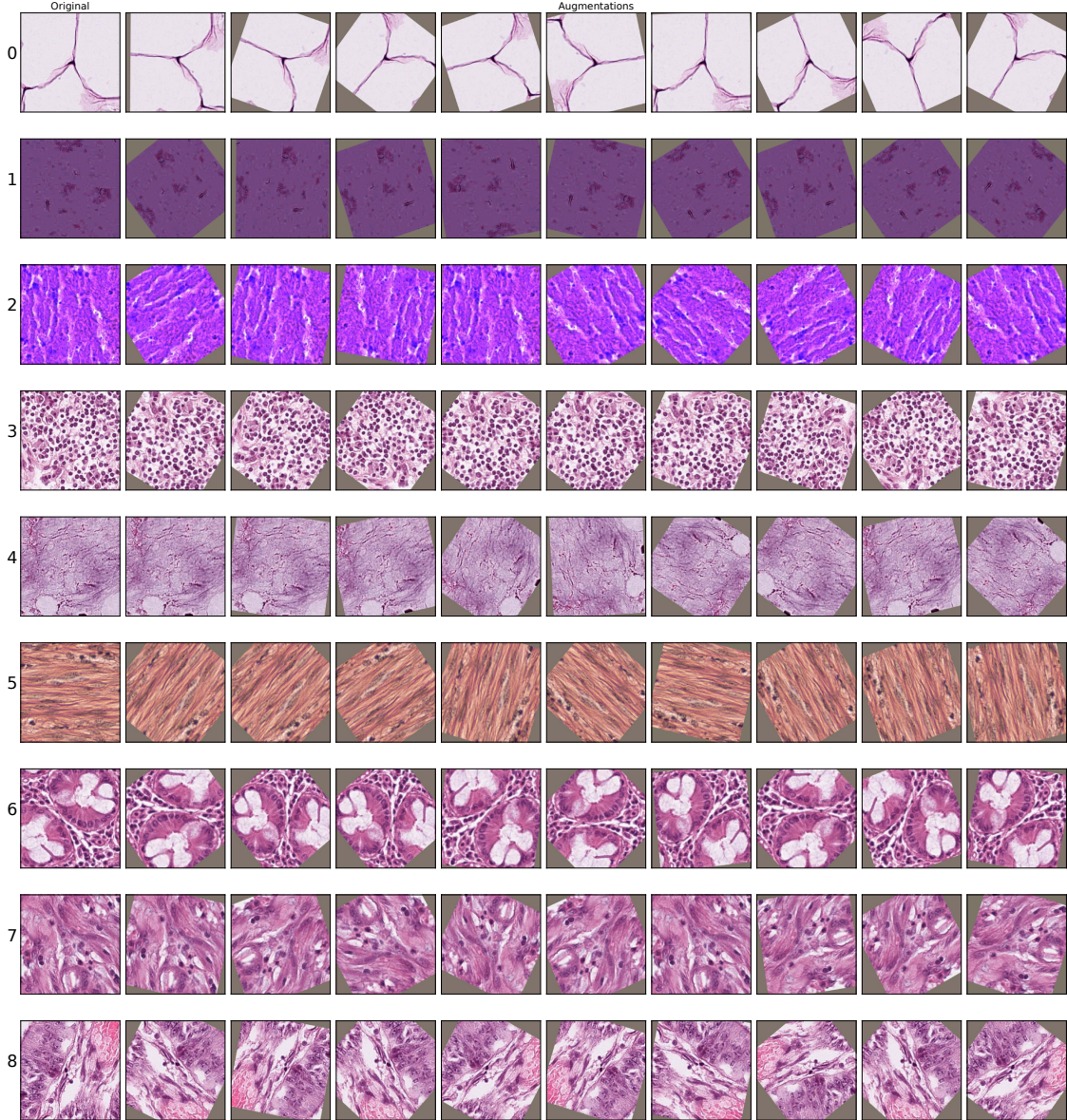


Figure 26: Example of augmentations generated by LieAugmenter for the CRC dataset. The first column shows the original samples, and the subsequent ones correspond to the generated augmentations.

E.11. Runtime Analysis

Next, we complement the analysis of the predictive performance in the different datasets that we considered by providing measurements of the train and test time associated with each model’s prediction results.

Although these measurements can be slightly influenced by the concurrent allocations of the GPUs we used for their execution, they exemplify the potential computational impact of our approach with respect to the different baselines. In addition, note that we have not attempted to optimize our implementation in detail, so it could still potentially be made more efficient.

Importantly, the time measurements for the prediction model that uses LieGAN augmentations corresponds to only the training and inference of the prediction network itself, and, thus, it would be considerably slower if we incorporated the additional time required to train LieGAN itself. That additional runtime for two-step equivariant prediction approaches can pose a significant limitation in practice, and it is one of the motivations behind our proposal of a single end-to-end method.

We present the runtime measurements for RotatedMNIST in Tables 15 and 16, for N -body dynamics in Tables 17 and 18, for QM9 in Table 20, for the no-symmetry experiment in Table 19, for the discrete rotation dataset in Table 21, and for partial permutation in Table 22.

From these results we can see the generally longer runtime of LieAugmenter over other augmentation baselines, which is mainly due to its additional loss and trainable parameters. In contrast, LieAugmenter can be trained much faster than hard equivariant models that consider a priori known symmetries, e.g., EMLP. Overall, we generally observe a trade-off between the flexibility and performance of the approaches and the length of their training time. This trade-off could be potentially minimized in the case of our approach, however, which more careful hyperparameter tuning and a more optimized implementation.

Table 15: RotatedMNIST runtime measurements (MM:SS) for in-distribution (ID) and out-of-distribution (OOD) evaluation of the different approaches. We report the mean over three random seeds.

	Equivariant architecture	No augmentation	Oracle augmentation	Symmetry discovery		
	GCNN (p_4)	Trivial	Rotation	Augerino+	LieGAN Aug.	LieAugmenter
ID train time	03 : 26	01 : 52	06 : 55	04 : 30	06 : 15	07 : 47
ID test time	00 : 00	00 : 00	00 : 02	00 : 03	00 : 01	00 : 01
OOD train time	03 : 56	01 : 50	06 : 57	04 : 47	05 : 03	07 : 04
OOD test time	00 : 00	00 : 00	00 : 02	00 : 03	00 : 01	00 : 01

Table 16: RotatedMNIST runtime measurements (MM:SS) for in-distribution (ID) and out-of-distribution (OOD) evaluation using the alternative inference strategy described in Appendix E.1. We report the mean over three random seeds.

	Oracle augmentation	Symmetry discovery	
	Rotation	LieGAN Aug.	LieAugmenter
ID train time	03 : 03	09 : 45	10 : 44
ID test time	00 : 00	00 : 00	00 : 00
OOD train time	06 : 57	06 : 18	10 : 48
OOD test time	00 : 00	00 : 00	00 : 00

Table 17: 2-body dynamics runtime measurements (MM:SS) for in-distribution (ID) and out-of-distribution (OOD) of the different approaches for one input and output timesteps. We report the mean over three random seeds.

		In-distribution		Out-of-distribution		
		Train time	Test time	Train time	Test time	
Equiv. architecture	EMLP	21 : 34	00 : 02	21 : 13	00 : 02	
	Data augmentation	Trivial	02 : 00	00 : 00	02 : 01	00 : 00
		Oracle	02 : 48	00 : 00	03 : 10	00 : 00
Symmetry discovery	Augerino+_0	05 : 25	00 : 02	05 : 25	00 : 02	
	LieGAN_0 aug	05 : 29	00 : 00	05 : 25	00 : 00	
	LieAugmenter_0	08 : 18	00 : 00	08 : 20	00 : 00	
	Augerino+_2	05 : 40	00 : 02	05 : 32	00 : 02	
	LieGAN_2 aug	05 : 19	00 : 00	05 : 15	00 : 00	
	LieAugmenter_2	08 : 28	00 : 00	08 : 26	00 : 00	
	Augerino+_4	05 : 33	00 : 02	05 : 30	00 : 02	
	LieGAN_4 aug	05 : 22	00 : 00	05 : 26	00 : 00	
	LieAugmenter_4	08 : 27	00 : 00	08 : 26	00 : 00	

Table 18: 2-body dynamics runtime measurements (MM:SS) for in-distribution (ID) and out-of-distribution (OOD) of the different approaches for three input and output timesteps. We report the mean over three random seeds.

		In-distribution		Out-of-distribution	
		Train time	Test time	Train time	Test time
Equiv. architecture	EMLP	17 : 32	00 : 02	16 : 55	00 : 02
Data augmentation	Trivial	01 : 36	00 : 00	01 : 32	00 : 00
	Oracle	02 : 34	00 : 00	02 : 33	00 : 00
Symmetry discovery	Augerino+_0	04 : 20	00 : 01	04 : 20	00 : 01
	LieGAN_0 aug	04 : 22	00 : 00	04 : 21	00 : 00
	LieAugmenter_0	06 : 37	00 : 00	06 : 35	00 : 00
	Augerino+_2	04 : 20	00 : 01	04 : 23	00 : 01
	LieGAN_2 aug	04 : 16	00 : 00	04 : 16	00 : 00
	LieAugmenter_2	06 : 43	00 : 00	06 : 40	00 : 00
	Augerino+_4	04 : 21	00 : 01	04 : 25	00 : 01
	LieGAN_4 aug	04 : 17	00 : 00	04 : 13	00 : 00
	LieAugmenter_4	06 : 46	00 : 00	06 : 48	00 : 00

Table 19: Runtime measurements (MM:SS) for the prediction results in the dataset without continuous symmetries. We report the mean over three random seeds.

		Train time	Test time
Data augmentation	No augmentation	00 : 44	00 : 00
	Oracle augmentation	01 : 12	00 : 00
Symmetry discovery	Augerino+	02 : 00	00 : 01
	LieGAN augmentation	03 : 28	00 : 00
	LieAugmenter	03 : 06	00 : 00

Table 20: Train and test time (HH:MM:SS) of LieAugmenter for the different considered prediction targets of the QM9 dataset.

	HOMO		LUMO	
	Train time	Test time	Train time	Test time
LieAugmenter	15 : 17 : 12	00 : 00 : 04	15 : 19 : 15	00 : 00 : 04

Table 21: Discrete rotation runtimes (MM:SS) for the different prediction approaches. We report the mean over three random seeds.

		Train time	Test time
Data augmentation	No augmentation	00 : 03 : 31	00 : 00 : 00
	Oracle augmentation	00 : 05 : 35	00 : 00 : 00
Symmetry discovery	Augerino+	00 : 09 : 29	00 : 00 : 01
	LieGAN aug	00 : 09 : 21	00 : 00 : 00
	LieAugmenter (continuous)	00 : 14 : 24	00 : 00 : 00
	LieAugmenter (discrete)	00 : 14 : 51	00 : 00 : 00

Table 22: Partial permutation runtimes (MM:SS) for the different prediction approaches. We report the mean over three random seeds.

		Train time	Test time
Data augmentation	No augmentation	00 : 03 : 40	00 : 00 : 00
	Oracle augmentation	00 : 05 : 33	00 : 00 : 00
Symmetry discovery	Augerino+	00 : 09 : 55	00 : 00 : 01
	LieGAN augmentation	00 : 09 : 54	00 : 00 : 00
	LieAugmenter (continuous)	00 : 15 : 09	00 : 00 : 00
	LieAugmenter (discrete)	00 : 15 : 04	00 : 00 : 00

E.12. Additional Equivariance Error Measure

Lastly, we expand our analysis of the equivariance error of the different prediction approaches by studying the behavior of another similar metric that differently measures the consistency of the generated predictions under augmentations from the ground truth symmetry group: $\frac{1}{N} \sum_{i=1}^N \frac{1}{K} \sum_{j=1}^K \|\Psi(\rho_{\mathcal{X}}(g_j)(x_i)) - \rho_{\mathcal{Y}}(g_j)(\Psi(x_i))\|$.

We present the associated results for RotatedMNIST in Tables 23 and 24, for N -body dynamics in Tables 25 and 26, for QM9 in Table 27, for the discrete rotation dataset in Table 28, and for partial permutation in Table 29.

As we can observe, the measurements for this metric are very close to ones we obtained with the previous equivariance error and follow similar trends in terms of which approaches provide a better result, thus reinforcing our previous analysis. In particular, we can once more see that LieAugmenter always provides among the lowest equivariance error measurements showing its strong and robust ability to encode the relevant equivariance into the prediction network.

Table 23: Additional equivariance error measure in the RotatedMNIST dataset for the in-distribution (ID) and out-of-distribution (OOD) evaluation of the different approaches. All values are reported as mean \pm std over three random seeds.

	Equivariant architecture	No augmentation	Oracle augmentation	Symmetry discovery		
	GCNN ($p4$)	Trivial	Rotation	Augerino+	LieGAN Aug.	LieAugmenter
ID Equiv. Error (\downarrow)	6.51 \pm 1.41	6.69 \pm 0.24	<u>4.86</u> \pm 0.36	6.35 \pm 0.98	6.12 \pm 0.25	3.82 \pm 0.38
OOD Equiv. Error (\downarrow)	7.16 \pm 1.52	8.74 \pm 0.61	<u>4.75</u> \pm 0.38	5.26 \pm 0.72	7.17 \pm 0.50	4.12 \pm 0.75

Table 24: Additional equivariance error measure in the RotatedMNIST dataset for the in-distribution (ID) and out-of-distribution (OOD) evaluation of the different approaches with the alternative inference strategy. All values are reported as mean \pm std over three random seeds.

	Equivariant architecture	No augmentation	Oracle augmentation	Symmetry discovery		
	GCNN ($p4$)	Trivial	Rotation	Augerino+	LieGAN Aug.	LieAugmenter
ID Equiv. Error (\downarrow)	6.51 \pm 1.41	6.69 \pm 0.24	<u>4.72</u> \pm 0.27	6.35 \pm 0.98	5.95 \pm 0.87	4.54 \pm 0.17
OOD Equiv. Error (\downarrow)	7.16 \pm 1.52	8.74 \pm 0.61	<u>4.96</u> \pm 0.13	5.26 \pm 0.72	8.35 \pm 0.97	4.29 \pm 0.56

Table 25: 2-body dynamics alternative equivariant error measurements for in-distribution (ID) and out-of-distribution (OOD) of the different approaches for one input and output timesteps. We report the mean over three random seeds.

		In-distribution	Out-of-distribution
		Equiv. Error (\downarrow)	Equiv. Error (\downarrow)
Equiv. architecture	EMLP	8.08e-05 \pm 1.76e-05	8.02e-05 \pm 1.72e-05
Data augmentation	Trivial	4.84e-02 \pm 1.58e-02	8.91e-02 \pm 6.24e-03
	Oracle	6.35e-03 \pm 1.44e-03	6.53e-03 \pm 1.25e-03
Symmetry discovery	Augerino+_0	4.20e-01 \pm 1.85e-03	4.21e-01 \pm 6.31e-03
	LieGAN_0 aug	3.93e-02 \pm 1.73e-03	7.25e-02 \pm 1.01e-02
	LieAugmenter_0	5.75e-03 \pm 2.26e-04	4.53e-03 \pm 2.52e-04
	Augerino+_2	4.30e-01 \pm 5.04e-02	4.00e-01 \pm 6.40e-02
	LieGAN_2 aug	2.83e-02 \pm 8.22e-03	6.68e-02 \pm 2.19e-03
	LieAugmenter_2	5.34e-03 \pm 1.35e-03	9.61e-03 \pm 4.93e-03
	Augerino+_4	4.16e-01 \pm 1.64e-03	4.16e-01 \pm 3.58e-05
	LieGAN_4 aug	6.03e-03 \pm 8.00e-04	7.08e-03 \pm 1.67e-03
	LieAugmenter_4	6.17e-03 \pm 1.61e-03	5.79e-03 \pm 7.28e-04

Table 26: 2-body dynamics alternative equivariant error measurements for in-distribution (ID) and out-of-distribution (OOD) of the different approaches for three input and output timesteps. We report the mean over three random seeds.

		In-distribution	Out-of-distribution
		Equiv. Error (\downarrow)	Equiv. Error (\downarrow)
Equiv. architecture	EMLP	4.47e-05 \pm 7.24e-06	4.46e-05 \pm 7.31e-06
Data augmentation	Trivial	7.17e-02 \pm 1.53e-02	8.36e-02 \pm 3.20e-03
	Oracle	1.10e-02 \pm 3.29e-03	8.62e-03 \pm 8.36e-04
Symmetry discovery	Augerino+_0	4.22e-01 \pm 3.07e-03	4.22e-01 \pm 8.34e-03
	LieGAN_0 aug	7.20e-02 \pm 1.13e-02	9.55e-02 \pm 1.45e-02
	LieAugmenter_0	7.62e-03 \pm 1.95e-03	1.04e-02 \pm 4.38e-03
	Augerino+_2	4.13e-01 \pm 1.26e-02	4.13e-01 \pm 1.53e-03
	LieGAN_2 aug	4.36e-02 \pm 2.40e-03	9.53e-02 \pm 1.06e-02
	LieAugmenter_2	8.50e-03 \pm 8.16e-04	2.13e-02 \pm 2.66e-03
	Augerino+_4	4.19e-01 \pm 4.20e-03	4.20e-01 \pm 3.19e-03
	LieGAN_4 aug	8.10e-03 \pm 1.21e-03	9.62e-03 \pm 3.32e-03
	LieAugmenter_4	8.37e-03 \pm 9.29e-04	8.11e-03 \pm 3.96e-04

Table 27: Alternative equivariant error measurements of LieAugmenter for the different considered prediction targets of the QM9 dataset.

	HOMO	LUMO
	Equiv. Error (\downarrow)	Equiv. Error (\downarrow)
LieAugmenter	0.0045	0.0019

Table 28: Alternative equivariant error measurements for the discrete rotation dataset. We report the mean over three random seeds.

		Equiv. Error (\downarrow)
Data augmentation	No augmentation	1.24e-01 \pm 2.39e-03
	Oracle augmentation	2.91e-03 \pm 2.35e-04
Symmetry discovery	Augerino+	1.36e-02 \pm 5.32e-03
	LieGAN augmentation	4.21e-03 \pm 4.20e-04
	LieAugmenter (continuous)	3.18e-03 \pm 4.07e-04
	LieAugmenter (discrete)	4.41e-02 \pm 2.06e-03

Table 29: Alternative equivariant error measurements for the partial permutation dataset. We report the mean over three random seeds.

		Equiv. Error (\downarrow)
Data augmentation	No augmentation	1.58e+01 \pm 4.25e+00
	Oracle augmentation	1.80e+01 \pm 2.68e+00
Symmetry discovery	Augerino+	3.20e+01 \pm 5.35e+00
	LieGAN augmentation	1.34e+01 \pm 2.59e+00
	LieAugmenter (continuous)	1.75e+01 \pm 5.80e+00
	LieAugmenter (discrete)	<u>1.49e+01</u> \pm 3.45e+00